TWO-DIMENSIONAL PHASES OF SILICON ON SILICON CARBIDE

A Dissertation
Presented to
The Academic Faculty

By

Hsin-Ju Wu

In Partial Fulfillment
of the Requirements for the Degree
Doctor of Philosophy in the
School of Physics

Georgia Institute of Technology

August 2020

TWO-DIMENSIONAL PHASES OF SILICON ON SILICON CARBIDE

Approved by:

Professor Phillip N. First, Advisor
School of Physics
Georgia Institute of Technology

Professor Walt A. de Heer
School of Physics
Georgia Institute of Technology

Professor Zhigang Jiang
School of Physics
Georgia Institute of Technology

Professor Andrew Zangwill
School of Physics
Georgia Institute of Technology

Professor Angelo Bongiorno
Department of Chemistry
*City University of New York,
College of Staten Island*

Date Approved: May 28, 2020

It does not matter how slowly you go as long as you do not stop.

Confucius

To my parents,

Wen-Chien Chen and Shih-Ming Wu

ACKNOWLEDGEMENTS

TABLE OF CONTENTS

LIST OF TABLES

LIST OF FIGURES

ACRONYMS

MoS_2 molybdenum disulfide. 1

2D two dimensional. 1, 2, 4, 5, 6, 10, 11, 18, 19, 21, 46, 55, 71, 75, 78, 83, 86

3-tet a triangular grouping of 3 tetramers. 70, 71, 72, 73

3D three dimensional. 1

AES Auger electron spectroscopy. 21, 28, 29, 37, 38, 39, 40, 85

AFM Atomic Force Microscope. 21, 23

BP black phosphorus. 1

CCM constant current mode. 43

CCS confinement-controlled sublimation. 2

CHM constant-height mode. 43

CMA cylindrical mirror analyzer. 38

CMP chemical mechanical polished. 23

DAS dimer-adatom-stacking fault. 11, 16

DFT density functional theory. 81, 82

FFT fast Fourier transform. 65, 67, 68, 71

SUMMARY

Two dimensional (2D) materials have been widely studied since single layer graphene, a 2D atomic honeycomb structure with unusual electronic properties, was obtained. Graphene grown on SiC by thermal decomposition is of interest because of its potential for fine control of the epitaxial growth directly on a crystalline semiconductor substrate. Control of this growth has been obtained by introducing Si vapor into the growth environment. Other work has shown that this approach is valuable for the production of unique nanostructures of graphene; in this work, we explore the possibility to grow 2D thin films of *silicon* on the SiC substrate.

An understanding of growth dynamics and surface phases is of interest for the creation of electronic-grade graphene on SiC, but there is also the potential for electronically useful 2D phases of silicon. For instance, the Si 2D honeycomb structure, silicene, is considered a potential next-generation material for electronic devices.

In this thesis, we describe experiments undertaken in order to understand growth dynamics and Si surface phases in the pre-graphene regime of quasi-equilibrium growth, determined by the temperature and Si vapor pressure. A novel LEED pattern ($\sqrt{43} \times \sqrt{43}R \pm 7.6°$) for a complex 2D Si structure is found on both the Si-terminated and C-terminated faces of SiC. The hexagonal structure and epitaxial matching constraints are consistent with silicene, but ultimately we show that a different structure is a more likely explanation.

Based on experimental data and established structures from other research groups, a model for the newly-discovered phase of Si on SiC(0001) is proposed. By comparing growth conditions and other experimental data collected, we conclude that the structure contains three tetramers similar to the Si-rich 3×3 structure and three bridge-atom formations, reducing the number of dangling bonds to just three per unit cell. Empirical methods underlying the development of this model are discussed. Similar approaches are potentially of use for other 2D phases of Si on SiC.

CHAPTER 1

INTRODUCTION

Two dimensional (2D) systems have been widely studied for a long time because of the unusual transport properties of electrons confined to a plane. From classical physics point of view, 2D materials are thermodynamically unstable at any finite temperature due to thermal lattice fluctuations [1]. However, the existence of three dimensional (3D) materials with layered structure such as graphite or molybdenum disulfide (MoS_2) ("van der Waals" materials) still implies the possibility to obtain single layers of such materials.

Exfoliation down to their 2D monolayer (ML) was considered to be possible only theoretically since Mermin demonstrated that low dimensional materials can exist if the crystal is described within the harmonic approximation in 1968 [2]. However, this topic has exploded after graphene, an atomic layer of honeycomb structure of C, has been successfully produced in 2004 [3, 4]. This honeycomb structure of C shows very special electronic properties such as high electron mobility and the integer quantum hall effect [5, 6]. After that, graphene-like or 2D structures from other van der Waals materials are also studied including transition metal dichalcogenides (TMDs), hexagonal boron nitride (h-BN) , black phosphorus (BP), and silicene [7]. Other than the material mentioned, there are also extensive discussion about possible existence of other 2D materials. Calculation has been done and predicted that more than 800 materials could be stable in 2D structure from exfoliation [8–11].

With the understanding of physical and electrical properties, the next step would be to develop ability to control the production of such material to make it suitable for use in large-scale integrated electronics.

Because of the importance mentioned above, the production methods for obtaining other 2D material are also widely studied. Epitaxial growth on a crystalline substrate, by vapor

deposition or other means, allows the production of *oriented* 2D single crystal films with low defect density [12].

The graphitic film on SiC was firstly found in 1975 [13]. Epitaxial graphene grown by thermal decomposition method on SiC allows us to have large uniform large graphene sheet on SiC substrate, which is an insulating substrate and can be potentially used to integrate with Si based electronic device [4].

While epitaxial growth result in large uniform graphene, the etch pits formation and nucleation phenomena make it difficult to control surface morphology [14]. Some experimental methods are provided to solve this problem such as confinement-controlled sublimation (CCS) over the growth process [15–17]. This is potentially valuable for creating unique nanostructures such as "sidewall" nanoribbons [18].

The CCS method provides a way to have better growth control by supplying more Si background pressure, which, at a given temperature, slows the growth of graphene, allowing large terraces to form. In a similar way, suppressing Si desorption rate from the SiC substrate by introducing a high pressure inert gas also improves the graphene growth. [19, 20], but further refinement such as forming graphene nanoribbons still requires a detailed understanding of the graphene growth mechanism [21].

Additionally, growth control that introduces Si vapor provides a potentially reversible process to turn a C-rich surface into a Si-rich surface to form a *silicon* thin film. While epitaxial graphene forms on a C-rich (or Si-depleted) surface of SiC, a Si-rich surface of SiC may form a 2D Si structure and we can speculate that perhaps a it could form epitaxial silicene, the 2D analog of graphene. To this end, questions are still open and need to be answered: What Si 2D structure can be formed epitaxially on SiC, and will it be possible to find silicene? Can we systematically find growth condition for silicene from graphene production? Can we understand the evolution of a patterned SiC surface to its final configuration of graphene or silicene nanostructures?

In this thesis, we will discuss 2D structure of Si on the Si-rich surface. Background

of related materials is introduced in the following sections in this chapter. Chapter 2 discusses experimental methods and equipment. Experimental methods with growth control is designed to obtain Si thin film and graphene, and *in situ* and *ex situ* measurement are done to answer these questions. Experimental data will be in Chapter 3. The result and analysis is in Chapter 4, with conclusions and outlook presented in Chapter 5.

1.1 Silicon Carbide

SiC has been extensively studied since 1989 when scientists start searching for materials for both properties from group IV element and compound semiconductors [22]. It has a large electronic band gap from 2.4 eV to 3.3 eV based on its polytypism [23]. It is also a high electron mobility and thermal conductivity material. These properties allow it to be used for devices in high temperature or high power and high frequency [24, 25].

To produce pure SiC, Lely method is used which was invented by Jan Anthony Lely in 1954 [26]. A modified Lely process by Tairov and Tsvetkov in 1978 is adopted to have improved high quality SiC wafer [27]. There are about 250 crystalline forms [29]. In
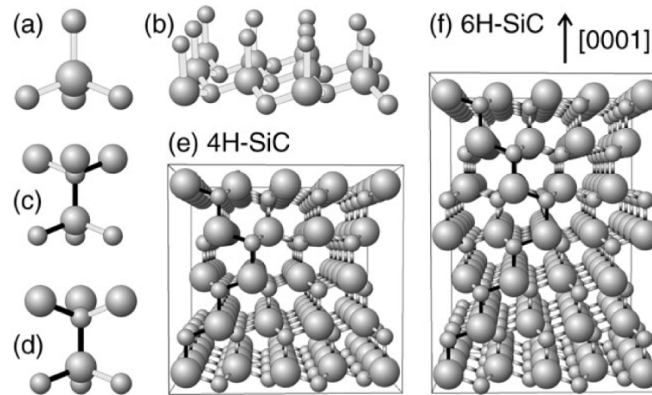
Figure 1.1: SiC structure, small and large atoms represents C and Si accordingly [28].

the following, we will introduce the ones we use in this thesis. The basic structure of SiC is similar to other sp^3-bonded semiconductors in group IV and the III-V zincblende semiconductors. This means that each atom bonds tetrahedrally to its neighbors [28] to form

bulk SiC. There are several approaches to see how different SiC structures are constructed. One way to consider is to have a buckled honeycomb structure as a bilayer, and the full crystal structure is formed by stacking multiple bilayers in specific ways.

Each bilayer is constructed by two elements, Si and C. Stacking each bilayer in rotational angle will result in different polytypes. Fig. 1.1(a) shows the basic tetrahedral structure with one Si atom at the center bonded with its four nearest C atoms. With one of these four Si-C bonds pointing up (i.e. in z direction), repeated structure in x-y plane can form a 2D Si-C bilayer as shown in Fig. 1.1(b). The C atoms on top of each Si atom can be seen as part of another bilayer tetrahedrally bond to other Si atoms in that layer.

By using bilayers as a building block, the bulk SiC is formed by stacking bilayers vertically. The three-fold symmetry of one bilayer indicates that there are two possible stacking configuration. One is "Linear Stacking" which all atoms are configured in the same way with a linear shift in an in-plane direction, and the other is "Switching Stacking" in which the bilayer rotates 60 degrees within the bilayer plane. Fig. 1.1(c) and (d) show, respectively, linear and switching stacking of two bilayers.

Different combination of linear and switching stacking form different polytypes. Some polytypes are common in production. If each stacking is linear, it is a three-bilayer translated cubic structure (3C-SiC), and if the stacking switches every other bilayer, it is a two-bilayer translated hexagonal structure (2H-SiC). If the stacking switches form a pattern periodically every fourth bilayer and sixth bilayer, it corresponds to 4H-SiC and 6H-SiC respectively as shown in Fig. 1.1(e) and (f). 6H-SiC is also known as α-SiC, which is the most common kind [30], and it is formed at $1700°$ C or higher. 3C-SiC is also known as β-SiC, and it forms below $1700°$ C.

With all the bilayer stacking sequences, bulk SiC terminates with one bilayer and leaves only one dangling bond on each Si atom and none for C atoms on one end, and one dangling bond on each C atom and none for Si atoms. For the Si-terminated surface, it is called Si-face or SiC(0001) face. On the other hand, the C-terminated surface on the other side is

4

called C-face or SiC($000\bar{1}$) face. In this thesis, the 2D Si structure growth is focused mostly on Si-face. While different stacking orders form different structures, the terminated face on Si-face and C-face still have Si or C atoms with single dangling bond per unit cell. When a SiC sample is heated up to high temperature, the Si and C bond on the first few bilayers will break. Si atoms will evaporate and leave C atoms on the surface to form 2D structure. One of the 2D structure is graphene, single atomic layer of graphite.

On the other hand, when annealing with lower temperature, Si-C bond on substrate won't break and if there are excessive Si atoms, they will diffuse and move within the surface and form a low energy configuration. The low energy Si configuration will epitaxially form different periodic patterns based on annealing temperature. The periodic Si pattern and SiC substrate can be seen by having low-energy electron diffraction (LEED) measurement under ultra-high vacuum (UHV) environment.

The LEED measurement gives some reconstruction information, and different regions of annealing condition such as temperature and pressure result in different LEED information, and because of this, the LEED notation is used to label different phases throughout the annealing process.

Starke et al. has done a series of study for LEED phases change on both Si-face and C-face [28]. Figure 1.2b shows different LEED phases when annealing a SiC sample within temperature from 800 °C to 1100 °C on Si-face. A sample surface is *ex situ* prepared and then annealed at 800° C under Si flux in UHV chamber. The Si-rich environment saturates the dangling bond on the surface, and excessive Si atoms form a 2D periodic structure. This 2D structure was then identified as 3×3 super lattice, and starting from 3×3, the LEED phase will change when raising annealing temperature, and this process gives some LEED phases which are easily reproduced. They are 3×3, $\sqrt{3} \times \sqrt{3}$, and $6\sqrt{3} \times 6\sqrt{3}$.

Other than the three reproducible phases, there is a region between 3×3 and $\sqrt{3} \times \sqrt{3}$ called "Metastable Phases." Some LEED phases were found in this region, and they can not be easily reproduced. Experimental result shows that they are very sensitive to annealing

temperature, and most of the time it contains multiple phases instead of having single well-ordered phase.

The LEED phases on Si-face indicates some interesting structure on the surface, and scientists started studying these structures and how they relates to the annealing condition. The Si-rich 3×3 surface was well studied by Starke et al., and this structure was built by Holographic LEED (HLEED) [31] with other experimental data. More details will be discussed in the next section.

Further annealing in higher temperature results in even more Si adatoms evaporated, the bonding for the first few bilayer of SiC will also starts to break. The C atoms left on the surface will form 2D structure to form a honeycomb structure of C atoms bonded to the substrate. At this condition, the structure is still not free from the substrate, and it is called Buffer Layer or "Layer Zero."

This buffer layer will show a $6\sqrt{3} \times 6\sqrt{3}$ on LEED. These two reproducible phases, $\sqrt{3} \times \sqrt{3}$ and $6\sqrt{3} \times 6\sqrt{3}$, under high temperature annealing above $1000°$ C will be discussed in more detail in later sections. After $6\sqrt{3} \times 6\sqrt{3}$ phase, Si atoms will continue evaporating, another buffer layer will start to form on top of the SiC bilayer (and beneath the original buffer layer). This will detach the original buffer layer to become quasi–free standing 2D honeycomb structure, which is graphene, and this is called "Layer 1." When annealing to even higher temperature, more and more graphene layers are pushed away from the substrate by inserting one new buffer layer each time, and the LEED phase does not change from here except the sharpness and intensity of the reconstruction spots on LEED image.

The above is a series of LEED phase change for Si-face based on annealing temperature. The Si evaporation rate and the breaking of Si-C bonds from substrate will determine whether the super lattice on the surface is Si-rich or C-rich. This will give us information about forming 2D structure on SiC.

Same analysis are done on C-face by Heinz et al. [28]. Comparing to Si-face, C-face has a similar structure, and it's the C atoms which form the dangling bond on the substrate.
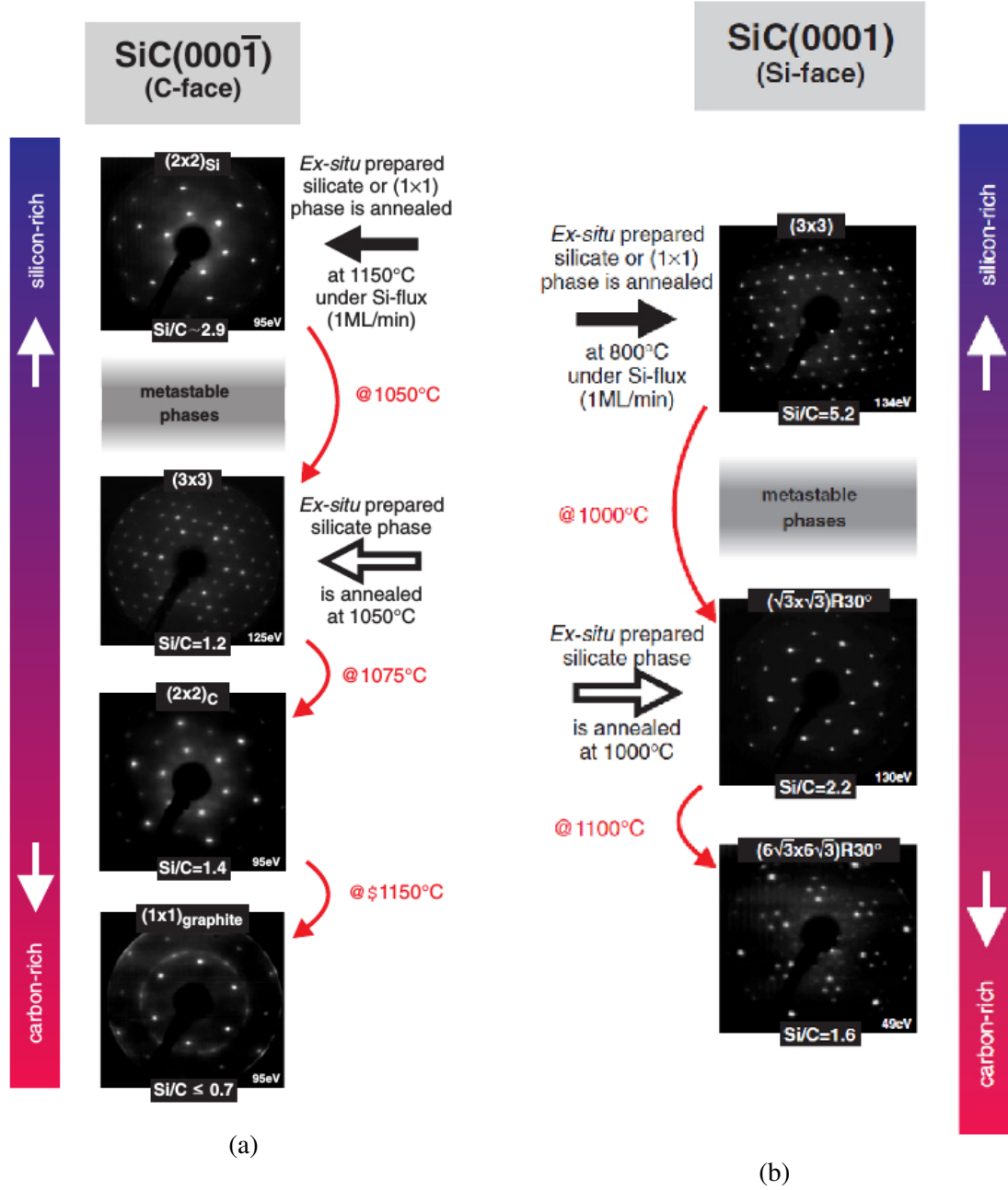
Figure 1.2: (a) SiC(000$\bar{1}$) surface in different phases [28] (b) LEED phase of Si-face on SiC based on annealing temperature [28]. (c) Temperature-Pressure diagram [19]

Without Si-C bond breaking from substrate, additional Si atoms are bonded with C atoms from substrate. While the dangling bonds from substrate still form the same 1×1 unit cell with lattice constant 3.08 Å, the bond length is shortened, and the low energy configuration is not the same as Si-face. Fig. 1.2a shows the LEED phases information for C-face of SiC substrate.

In Heinz's paper [28], samples studied for C-face were prepared by the same initial treatment as Si-face. However, instead of just a single 3×3 phase, the initial C-face condition could be a 3×3 or 2×2 Si-rich reconstruction. Starting from initial phases, further annealing with higher temperature showed LEED phases information. Comparing to Si-face, the LEED reconstruction phases also showed two stable structures, which are the C-rich 2×2 and graphene rings. Some reproducible structures on C-face will be discussed in the next section. The surface condition for each phase depends on the amount of Si and C adatoms, and it is essential to understand how a Si-rich surface transits to almost no adatoms, C-rich surface, and then become graphene. This information could potentially be helpful for controlling the graphene quality.

While both Si-face and C-face does show potential to grow graphene based on LEED phase, graphene grown on Si-face does have a better control comparing to C-face. Because the honeycomb structure forms after the surface reach C-rich condition, the evaporation rate for Si atoms is one of the main factor to affect the quality and quantity of graphene. Faster and more rapid Si evaporation will cause fluctuation of local C density and therefore affect how fast and where the honeycomb structures are formed. To this end, controlling Si background pressure when annealing to high temperature could potentially lower the fluctuation for local carbon density and improve graphene quality.

In this thesis, we mainly focus on Si-face, and based on the amount of adatoms on the surface, one can separate the process to two different steps: One is from Si-rich environment to no adatoms, and another is from no adatoms to C-rich surface.

While growing graphene from annealing SiC substrate can provide the quality that other
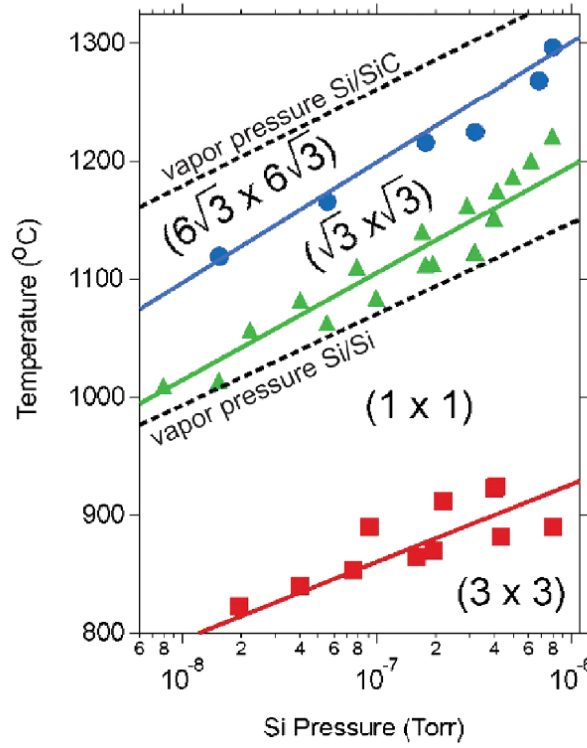
Figure 1.3: Temperature-Pressure diagram [19]

material or growing method can't, there are still some problems with this method such as forming etch pits and small grain size of graphene [14]. Si atoms decomposed from surface randomly to form nucleation phenomenon, and it is possible to be avoided with background Si pressure. Tromp et al. used disilane to supply background Si pressure to compensate Si desorption from surface [19]. The disilane gas decomposes to Si and H atoms when temperature is higher than $420°$ C. H atoms can not affect the surface much by etching due to the fact that the pressure and temperature are far from this region. Fig. 1.3 shows a temperature-pressure diagram from that paper, and the temperature of phase transition can shift up to $250°$ C, and all the transition are fully reversible. In Ref. [19], two phases can coexist in a temperature range, and this is the same as the transition process for Si(111) 1×1 to 7×7, which the temperature shift due to 1.0×10^{-5} Torr Si background pressure is $3°$ C, but the temperature shift for phase change can go up to $205°$ C for phase transition for Si reconstruction.

The coexist temperature range is 10 °C to 15 °C, and in this range, the time it costs for phase transition to occur at low end of the range is on a time scale of minutes, on the contrast, it only take a few second at the high end.

When sample is annealed at 1300° C under 2×10^{-5} Torr of Si pressure, it shows an improved surface morphology with mostly one layer of graphene comparing to samples annealed at the same temperature under vacuum, which has graphene coverage from 1 to 4 layers.

Tromp et al. [19] demonstrated the reversible phases while annealing on SiC surface, and this shows that with adjusted temperature and pressure, it is possible to control the surface to be Si-rich or C-rich surface under a quasi-equilibrium status.

While controlling Si background pressure is a potential great way to control the quality for graphene production, it is also possible to grow only buffer layer of graphene and isolate it from substrate. The covalent bonds between buffer layer graphene and substrate cause charge transfer and resulting an intrinsically n-doped graphene [32]. Other than continue annealing to obtain another buffer layer, it is also possible to saturate the dangling bond from substrate, after that the buffer layer will turn into a quasi-free-standing graphene. Several groups have used different elements to successfully passivate the substrate, such as hydrogen [32–34], silicon [35], or oxygen [36, 37].

The hydrogen intercalation is done by annealing sample to a temperature range 600 °C to 1000 °C under 950 mbar molecular hydrogen for 10 min. Si intercalation , in contrast, is done by depositing 1–3 ML of Si on buffer layer and annealing to 800° C under vacuum.

While extensive studies are done on Si-face for better graphene production, the Si-rich side of the surface is mainly treated as a preparation phase before graphene growth. However, the success of graphene does ignite a wide search on other possible 2D material, and Si, as part of the group IV element, is certainly a good candidate for this purpose. The quasi-equilibrium experiment from Tromp et al. [19] shows the potential to control Si 2D structure on the Si-rich side of the SiC surface when annealing, so in the next section, we

will discuss the 2D Si structure obtained so far.

1.2 Two dimensional structures of Si on SiC

The reconstruction patterns for different annealing temperature and Si background pressure forms different structures on the surface, and by studying the structure on the surface, we can understand the growth process and potentially control it for further 2D Si thin film application. Some structures of the LEED phases such as 3×3 and $\sqrt{3} \times \sqrt{3}$ were well studied in details [28], and other than these two phases, there were also some proposed structures for the phases found in Metastable Phases. In the following, the accepted and proposed Si structures on both Si-face and C-face are discussed. Other possible Si 2D structure will also be discussed. We will start with the known structures such as 3×3 and $\sqrt{3} \times \sqrt{3}$. In the study from Heinz et al., some techniques and calculations were done for Si deposition on SiC from LEED in order to determine the structure [28].

The 3×3 phase is one of the most common phases found, and extensive research has been done to study this phase [38–40]. Some groups had proposed structures based on Si(111) 7×7 structure [22, 38, 41, 42], which is the dimer-adatom-stacking fault (DAS) model [40]. However, there is no scanning tunneling microscope/microscopy (STM) data to support the structure with proper dangling bonds information [31, 43]. There are also some other proposed structure for this phase [44]. Starke et al. has built a model from Holographic LEED method which is widely accepted and will be discussed and used in this thesis [43]. In that paper, the STM image for reconstruction surface 3×3 shows only one protrusion per 3×3 unit cell, and because of this, the wave emitted from the protrusion atom can be seen as a reference wave, and other waves emitted from others can be seen as objective waves. To this end, the interference between a reference wave and objective waves can be measured. By obtaining the information of the interference, the surface structure can be calculated. Figure 1.4a shows the principle to form holographic image based on the single protrusion sticking out of the surface. Fig. 1.4b shows the result from holographic

11

(a)

(b)

(c)
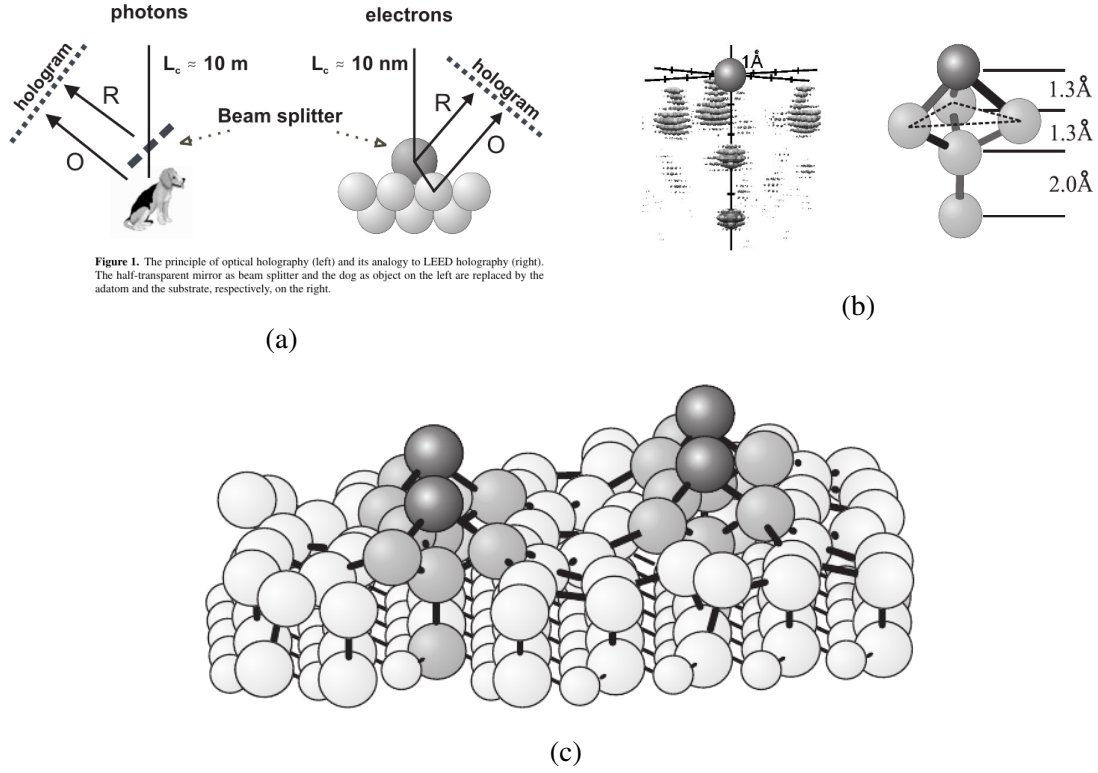
Figure 1.4: (a) The principle of hologram and the application for Si structure on the surface. (b) Result from holographic image which indicates the tetrahedral structure. (c) The Si structure based on tetrahedral structure from holographic result [45].

methods showing the tetrahedral structure under the beam-splitter atom. Fig. 1.4c shows the 3×3 structure with relaxed bonding atom position based on the tetrahedral structure from HLEED.

Starting from the structural element in Fig 1.4b, the 3×3 Si structure has also been determined. One Si atom is put directly above each Si atom from Si-face to form one Si adlayer. Then, three adatoms are added on a local structural element as a "trimer" structure, and then another Si adatom is put on top to form the local adatom structure that we refer to throughout this Thesis as a "tetramer."

Thus, four extra Si adatoms are added to the 3×3 unit cell on top of the adlayer. The adlayer and adatoms will finally form bondings to have only one dangling bond per unit cell on the top. Finally this structure has been calculated and obtained relaxed positions as mentioned in Fig. 1.4.

The tetramer structure tend to rotate counter clockwise after relaxation. There are some evidence indicating that the relax direction could also be clockwise direction [46]. And the structure would only prefer one direction locally aligned with other tetramers.

The Si coverage, with one adlayer and four additional adatoms in a 3×3 unit cell, is $(9 + 4)/9 = 13/9$ ML.

In addition to 3×3, $\sqrt{3} \times \sqrt{3}$ is another common phase on Si-face. Several groups have found and studied this phase [47–51], and Coati et al. used grazing-incidence x-ray diffraction to determine that the adatom is on T4 site instead of H3 site [52]. Details for T4 and H3 configuration is in Fig. 1.5. The Si coverage for $\sqrt{3} \times \sqrt{3}$ is one adatom per unit cell, and this gives $1/3$ monolayer of Si coverage.

The study for $\sqrt{3} \times \sqrt{3}$ on Si-face from Starke et al. also discussed the structure of the substrate [53]. By using "Pendry R Factor" to calculate the intensity of single reconstruction spot from LEED image, they found out that the calculation for 4H-SiC, which there is a "Switch Stacking" every 2 bilayers of SiC, preferably have S3 stacking, "Switch Stacking" every three bilayers like 3C-SiC or 6H-SiC instead of two on the surface when obtaining $\sqrt{3} \times \sqrt{3}$ phase. To this end, it is suggested that the bilayer structure, at least for the top three bilayer of the substrate, will rearrange when sufficient Si and C atoms are provided with proper annealing temperature. This also that the Si thin film on Si-face or C-face of SiC will have the same structure when obtaining the same LEED phase from different polytype of SiC.

The Holographic LEED provides a great way to explore Si structures, and the 3×3 structure is the initial surface condition after Si flux treatment for sample preparation. In other words, it can be considered as the extreme case for Si-rich surface on Si-face. $\sqrt{3} \times \sqrt{3}$ is the case that almost no Si adatoms on the surface and the Si-C bonding from the substrate does not break so that no Si atoms was released from substrate yet. So the Metastable Phases in between can be seen as a progression from 3×3 to $\sqrt{3} \times \sqrt{3}$ equilibrium phases.

This means that we can use the amount of Si adatoms and the tetramer structure as a

starting point to construct possible Si structure for the Metastable Phases. Unfortunately, the beam-splitter method requires the single protrusion per unit cell in order to have a reference wave and an object wave, and most of the LEED phase information in Metastable Phases do not contain this feature from STM image, so one needs to collect other information in order to determine the Si structure. However, the tetramer structure is still a reference for entering this phase.

The Holographic LEED can be done to obtain the location of the adatoms on the surface above substrate [45], and this method is also used to determine the structure for 2×2 reconstruction on C-face. Unlike 3×3 from Si-face, the HLEED image shows a combination of two possible reconstruction patterns from different domains. So other information are needed to determine the symmetry of the structure.

For different LEED phases around this region, the Auger peaks shown from Auger measurement suggests that all Si on the surface are sp^3 bonds, in other words, all Si adatoms have four covalent bonds as the substrate. Considering the bonding methods, there are three possible locations for the Si adatoms tetrahedrally bond on the surface. Figure 1.5
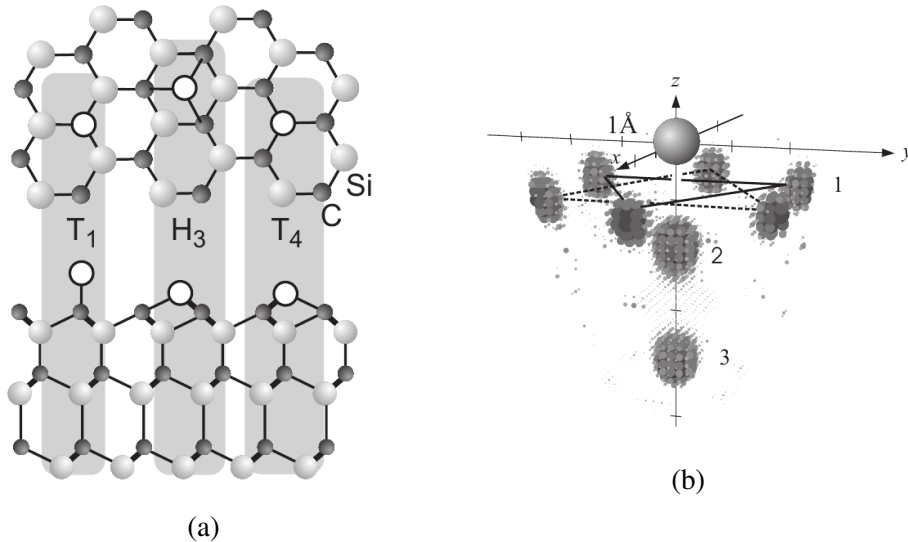
Figure 1.5: (a) Possible Si adatom site based on the Si atom from substrate. T1: Directly on top ; H3: On top of a hollow site ; T4: On top of a Si atom. (b) The Holographic LEED image showing the combination of two sets of tetrahedral bonding on the top layer [45].

shows the possible Si adatom sites on SiC bilayer substrate. T1 is for one Si adatom right on top of the Si atom from substrate for C-face, H3 indicates a three-fold hollow site, and T4 is at a hollow site right on top of a Si atoms from substrate. By comparing Holographic LEED structure along with choices of locations for adatoms on the surface, a structural element of 2×2 has been determined, which is one Si adatom at the H3 site [54, 55]. And the Si coverage, with only one adatom per 2×2 unit cell, is 1/4 ML.

The structures discussed above by using Holographic LEED method were used to determine the common phases on Si-face, which are 3×3 and $\sqrt{3} \times \sqrt{3}$. However, there is no indication that any structure from Metastable Phases shows single protrusion in local site, therefore the Holographic LEED method might not be able to be used to explore the structure found in this region.

While Metastable Phases is not easily reproduced and structures can not be determined from Holographic LEED method, there are some results in STM from other groups who have found reconstruction patterns with proposed structures [56, 57]. The LEED phases found in Metastable Phases will be discussed in the following.

One of the phases found in Metastable Phases is 6×6 [58, 59]. The experimental details revealed that this 6×6 phase is different from the one found near C-rich reconstruction which is treated as the buffer layer. This 6×6 is a Si-rich surface reconstruction. In these papers, they concluded that the 6×6 is evolved from 3×3, and it is possible that the tetramer structure has shifted (or deform and reform) to move to the location further apart to form 6×6.

Another reconstruction pattern found in this region is from Naitoh et al. in 1999. With LEED and STM information, a Si-rich surface structure was proposed [60]. In that paper, a reconstruction phase $2\sqrt{3} \times 2\sqrt{13}$ was found coexisting with 3×3. According to STM data, the $2\sqrt{3} \times 2\sqrt{13}$ was formed by two rows of "thick belts" and two rows of "thin belts." The defect and filled/empty states information indicated two features of the structure on the surface: One is the "thick belts" consists with square shape patterns which suggests four
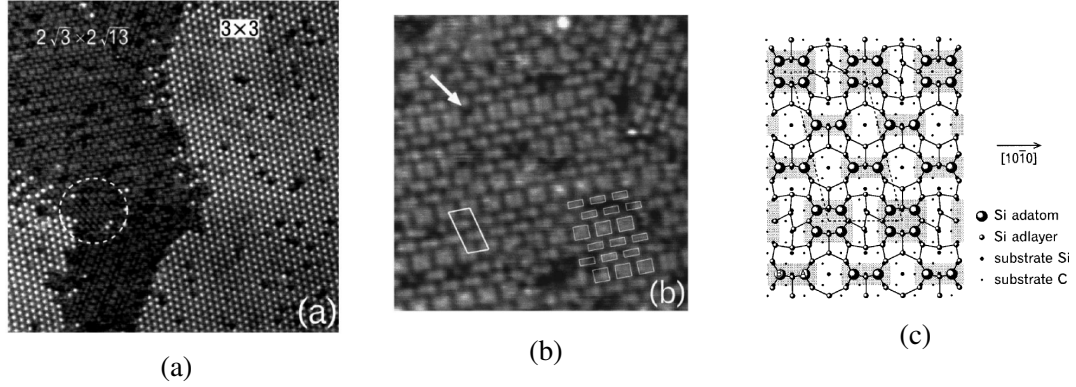
Figure 1.6: (a) STM image showing coexistence of 3×3 and $2\sqrt{3}\times2\sqrt{13}$. (b)Zoom-in area from (a) showing thick and thin belts feature. (c)Structure proposed for $2\sqrt{3}\times2\sqrt{13}$. This structure contains one Si adlayer and two/four adatoms to form thin/thick belts. STM data and structure proposed [60].

protrusions, and the "thin belts" suggesting two protrusions. While the STM image shows the thick and thin belts feature, the proposed structure has not been confirmed. In order to satisfy dangling bonds other than the belts, the bonding structure still could have a lower energy configuration.

Other than the $2\sqrt{3}\times2\sqrt{13}$ pattern, a local area shows a pattern found coexisting with 3×3. This structure only contained thin belts (The white broken circle in Fig. 1.6a), and this resulted in the reconstruction pattern $2\sqrt{3}\times\sqrt{7}$.

The coexistence of $2\sqrt{3}\times2\sqrt{13}$ and 3×3 suggests that the Si coverage is similar, and the configuration of adlayers and adatoms for 3×3 structure suggests that $2\sqrt{3}\times2\sqrt{13}$ can have a similar structure which is modified from 3×3. In other words, it is a four adatoms(thick belt) or two adatoms(thin belt) on top of one Si adlayer. The Si coverage, with six adatoms and one adlayer in a unit cell, is $(6+28)/28 = 34/28$ ML.

Another phase found in this region is $2\sqrt{3}\times2\sqrt{3}$ phase coexisting with 3×3 after $900\,^{\circ}$C heat treatment of a Si-rich 3×3 surface in UHV [61]. The proposed structure is based on DAS model [41]. In addition to one tetramer added per unit cell, some atoms were removed from the adlayer, and this gives the Si coverage $(4+12-3)/12 = 13/12$ ML of Si coverage. While this structure is not confirmed, the main idea is to have the adatoms

16

rearranged on top of a Si adlayer. This rearrangement could potentially be the key to form other reconstruction in Metastable Phases.

The Si structures discussed so far are mostly based on either the tetramer structure from Starke et al. or the DAS model from Takayanagi et al. However, more data is still needed to confirm those proposed structure.

In 2018, Martrou et al. published a paper about finding new Si structures on Si-face of SiC [57]. The experimental method is to deposit Si on Si-face first and then anneal the sample for several cycles. Each cycle will increase the Si coverage on the surface and therefore different LEED phases have been found. The starting phase is $\sqrt{3} \times \sqrt{3}$ and after several cycles, some phases were found as mentioned before and there are also new reconstruction patterns found, and they are 12×12 and 4×8.

The 4×8 phase found in that paper is the same as the $2\sqrt{3} \times \sqrt{7}$ made with all "thin belts" from Naitoh et al. [60]. However, the giant 12×12 phase has not been found, and this new pattern contains one regular and one distorted hexagonal patterns according to STM. The proposed structure is based on one adatom tetrahedrally bonded to one Si adlayer. After adatoms are placed, rearrangement of Si atoms is done in order to reduce number of dangling bonds. The STM data indicates that only one dangling bond at each corner of the regular and distorted hex, so all bonds from other atoms need to be saturated. In order to minimize the dangling bonds, a systematic method for constructing the proposed structure has been built, and this includes the bridge formation on the adlayer. In Figure 1.7,
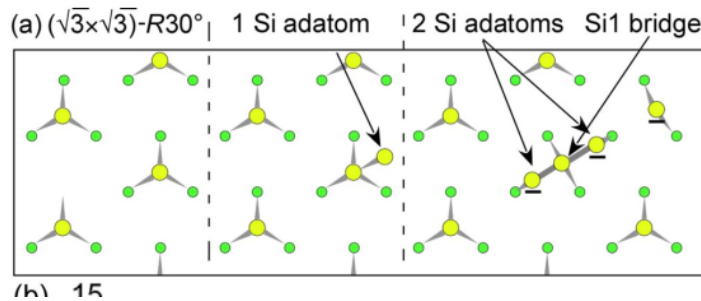
Figure 1.7: The bridge structure and cause of formation from [57].

17

the bridge formation has been demonstrated from Martrou et al. [57]. The green atoms represent Si atoms from substrate on Si-face, and the yellow ones are from Si adlayer. This figure shows the $\sqrt{3} \times \sqrt{3}$ surface, and in each Si enrichment cycle, extra adatoms are deposited on the surface. On the right side of the figure, three adatoms are bonded as a bridge, and the middle one is also bonded with the substrate (The "Si1 bridge"). Even though Fig. 1.7 is demonstrated based on $\sqrt{3} \times \sqrt{3}$ surface, this bridge formation is also possible to be formed when the whole surface is covered with one adlayer of Si. And this bridge formation is the key to systematically construct the proposed structure for this giant 12×12 [57].

Martrou et al. also apply the bridge formation to other Si structure in Metastable Phases [57]. By applying bridge formation, the Si coverage for each phase is reduced a little. The $2\sqrt{3} \times 2\sqrt{13}$ has 33/28 instead of 34/28 ML. And the giant 12×12 pattern is 1 monolayer of Si coverage.

The bridge formation from Martrou et al. [57] provides a unique way to minimize number of dangling bonds on adlayer. Even though this method still have some concern such as the bond length and the location of the bridge, it does provide a way to systematically build the structures in Metastable Phases.

The 2D Si structures discussed so far in this section are mostly the Si structures on Si-face. The discussion for Metastable Phases on C-face is not as much. However, other than the 2×2 discussed previously, there is another LEED phase found on C-face that is unique, and it is $\sqrt{43} \times \sqrt{43}$ on C-face from Li et al. [62].

A $\sqrt{43} \times \sqrt{43}$ LEED reconstruction was firstly found in 2012 by Srivastava et al. [63]. From Srivastava's experiment, the graphene growth on C-face under Si-rich environment shows not only graphene ring from LEED measurement, but also a reconstruction patter $\sqrt{43} \times \sqrt{43}$. This phase was considered as a buffer layer on C-face. More experiment and calculation are done in recent years and suggests that even though the annealing condition indicates a C-rich condition, one Si adlayer is preferable for this phase [62]. The proposed

structure is a few Si adatoms on top of one Si adlayer. This gives the Si coverage to be 56/43 monolayer with 13 dangling bonds per unit cell. Figure 1.8 shows the proposed model.
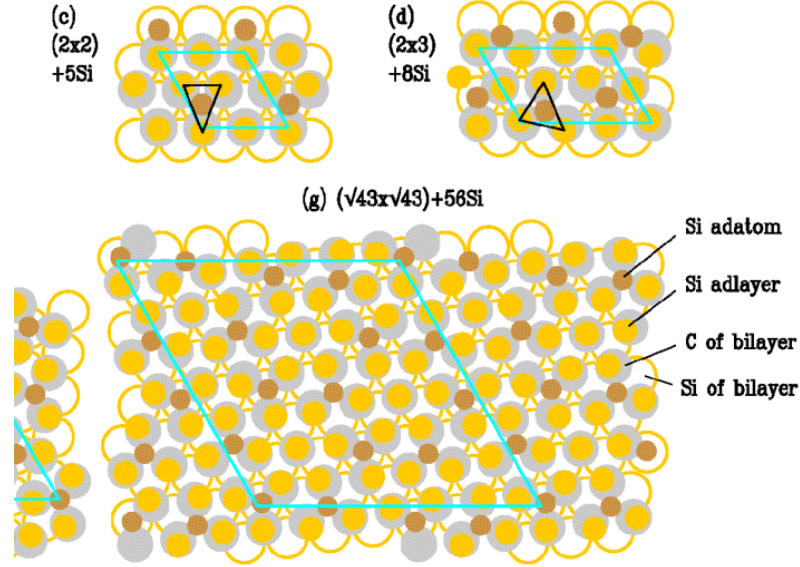
Figure 1.8: Proposed structure from Li et al. [62]. The top two figures shows the "biaxial" and "twisting" distortion, and the lower figure shows their reconstruction model for $\sqrt{43} \times \sqrt{43}$ with the applied distortion.

Other than the 2D Si thin film found above, another Si thin film structure also attracts a lot of interest, and that is the silicene, the Si version of 2D honeycomb structure. As mentioned in previous section, one of the main reason to have high electron mobility in graphene is its honeycomb structure and symmetrical lattice. This property makes graphene a potential material to have better performance in electronic device. While research interest on graphene increases significantly, the possibility of having similar properties in other two dimensional material has been considered, and silicene is a desirable choice. Like graphene, silicene also consists of honeycomb structure and symmetrical lattice, which means that it also contains high electron mobility [64]. However, the first principle calculation suggests that this 2D structure is formed in a low buckled structure instead of planar as shown in Figure 1.9, which means that one sub-lattice is shifting along perpendicular direction from the silicene plane. Because of this buckling feature, it is possible to open a tunable band gap
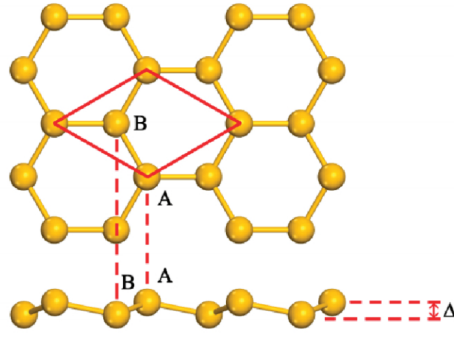
Figure 1.9: Silicene structure [64], the buckling height is around 0.46 Å

by applying external electric field. The stronger spin-orbit coupling also provides interesting transport properties such as Quantum Spin Hall Effect[64].

Experimentally, there is some evidence to indicate that silicene can be grown on Ag(111) and Ag(110) surface [65, 66]. However, questions were brought up about the validation [67–69]. Recent research has shown some new evidence claiming that silicene grows epitaxially on the Ag(111) surface [69] [70]. With similar growing condition from before, experimental data from Vogt et al. shows that one can obtain silicene by heating a silver substrate to 220 °C to 260 °C while Si atoms are deposited (vaporized by direct current heating method), and the surface will form a 4×4 reconstruction pattern [69]. Another pattern, $\sqrt{13} \times \sqrt{13}$, and its possible structure model is also presented in later research [70].

Silicene can be grown on different substrates such as diboride thin films [71] and iridium [72], but free standing silicene or epitaxially grown on insulating substrate still have not been successfully produced [73].

CHAPTER 2

EXPERIMENTAL METHOD

In order to study 2D materials, several conditions need to be considered to obtain well ordered structure, and surface science techniques are essential to examine interesting properties. For epitaxially growth process, the surface of the substrate need to be chemically clean and flat in order to obtain larger uniform area of Si thin film. The Si film grown on the substrate can also easily be contaminated or oxidized. It is common to have surface science experiment under UHV environment.

In this thesis, the sample growth and measurement for all samples are conducted in this matter. The experimental methods involve different systems: home-built growth systems with LEED Auger electron spectroscopy (AES), and STM. These systems are operated under UHV environment. Other than that, other tools such as Atomic Force Microscope (AFM), Raman, are also used for preparing and examining samples.

In this chapter, the UHV environment will be introduced, and details for sample preparation are provided. After that the tools for characteristic measurement under UHV are introduced.

2.1 UHV system

Vacuum system has been widely used for experimental research purpose. For surface science, clean sample surface without interaction between sample surface and unwanted particles is crucial to determine surface structure and condition. Also, analysis techniques used to acquire information from surface condition by incidental electron beam or electromagnetic wave requires clean traveling path without colliding any particle. The formula for mean free path (MFP) which indicates the average distance traveled by a moving particle

between successive collisions, is used:

$$l = \frac{k_B T}{\sqrt{2}\pi d^2 n} \tag{2.1}$$

In this equation, k_B is the Boltzmann constant, T is the temperature, d is the diameter of gas molecules, and n is number of particles per volume. MFP is one of the major method to estimate the proper pressure for conducting experiment for this purpose. Several UHV systems are used in this thesis, and they are all equipped with several pumping stages in order to effectively maintain UHV pressure.

The UHV systems are equipped with a roughing pump operating from atmosphere pressure down to 1.0×10^{-3} Torr, and a turbomolecular pump operating from 1.0×10^{-3} Torr to 1.0×10^{-6} Torr range. Then an ion pump will maintain the pressure down to 1.0×10^{-9} Torr. In addition, a titanium sublimation pump (TSP) is also used to help maintain UHV pressure. To speed up the process from atmosphere to UHV, a thorough bake-out is performed. The system is heated to more than $100°$ C to excite absorbed gas particles on the wall such as water. This bake-out process takes approximately 24 hours, and all filaments in the system should be heated to while the system cools down.

2.2 Sample Preparation

SiC wafers purchased from commercial companies were polished to certain degree. Two sample wafers were purchased from Cree Research Inc. They are semi-insulator 4H-SiC and conductive 6H-SiC wafers. All wafers are on-axis facets with SiC(0001) on one face and SiC(000$\bar{1}$) on the other. In this thesis, information including naming system and growth conditions for all samples discussed is described in appendix A. Figure 2.1 shows an image of a wafer used and the direction of the diced samples. For experimental purpose, the wafers are subsequently diced into 3.5 x 4.5 mm^2 in Cleanroom at Georgia Tech. The short and long edges of the diced sample is along [1$\bar{2}$10] and [1$\bar{1}$00] direction. The notch on the

(a)

(b)
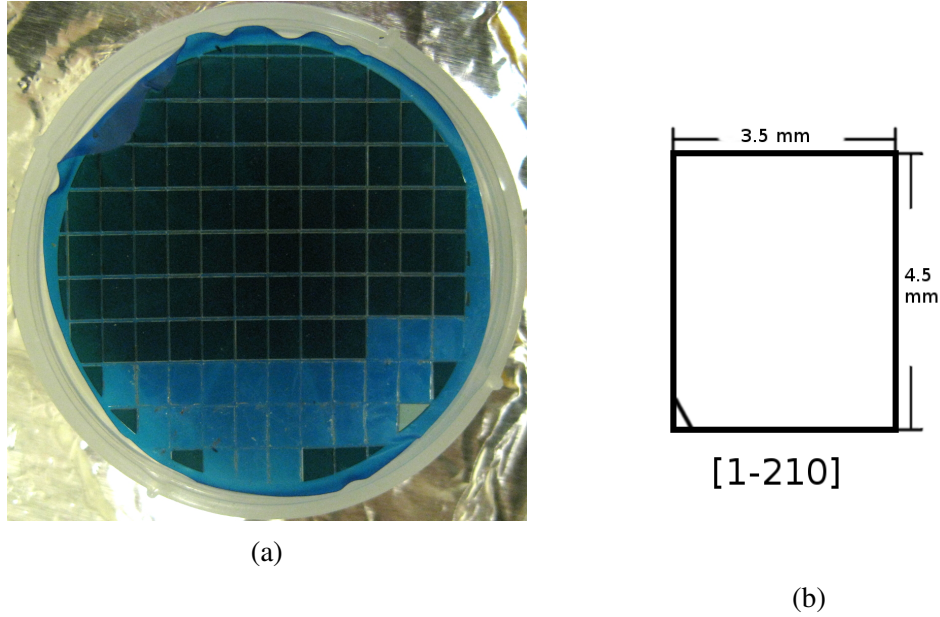
Figure 2.1: (a)A picture of a wafer with C-face up diced into 3.5 x 4.5 mm^2 samples. (b) Drawing of diced 6H-SiC sample. Short edge is along [1$\bar{2}$10] direction, the notch at the left down corner indicates Si-face.

left down corner marks the face. For research purpose, further cleaning to atomically flat is needed to remove scratches and damage. Figure 2.2 shows AFM images for a sample surface condition before and after hydrogen etching on C-face. The purchased wafer has different polishing process for Si-face and C-face. The C-face is mechanical polished, and the Si-face is chemical mechanical polished (CMP). The mechanical polished surface shows clear scratches, and CMP surface is relatively flat with a small mis-cut angle approximately 0.25° and no step edges. Samples are heated to at least 1400° C under flow hydrogen [74]. Surface of the wafer is etched, and after the sample cools down, hydrogen atoms saturate the dangling bonds to prevent contamination.

Other than hydrogen etching, another method for cleaning surface is used as well. By having excessive Si coverage on the surface while annealing, high temperature annealing will break the Si-C bond and these two atoms will rearrange and form well-ordered bilayer. The high Si density is achieved by having two SiC samples facing each other when annealing. This method is referred as Face-to-face method. The Face-to-face method for cleaning

(a) (b)
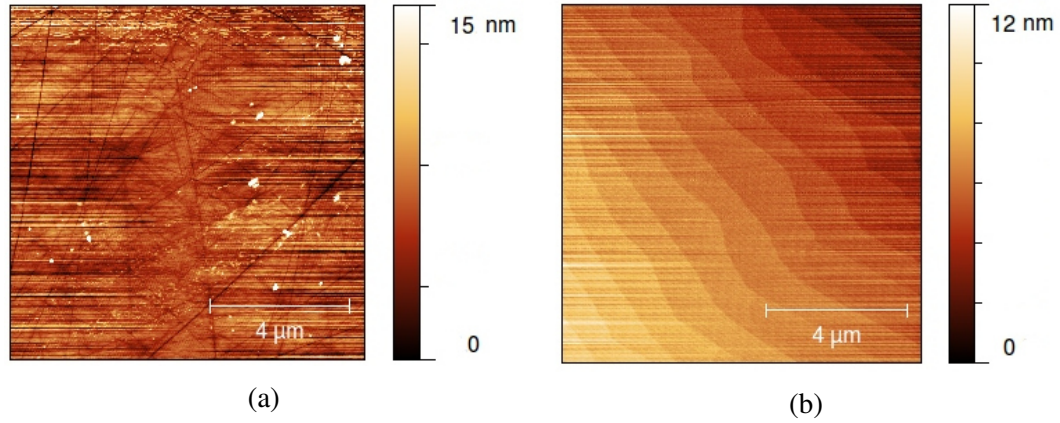
Figure 2.2: (a) AFM on a raw C-face with only mechanical polished process.(b) Same surface with uniform steps after hydrogen etching. Unit cell step heights shown on the sample.

sample surface was prepared by Hu et al. from Prof. Walt de Heer's group. Figure 2.3

(a)

(b)
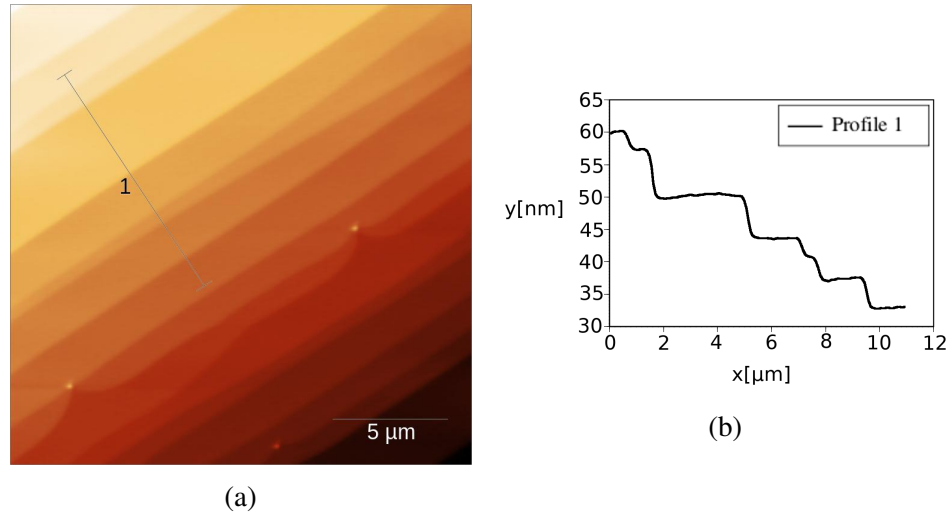
Figure 2.3: (a) AFM image for a sample surface after Face-to-face cleaning method. (b)Profile of the surface showing uniform unit cell step height.

shows a Si-face condition after Face-to-face annealing. Two samples stacking together with Si-face facing each other are annealed to around $1500° C$. By doing this, the Si density remain high between two Si faces to maintain equilibrium. The surface shows half or full unit cell step height and 2 μm terrace width.

2.3 Growth System
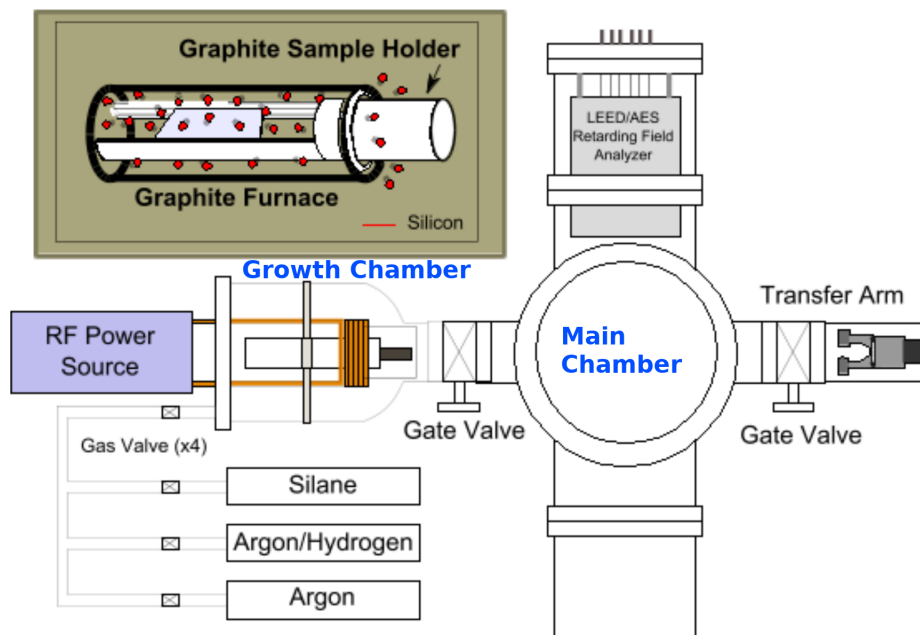
Figure 2.4: Configuration of home-built graphene growth system (GGS). The system consists of a Main Chamber for sample characterization, a Growth Chamber for sample annealing, and two load-lock chambers as shown in Figure 2.5b. A dark colored box on the top left corner shows a graphite furnace for induction heating in Growth Chamber, and a graphite sample holder to hold up to three diced SiC samples.

The graphene growth system (GGS) was originally designed by Dr. David Lee Miller and modified by Dr. D. Britt Torrance, Dr. Tien Manh Hoang, and myself. Figure 2.4 shows the configuration of the GGS. This system consists of a Main Chamber for sample characterization, a Growth Chamber for sample annealing, and two load-lock chambers as shown in Figure 2.5b. A dark colored box on the top left corner shows a graphite furnace for induction heating in Growth Chamber, and a graphite sample holder to hold up to three diced silicon carbide (SiC) samples. A picture of the real graphite sample holder is shown in Fig. 2.6b. Figure 2.5 shows pictures of the home-built UHV system. Fig. 2.5a shows the Main Chamber and Growth Chamber, and Fig. 2.5b shows the load-lock chamber(i) and (ii). The two load-lock chambers are designed to be used for reducing loading time in UHV system. Samples with a sample holder are loaded on an Al adapter attached to

25
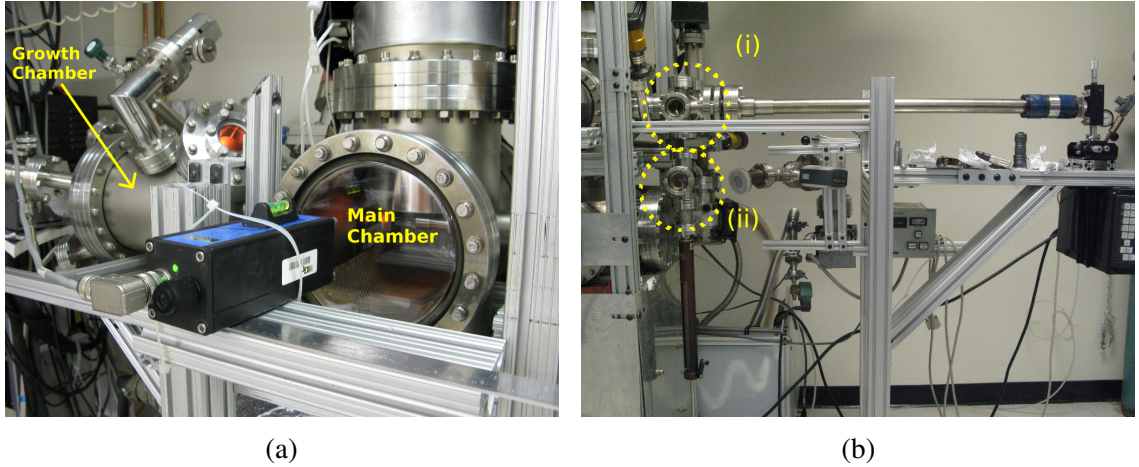
Figure 2.5: (a) A picture of the Growth Chamber and Main Chamber. (b) Two separate load-lock chambers indicated in yellow circles. The main chamber and two chambers were separated by two valves for pumping purpose.

a Linear Motion Feedthrough from MDC product, LLC in the first load-lock chamber as shown in a yellow circle (ii). A separate pumping system including a roughing pump and a turbomolecular pump will operate only on the this load-lock chamber. Once this chamber is pumped down to around 1.0×10^{-6} Torr, the sample can be moved to the upper load-lock chamber(i). After the sample holder is sent to the load-lock chamber(ii), the Magnetically-coupled Linear-Rotary Feedthrough from Thermionics Northwest, Inc. as the transfer arm will grab the holder and transfer it to Main Chamber or Growth Chamber for further experiment.

The load-lock chamber(ii) and the Linear Motion Feedthrough below it is also used as a vacuum suitcase for transferring samples to other UHV system for further experiment, so different machined adapters can be attached to the end of the feedthrough. Figure 2.6 shows one of the Al adapters designed with another sample holder for transferring samples to CreaTec STM system. The blue Al cylinder block in Fig. 2.6a is attached to the feedthrough, the light gray plate is the sample holder for CreaTec STM system. The black fork shaped holder is the graphite sample holder. A molybdenum plate and two tungsten wires were used in order to trap the sample when transferring from our graphite sample holder to the space between two wires and the molybdenum holder. This transferring mechanism is designed

<table>
<tr><td>(a)</td><td>(b)</td></tr>
</table>
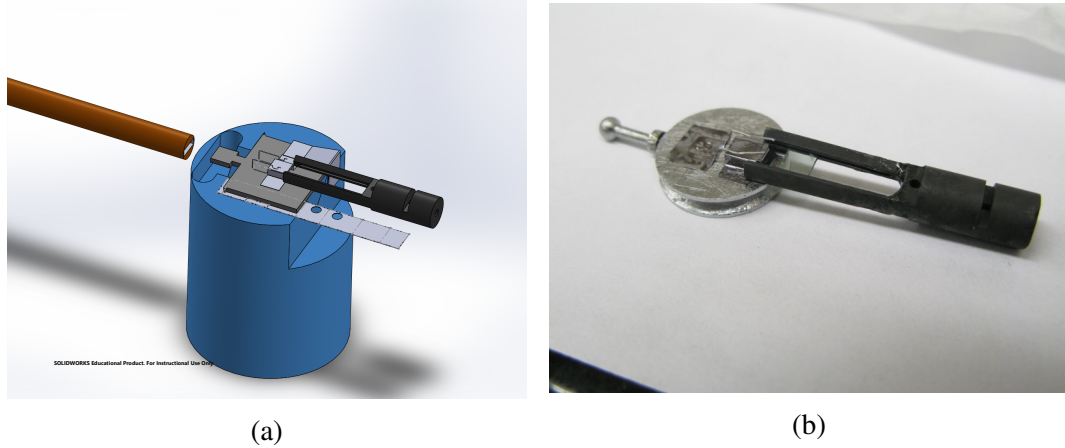
Figure 2.6: (a) Assembly of the adapter drawn from SOLIDWORKS for transferring sample to CreaTec STM system. (b) A sample holder with adapter for STM and graphite sample holder.

originally by Dr. Tien Manh Hoang and modified by me for the CreaTec STM.

The graphite sample holder is designed to hold sliced SiC samples along the 3.5 mm edge. Figure 2.6b shows a picture with a graphite holder and another assembly for transferring a sample to our home-built room temperature STM system. Up to three samples can be slid into the space between the fork, and outermost sample can be transferred.

After the sample holder is grabbed from the transfer arm in Fig. 2.4, it can be sent to the Main Chamber to determine the sample characterization. The Main Chamber consists of a Reverse View LEED/Auger device(RVL2000) from LK Technologies on the top. A TSP and an ion pump are at the bottom of the Main Chamber to keep pressure at UHV level. The holder can also be sent to the Growth Chamber for annealing. Figure 2.7 shows the furnace configuration inside the Growth Chamber. It consists of a RF heating coil with a graphite furnace. The graphite sample holder was designed to have samples annealed in a relatively closed furnace in order to keep local Si density high, and with silane in the annealing environment, a hole is drilled through the solid portion of the holder for better ventilation. By having a leak valve connected to the annealing chamber and a gate valve connected to a turbo pump, filled or flow gas environment can be introduced under different pressure by opening the gate valve slightly while monitoring the pressure. For growth experiment, Ar

(a)   (b)
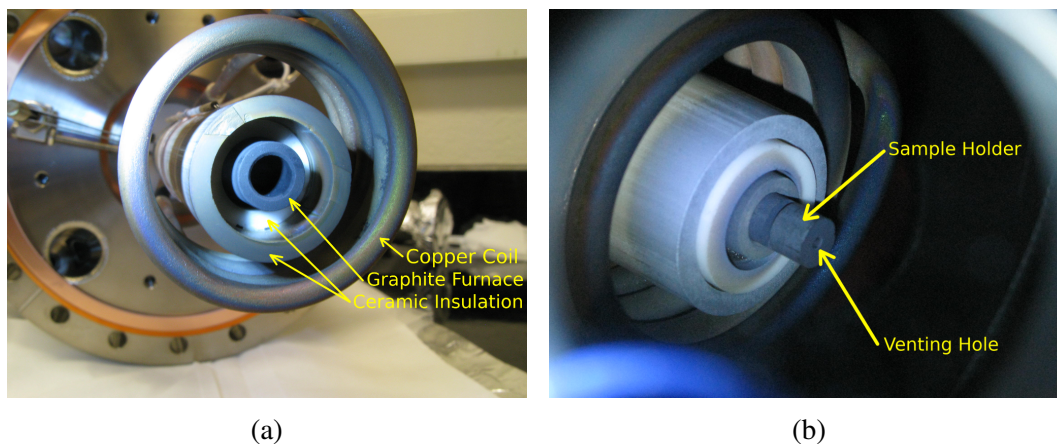
Figure 2.7: (a) Front view of the graphite furnace (b) Side-view of the graphite furnace through the glass window with graphite sample holder.

and mixture of Ar and silane are used to control Si background pressure.

2.3.1   Vacuum Suitcase

The GGS allows us to study sample characterization. However, while LEED and AES can give us useful information, further experimental data is still needed. To this end, vacuum suitcases are used for transferring a sample under vacuum to avoid contamination or oxidation when necessary. Figure 2.8 shows one of our designed vacuum suitcases.

(a)

(b)
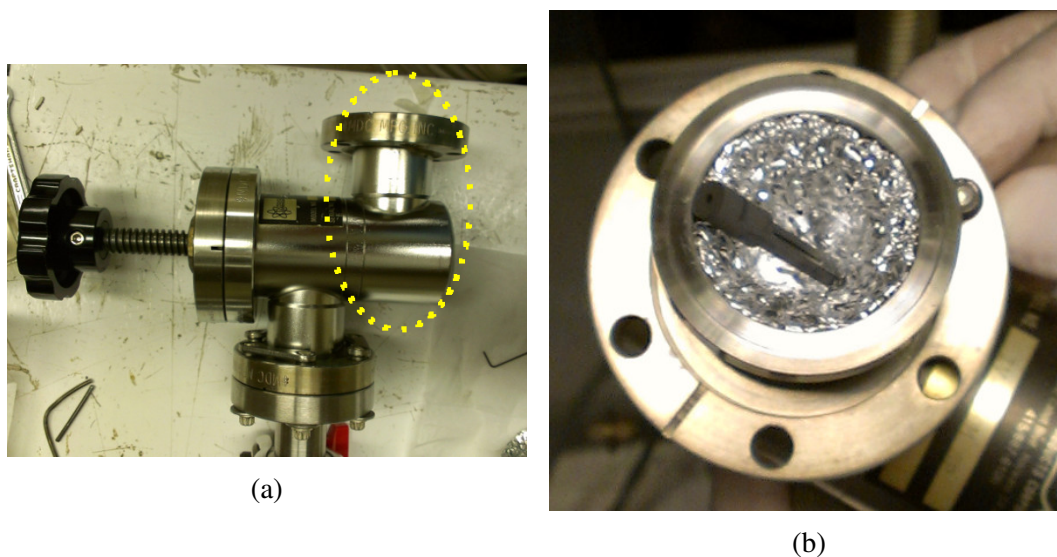
Figure 2.8: (a) An adapting valve as a vacuum suitcase for transferring sample. (b) sample holder with adapter for STM and graphite sample holder.

An Al support was inserted in the circled part in (a), and this adapting valve is replacing the load-lock chamber(ii) when used for transferring a sample. After the sample holder is dropped into this suitcase, the adapting valve and the valve on top of it will be dismounted and then moved to a glove box in pure nitrogen environment for further processing to avoid contamination.

While the small adapting valve could possibly move a sample without contamination, it is still better to transfer a sample without exposing to atmosphere, especially for experiment which required UHV environment as well. To this end, another vacuum suitcase was used. For transferring purpose, the suitcase needs to have a feedthrough in order to move the sample. So the load-lock chamber(ii) and the feedthrough below it in Fig. 2.5b are used. An adapter design is also used as shown in Fig. 2.6b.

The pressure in the suitcase needs to maintain UHV condition while transferring, so a portable pump device is needed for this purpose. A few options was tested, and having a copper rod feedthrough mounted was adopted. The copper rod is in contact with liquid nitrogen while transferring a sample. Low temperature of the copper rod will attract particles to avoid sample contamination. Inside the suitcase a copper braid was tied on the rod to increase surface area. With this setup the large surface area from copper braid will be able to trap particles and keep pressure low in the suitcase.

2.4 Measurement

The growth process starts with a raw SiC sample sent into the GGS. After surface cleaning and proper preparation, this sample will be annealed at proper temperature in order to study surface character. The LEED/AES device RVL2000 installed in the Main Chamber is used for this purpose. After that, additional measurements are done by transferring samples under UHV. In this section, we will discuss details about such measurement.

2.4.1 Low-Energy Electron Diffraction

LEED measurements are a major source of information for our surface study. This versatile technique is used to detect ordered superstructures on an atomically-clean surface in UHV. Figure 2.9a shows a picture of the LEED instrument used in this work, and its operational
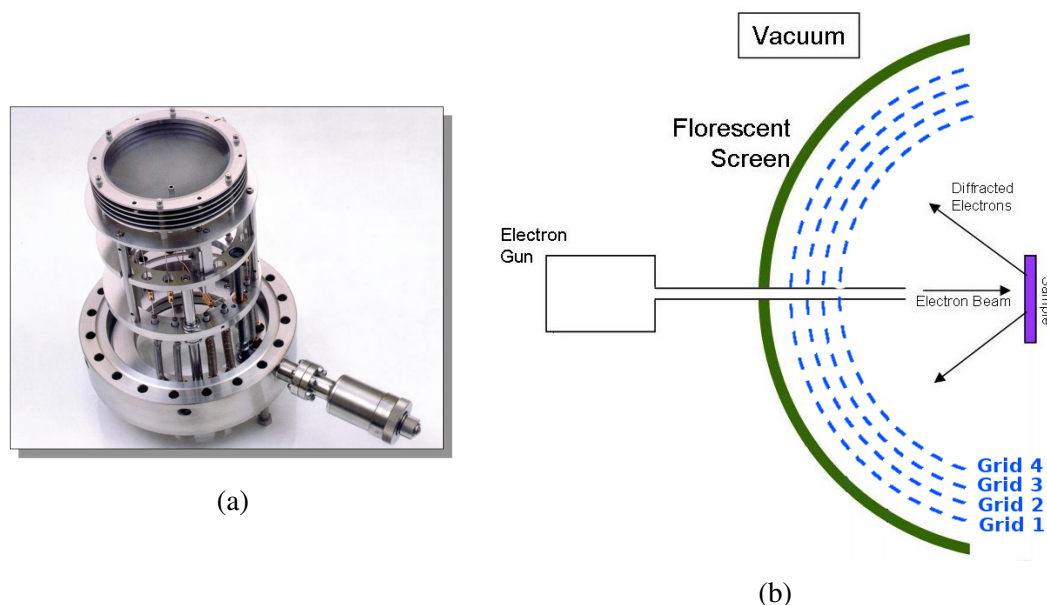
Figure 2.9: (a) Reverse View LEED/Auger device(RVL2000) from LK Technologies [75]. (b) A diagram showing the principle for LEED [76]. Note that functional LEED systems typically use 4 grids; "Grid 2" in the (b) is replaced by two grids at equal potential, and a fourth grid, at ground potential, is placed between the retarding-field grids and the fluorescent screen (this arrangement allows the instrument to be operated as a retarding-field analyzer for Auger electron spectroscopy). The screen is biased to a high positive voltage (1 kV to 4 kV) to increase the fluorescence brightness.

details are shown schematically in Fig. 2.9b. The LEED unit mounts to the UHV system. Electron diffraction was understood after 1924, when Louis de Broglie postulated that the wavelength of a particle is given by

$$\lambda = \frac{h}{p} \tag{2.2}$$

where h and p are Planck's constant and the momentum of the particle, respectively [77]. The wave nature of electrons was confirmed experimentally by Clinton Davisson and Lester Germer, who, in 1927, conducted an experiment firing low energy electrons at a crystalline

nickel target to obtain diffraction patterns. In a modern LEED experiment, an electron gun shoots electrons to the sample, as shown in Fig. 2.9b. The range of electron energies is 20 eV to 200 eV, which corresponds to wavelengths of 0.8 Å to 2.7 Å; i.e., comparable to the interatomic spacing in crystalline solids. Those electrons which reflect elastically from the sample (no energy loss) can undergo constructive and destructive interference. On the other hand, inelastic collisions within the sample may cause an electron to lose energy (change wavelength) which destroys the coherence necessary for wave diffraction/interference. Wire mesh grids, shown as dotted lines in the Fig. 2.9b are biased to filter out electrons which have suffered inelastic collisions. The interior grid (smallest radius) remains at sample potential (ground), while the inner grid is biased to a negative potential of magnitude slightly less than the electron-gun accelerating voltage. Elastically-scattered electrons will pass the high-voltage grid and will hit the fluorescent screen. The angles for which electron waves interfere constructively show as bright spots (assuming a single-crystal sample). Crucial information about the surface structure of a crystalline material can be determined by this method.

A key aspect of the LEED technique is that electrons can penetrate only several Å before suffering inelastic collisions, so LEED probes only the top few atomic layers of a crystal. Within these layers, LEED often reveals a rearrangement of atoms from their positions within the bulk crystal, i.e., a surface reconstruction. Diffraction spots (angles of constructive interference) can be described in "reciprocal space," using $k = (2\pi/\lambda)\hat{n}$ where $\hat{n}$ is the direction of wave propagation. The diffraction angles correspond to constructive interference between portions of the wavefront reflected from different positions on the crystal. The change in electron k which gives constructive interference is known as the Laue condition:

$$k - k_0 = G = ha^* + kb^* \tag{2.3}$$

where k and k_0 are scattered and incident wave vectors, and G is a vector of the reciprocal lattice. G is defined as integer multiples (h, k) of the primitive translations a^* and b^* that

define the unit cell of the surface reciprocal lattice. The Laue condition can be visualized

(a)

(b)

(c)
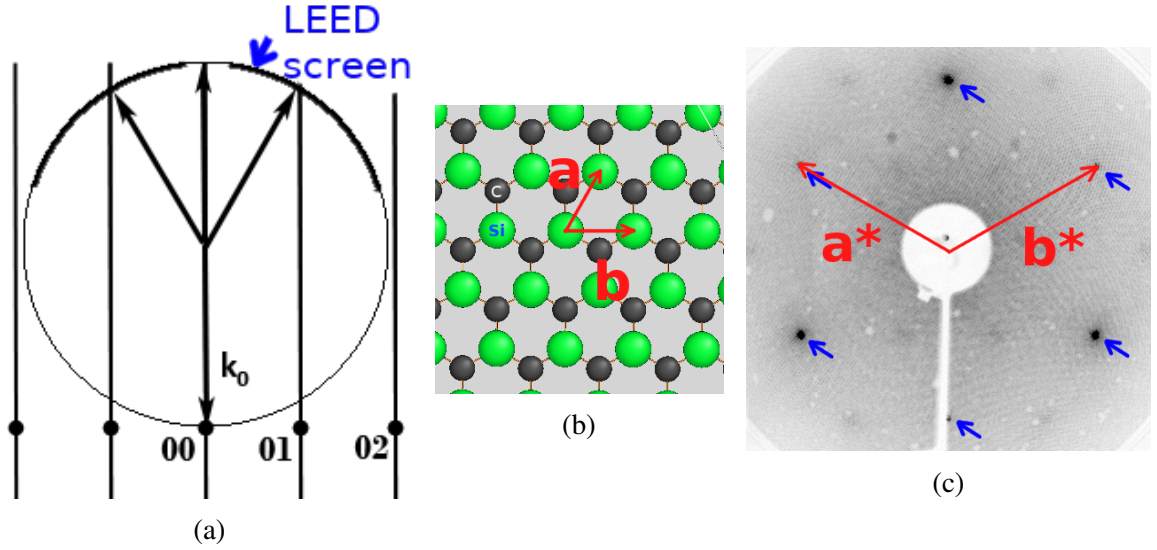
Figure 2.10: (a) Ewald's sphere showing the incident wave vector $\boldsymbol{k}_0$ and 3 scattered wave vectors corresponding to $(hk) = (0\bar{1}), (00), (01)$ [76] (the notational convention is to use $\bar{1}$ for -1). (b) Plotted model of one bilayer of SiC with real-space lattice vectors $\boldsymbol{a}, \boldsymbol{b}$. (c) LEED pattern for 1×1, with primitive reciprocal-lattice translation vectors $\boldsymbol{a}^*, \boldsymbol{b}^*$.

by Ewald's sphere construction to find the angles (bright spots) which satisfy both elastic scattering ($|\boldsymbol{k}| = |\boldsymbol{k}_0|$) and the Laue condition (Eq. 2.3) for indices h, k as shown in Fig. 2.10a. Fig. 2.10b is a model of one bilayer of Si-face SiC, and Fig. 2.10c is a LEED pattern acquired from Si-face SiC, imaged from the rear of the glass fluorescent screen. The central white circle and contiguous white region is blocked by the electron gun and its support.

One of the important information from LEED pattern is the superstructures on top of the substrate. Regular SiC substrate on Si-face and C-face are periodic hexagonal structure, and this structure forms a hexagonal pattern on the LEED screen. If extra structure forms on top of the original structure to form another periodic pattern associated with the original structure, the reciprocal lattice will form extra spots, and this can give us extra information about the surface structure. Figure 2.11 shows a plotted version of relaxed 3×3 superstructure from Schardt et al. [31] and its LEED image. In Fig. 2.11a, all atoms are Si atoms. The "Si" represents the substrate, "Si2" are from the adlayer, "Si4 and Si5"
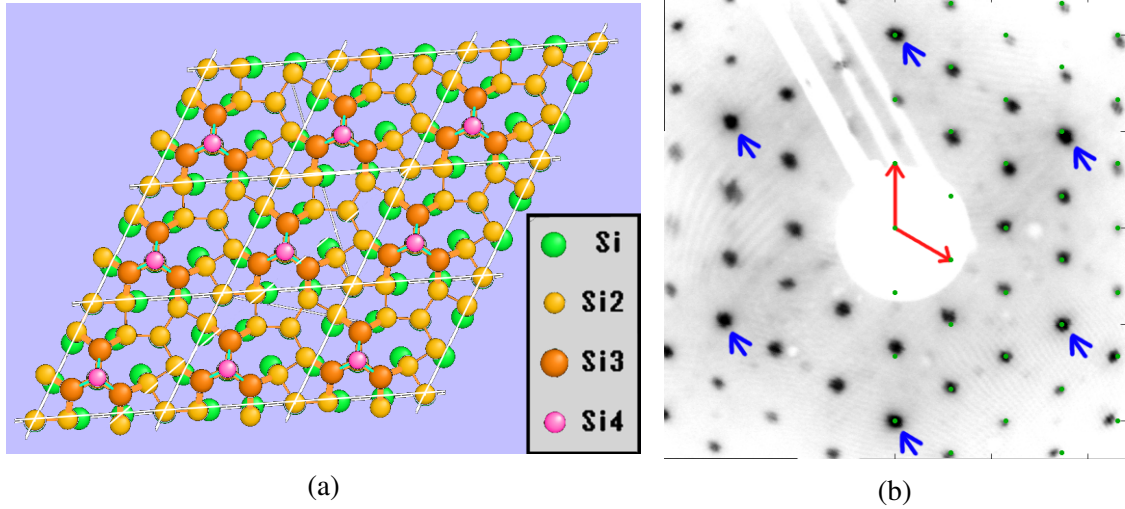
Figure 2.11: (a) Plotted version of 3×3 reconstruction structure on Si-face. (b) LEED image of 3×3. Blue arrows indicate the SiC 1×1 spots, and the green spots in (b) indicate the 3×3 grid. The red arrows in both (a) and (b) are the lattice and primitive translation vectors.

represent the tetramer structure. The red arrows shows the lattice vectors in (a) and their primitive translation vectors in (b). The blue arrows indicate 1×1 SiC spots. The green spots indicate the 3×3 spots on Fig. 2.11b.

The superstructures on top of SiC surface can be seen as superstructures of hexagonal patterns, and a table of possible combination of superstructures as periodic mesh on top of a hexagonal structure is recorded in a handbook up to 7×7 unit mesh [78]. Patterns in this handbook is used as the first step to identify any unknown LEED pattern found experimentally. A matrix notation can be found for a reconstruction in real space, and this matrix is then transformed into the corresponded matrix in reciprocal space. Figure 2.12 shows some cells as part of the reconstruction table. Each cell contains one reconstruction pattern. Cell No.63, for example, shows a $2\sqrt{3} \times 7$ pattern. The notation "R30°" indicates that the pattern is 30 ° counterclockwise from SiC direction, and the matrices for real space and LEED pattern are also included. The 3×3 grid in Fig. 2.11 is also generated by this method.

For any unknown pattern acquired, the handbook is firstly used for recognized pattern.

Figure 2.12: Part of the table in the handbook [78]. Each cell shows information about a hexagonal pattern in real space, LEED phase, and the transformation matrix.

Any unknown pattern which can not be identified from the handbook will be identified by generating reconstruction patterns with lattice constant larger than 7×7 first, and they are also manually compared in an image processing software such as GNU Image Manipulation Program (GIMP).

The $2\sqrt{3} \times 2\sqrt{13}$ pattern found from Naitoh et al. in Fig. 1.6 [60] is one of the example for successfully being identified by this method. This pattern is not found in the handbook since $2\sqrt{13}$ is larger than 7 so that this pattern is not listed in the handbook.

Other than unknown patterns which could not be identified from the handbook, it is also time consuming process even if a pattern can be found from the handbook. The number of patterns generated for comparison in a 7×7 superstructure table is 168, and the patterns generated exceeding 7×7 lead to an effective way to compare patterns by overlapping patterns one by one. To this end, it is more effective to filter out unnecessary ones at first to speed up the comparison.

Another way to identify a pattern is to measure the lattice constant directly from the

34

LEED screen. However, the camera mounting mechanism and the focus function from the camera did not allow us to properly take photos directly. A slightly tilted angle from the camera or different zoom-in range could distort the image easily. Other than that, the LEED screen which is a curved surface also distort the image depending on how far the camera was mounted.

To attempt solving this problem, several correction methods for image distortion was used, but there is no effective way found to embed in the code when processing images. To this end, another approach has been used to reduce processing time for identifying patterns. This approach is done by comparing the real LEED image and the generated patterns. The distortion and the intensity of the image will reduce the effectiveness for image comparison, so both images from real and generate patterns need to be processed first in order to reduce the comparing process time. Fig. 2.11b shows one of the example for distortion at the edge of the image. The reconstruction spots at the right top corner are shifted from 3×3 grid. Figure 2.13 shows the procedure for identifying LEED patterns. The left half of Fig. 2.13a

(a) (b) (c)
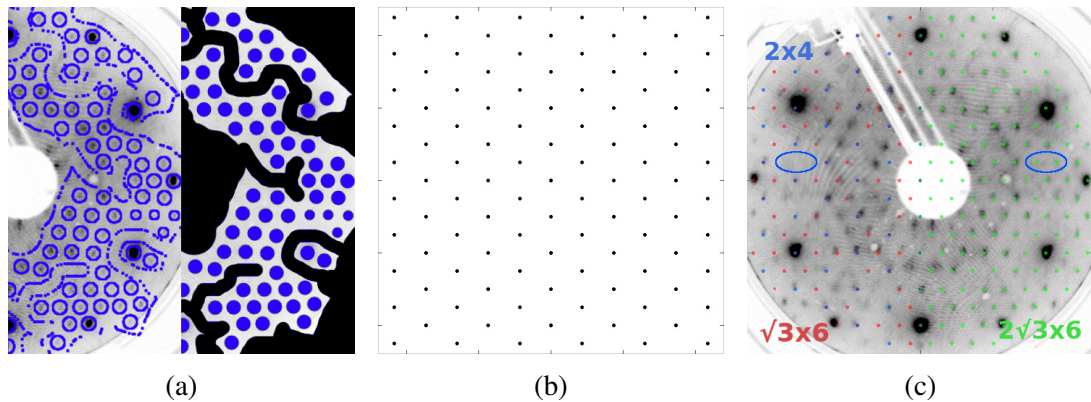
Figure 2.13: (a) A comparison of an original LEED and a processed image. The blue outline on the left shows the region of visible reconstruction spots. The right half shows the processed image with three different colors: Black area is not used for comparison, the white area indicates where there is no spots at all, and blue area shows location of possible reconstruction spots. (b) One of the generated patterns used to be compared with the processed image in order to estimate the matching percentage. (c) The top three results obtained after image comparison with all possible patterns generated.

is an unknown LEED image displayed in an inverted gray scale (white to black is zero to

maximum intensity). The blue circles and dotted lines indicate the locations where visible reconstruction spots are located. If there is no distortion, one can simply adjust the contrast to extreme black/white and compare them with generated image in Fig. 2.13b and compare the matching rate; however, because of the distortion, the area of each spots are expanded manually as shown in right half of Fig. 2.13a. To this end, three colors are used in this processed image for image comparison purpose. The black area is being masked out, the white area indicates the location where there is no spots at all, and the gray area indicates where the spots are supposed to be.

By comparing the processed image in Fig. 2.13a with each generated pattern such as Fig. 2.13b. A pixel-by-pixel comparison will give a matching rate, and the patterns with highest matching rate are selected for the next comparison. After some patterns are chosen from the matching rate ranking, these patterns are loaded into GIMP to be compared manually. Further selection rules can be made for this process as well; however, after the first step, there are no more than 10 patterns left to be determined, and manually choose the proper patterns is possible from this step.

Figure 2.13c shows three possible reconstruction patterns chosen after manually comparing them to the LEED image. The blue spots show 2×4 grid, the red spots show $\sqrt{3} \times 6$ grid, and the green spots show $2\sqrt{3} \times 6$ grid. If one pattern can fit all reconstruction spots such as $\sqrt{43} \times \sqrt{43}$ on C-face from Feenstra et al. [79], then it's likely to be the reconstruction pattern. However, if no single pattern can fit all reconstruction spots, either the lattice constant is larger than 7×7 such as $2\sqrt{3} \times 2\sqrt{13}$ from Naitoh et al. [60] or multiple reconstruction from different area on the surface contribute to this LEED image. For this unknown pattern, the simplest reconstruction pattern is the combination of 2×4 and $\sqrt{3} \times 6$. This two patterns are able to cover almost all spots on the surface. The blue circles in Fig. 2.13c show two very blur spots, and this combination did not cover them. On the other hand, $2\sqrt{3} \times 6$ pattern seems to cover all. So to this end, it is likely that this LEED image should be identified as $2\sqrt{3} \times 6$.

This pattern was found in the Metastable Phases on Si-face on SiC, however, other LEED images found similar to this phase all have missing spots when being compared to $2\sqrt{3} \times 6$, so it is less likely to be only one single pattern for this phase. Instead, it should be a combination of multiple reconstruction patterns from different area on the surface. Further analysis is needed to confirm. However, the paper for $2\sqrt{3} \times 2\sqrt{13}$ from Naitoh et al. [60] indicates two features on the surface referred as "Thin Belts" and "Thick Belts." The combination of these two features can explain the combination of 2×4 and $\sqrt{3} \times 6$, so this LEED analysis can be explained by the "Belts" feature. More details are discussed in Chapter 1.2 and 4.

2.4.2 Auger Electron Spectroscopy

AES is another common analytical technique used to study surface. It is operated based on Auger Effect and was first discovered by Lise Meitner in 1922. Pierre Victor Auger independently discovered the effect shortly after and is credited with this discovery [80].

The Auger Effect is an effect starting with a vacancy in an inner shell of an atom. An electron from another shell transit into the vacancy and the energy released let an electron from outer shell to overcome the binding energy and escape [81]. Figure 2.14 shows the transition process when an Auger electron is released. A vacancy is created by a collision between an electron in inner shell and an incident electron or a phonon. Then an electron from higher level jumps in to fill the vacancy and one electron from outer shell is released. One of the common ways for the energy level associated with the electrons transited to be labeled by using X-ray notation. So this particular transition is referred as a $KL_1L_{2,3}$ transition. By bombarding a sample with energetic electrons and measure intensity of Auger electrons as a function of energy, the result can be used to determine emitting atoms. The energy of the electron from Auger Effect can be calculated from energy conservation. There are different pathways to fill the core hole, and different pathways will have different signature detected from the collector.
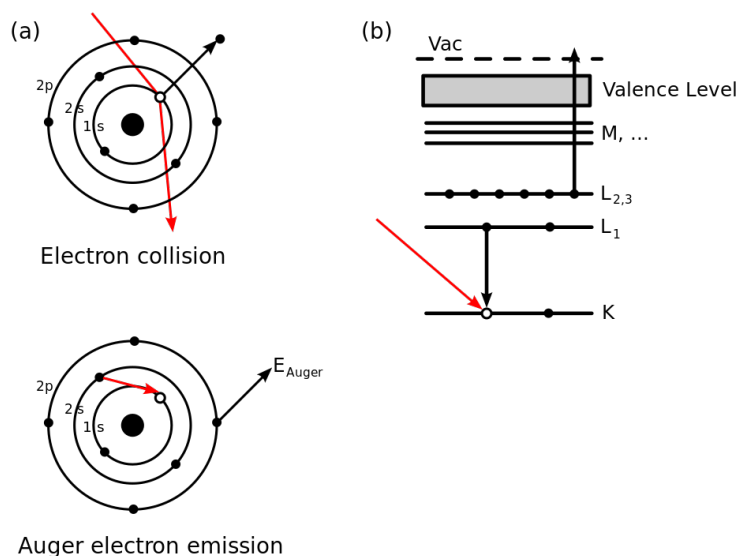
Figure 2.14: Schematic diagram when an Auger electron is released [80]. (a) An electron in the inner shell is removed by a collision with a phonon or an electron. When another electron from higher level jumps in and fill the vacancy, an electron from outer shell was released. (b) One of the common way to generate an Auger electron. The transition in this case is noted as $KL_1L_{2,3}$ transition.

There are two classes for AES instruments. One is retarding field analyzer (RFA), and the other one is cylindrical mirror analyzer (CMA). For CMA, the collector will only accept electrons within an energy window, and RFA will collect all electrons above a potential from a cut-off grid. In this thesis, we mainly use RFA which is integrated with LEED as a single device.

Figure 2.9b shows a diagram for LEED instrument setup. For the device we use, LEED/AES device(RVL2000) from LK Technologies, this setup is used for AES with two additional grids as well. The primary beam of electrons strike the sample at normal incidence, and the reflected electrons pass through the grids and are collected by the screen. "Grid 1" and the sample are grounded so that there is no electric field in the space between them. This allows the electrons to radially travel towards the screen. "Grid 2" and "Grid 3" are retarding grids, and electrons with less energy will be stopped from these grids. "Grid 4" is also grounded to reduce capacitive coupling. The collector is the Florescent Screen

which is positive biased for collecting electrons. After the electrons are reflected to the screen, "Grid 2" and "Grid 3" will block electrons from passing with energy lower the the voltage applied. The current is recorded as a function of retarding field voltage.

$$I(V) \propto \int_{E}^{E_{max}} N(E')dE' \ (E = eV) \tag{2.4}$$

where $N(E')$ is the number of electrons reflected from the surface at energy E. To obtain energy distribution, the differentiate of this curve with respect to V, dI/dV, is obtained. To acquire Auger intensity which is small comparing to noise, an experimental method is used. The Taylor series of a current as a function of voltage can be written as

$$I(V + \Delta V) = I(V) + I'(V)\Delta V + \frac{I''(V)}{2}(\Delta V)^2 + \frac{I'''(V)}{3!}(\Delta V)^3.... \tag{2.5}$$

With small AC modulation $\Delta V = k \sin \omega t$ we can write

$$I(V + \Delta V) = I_0(V) + [I'(V)k + \frac{I''(V)}{8}k^3 + ...] \sin \omega t + ... \tag{2.6}$$

With small amplitude k, higher order terms can be neglected, and this makes the second term proportional to $I'(V)$. By applying a small AC modulation voltage on the retarding grids, the intensity of the Auger electrons can be measured by measuring the amplitude by lock-in amplifier. Figure 2.15 shows one of our AES data for the Si-face of a bare SiC annealed at $1000°$ C under vacuum. The valley located at 92 eV is a Si(LVV) peak, and the valley at 272 eV is a a C(KLL) peak. The ratio for peak-to-peak value of these two transitions is the major indication for Si coverage on the surface. For our experiment, SiC substrate with Si thin film on top is studied, and the AES spectrum can give us the amount of Si and C ratio on the surface, and this is one of the way to acquire information about number of Si adlayer or adatoms on the surface.
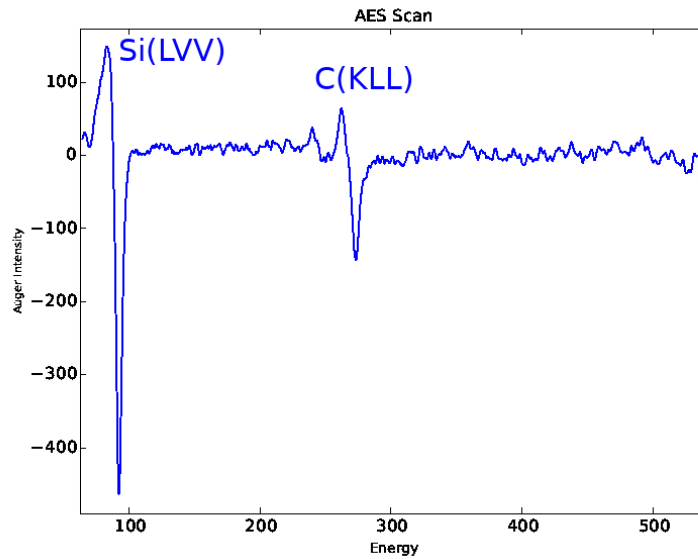
Figure 2.15: AES data for the Si-face of bare SiC

2.4.3   STM

While LEED and AES allow us to obtain structural and chemical information from sample surface, a visualized atomic detail is still needed to obtain a real structure. To this end, STM instrument is used for imaging surfaces information at the atomic level. The development was firstly done in 1981 by Gerd Binnig and Heinrich Rohrer, and they shared half of the Nobel Prize in Physics in 1986 [82].

STM is to use a tip close to surface to scan a sample surface, and a bias voltage difference between tip and sample cause tunneling current, and the resulting current for each position forms an image [83]. Thus, the tunneling current allowed Binnig and Rohrer to "see" atoms on the surface of the famous Si(111) 7×7 reconstruction [84].

Without any contact between a tip and a sample, there should be no current in a classical view. However, when the gap between the tip and sample is in atomic scale, electrons and jump from through vacuum and produce the current by a phenomenon "Quantum Tunnelling".

Schrödinger's fundamental equation of quantum mechanics defines the total energy of

a system:

$$\hat{H}\Psi = E\Psi \tag{2.7}$$

where $\hat{H}$ is the Hamilton operator, E is the total energy of the system, and Ψ is the wave function.

Based on the Figure 2.16 shows a simple one-dimensional model for a particle traveling
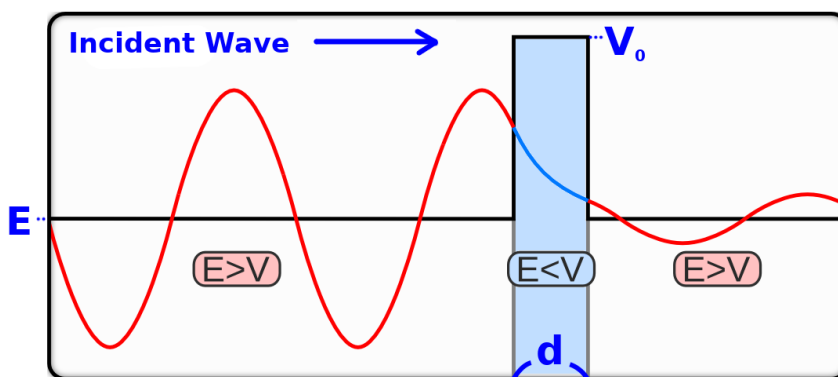
Figure 2.16: A wave tunneling through a barrier with potential higher than total energy [85].

with total energy E. The blue area in the middle indicates the vacuum gap between the tip and sample. A tunneling probability, T, when an electron is traveling from left to right through the barrier can be written as:

$$T = \frac{4E(V_0 - E)}{V_0{}^2} e^{-\frac{2d}{\hbar}\sqrt{2m(V_0 - E)}} \tag{2.8}$$

In principle, the tunneling current can be measured without any bias voltage applied, but in order to maintain difference between Fermi energies, a bias voltage is applied.

In the case for this figure, electrons will tunnel from sample to the tip. The tunneling current is proportional to the following quantitative:

$$I \propto V_{bias} \cdot \rho_s \cdot e^{-\frac{2d}{\hbar}\sqrt{2m\phi}} \tag{2.9}$$

41
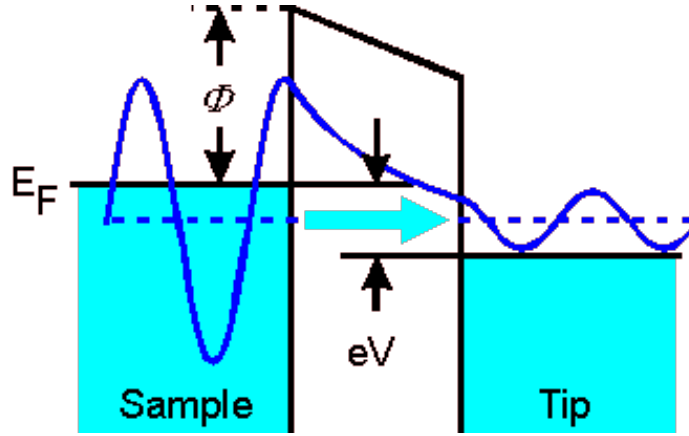
Figure 2.17: A wave tunneling when a bias voltage is applied to the sample[86].

where ρ_s is the local density of states (LDOS) at the sample surface and ϕ is the work function. LDOS is defined as number of electrons per unit volume per unit energy at a certain point in space at a specific energy [87]. LDOS also provides information about the electronic structure of the surface. The exponential dependence provides high z-sensitivity of the tip, and the tip position in each location is recorded. Figure 2.18 shows a schematic
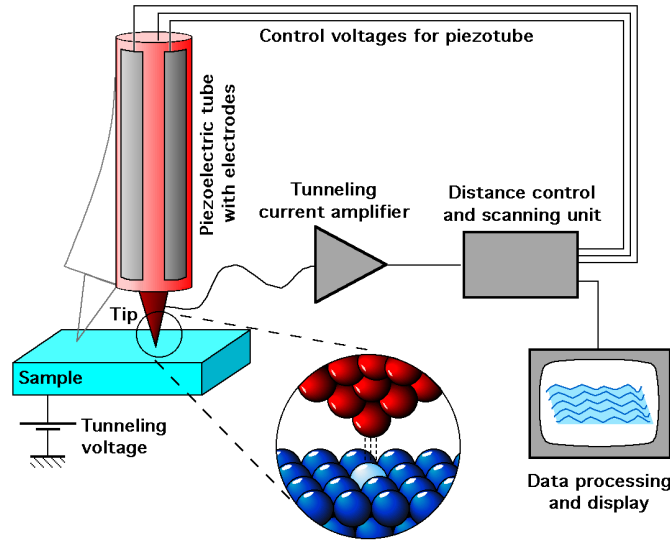
Figure 2.18: A schematic for STM instrument with tip, piezoelectric and the feedback for controlling height of the tip [83].

drawing for operation [83]. A bias voltage is applied to the sample. The tunneling current is measured, amplified, and sent to the feedback loop for distance control. The tip movement

42

is controlled by applying specific voltage at a piezoelectric scanning tube where the tip is mounted.

When recording the data, certain modes can be chosen in order to limit the variables. The most common two modes are constant current mode (CCM) and constant-height mode (CHM).

For CCM, the sample is scanned at a constant tunneling current, and the vertical position of the tip is recorded. It gives a constant charge density surface. However, this mode is limited by the reaction time of the feedback loop.

For the CHM, on the other hand, the tip height is fixed while scanning and tunneling current is recorded. This mode gives a constant charge density surface And because of the constant height, feedback loop is not needed and therefore the scanning time is reduced. However, a relatively flat surface is required [88].

The geometry of the tip can also affect the result. Tersoff and Hamann published the first model based on time-dependent perturbation theory [89, 90]. However, this model was not able to explain atomic resolution of various substrate.

In 1984, Baratoff proposed a model concerning STM resolution of Si(111) 7×7 reconstruction [91]. This model was based on localized d_{z^2} orbital located at the apex of the applied tungsten tip. The importance of the d_{z^2} orbital was then shown by first principle calculation [92]. Figure 2.19 shows our home-built room temperature STM system. The green dotted circle indicate a four-way cross where the vacuum suitcase in Fig. 2.5 is mounted from the bottom.
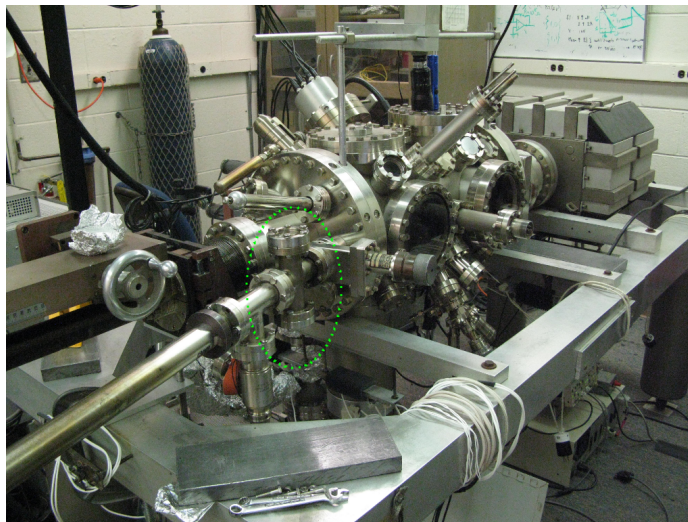
Figure 2.19: The home-built room temperature STM in the lab. Green dotted circle shows a four-way cross where the vacuum suitcase is mounted.

CHAPTER 3

RECONSTRUCTION ON SILICON CARBIDE

In Chapter 2, we have discussed the experimental method for controlling Si background pressure when growing Si or C thin film on Si-face and C-face of SiC. In this chapter, we will discuss experimental details about LEED phases obtained on both faces. Some phases are confirmed from previous work, and some phases are firstly found.

The GGS allows us to study both Si-rich and C-rich phases on both Si-face and C-face. A series of Si deposition studies on both faces have been done previously by other research groups. In this chapter, we will present our experimental data to confirm the LEED phases found so far, and we will also show some newly-discovered phases found in Metastable Phases.

Samples discussed in this Thesis were prepared in two steps. Before insertion into the UHV system, sample surfaces have been cleaned by hydrogen etching in order to have clean and flat surfaces. After that, samples were out-gassed in UHV environment. After LEED measurement on the sample indicating a clean 1×1 surface, which means well-ordered Si or C terminated surface, Si adatoms were deposited to start the experiment.

Obtaining reproducible LEED phases in Metastable Phases by controlling temperature and pressure condition is challenging. Therefore, sample ID will be used when discussing growth condition, and details for annealing process will be in Appendix A.

3.1 Samples Growth and Their Phases

The starting LEED phase is the 3×3 reconstruction as shown in Figure 1.2b or Figure 2.11b. Starting from 3×3 phase, samples are annealed again around $1000°$ C under vacuum, and after annealing, the LEED phase of the samples become $\sqrt{3} \times \sqrt{3}$ reconstruction. These two phases are obtained in order to compare our experimental data to previous work as a

confirmation.

Experiments from Tromp et al. [19] and Heinz et al. [28] show well-ordered structures of Si 2D growth on Si-face or C-face of SiC. These two studies also show an alternative way to control the quality of sample surfaces and therefore grow one layer of graphene. To this end, with our experiment setup, we looked for alternative ways to control Si background pressure on both Si-rich and C-rich side of the growth on both faces.

First, we annealed one high conductive 6H-SiC and one low conductive 4H-SiC (see Appendix A) at the same time to compare the difference on both faces. Both samples were annealed at 1350° C under backfilled pure silane pressure 1.0×10^{-4} Torr for 20 minutes. The temperature and background pressure in the phase diagram (Fig. 1.3 and extended for this work in Fig. 3.6) indicates that this growing condition is near a phase transition from $\sqrt{3} \times \sqrt{3}$ to $6\sqrt{3} \times 6\sqrt{3}$ for Si-face. As shown in Figure 3.1, the Si-face on both samples have

(a)   (b)
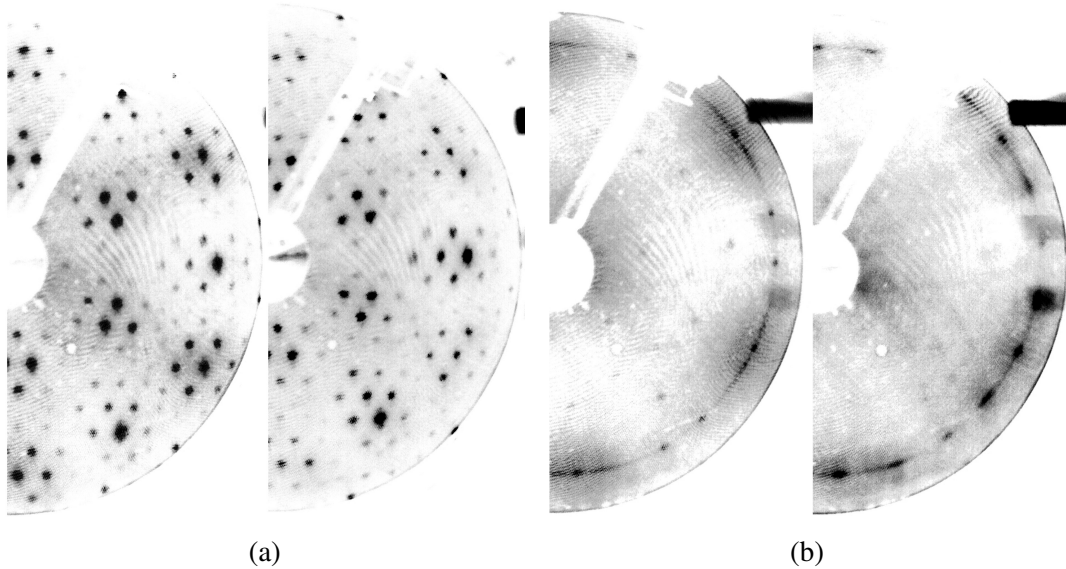
Figure 3.1: One high conductive 6H-SiC sample(left) and one low conductive 4H-SiC sample(right) annealed at 1350° C with pure silane pressure 1.0×10^{-4} Torr. LEED comparison for (a) Si-face, and (b) C-face. Both Si and C face of the high conductive sample has sharper reconstruction spots comparing to the low conductive sample. Sample ID: HF18, LF42

$6\sqrt{3} \times 6\sqrt{3}$ reconstruction pattern in LEED image, and C-face of both samples have graphene rings. This approximately agrees with the phase diagram (Fig. 1.3). By comparing both

samples, the intensity of the reconstruction patterns are slightly different, but other than that, the general location of the spots are the same.

On the other hand, while C-face on both samples have a ring pattern indicating graphene structure, there are additional spots showing on the 6H-SiC sample, but it is blur on 4H-SiC. This suggests that both high and low conductive samples have similar structure on Si face, but the reconstruction on C-face is relatively well-ordered on 6H-SiC sample.

With silane as background pressure, this suggests that unknown Si structure are forming on C-face of SiC within this temperature range, and to this end, more annealing condition will be used to study Si deposition on Si-face to see if longer annealing time will have the surface transferred to well-ordered surface.

Other than Si deposition on C-face, we also studied Si-rich growth condition on Si-face. The result from this experiment indicates that different structure of the substrate could have the same Si structure, but it might be different in C-face.

In order to compare the phases found from Tromp et al. [19], we also changed the annealing method from backfilling silane gas to flowing silane and argon mixture in order to provide constant Si background pressure while annealing. This is done by opening a small crack from the gate valve connected to the main chamber while monitoring the pressure.

3.1.1   C face

After growth of the high and low conductive samples previously, Si-rich surface with graphene on C-face becomes an interesting condition to study. In order to compare the data for quasi-equilibrium growth from Hannon et al. [19], flowing argon silane gas was used instead of backfilled pure silane.

Two samples were used for this annealing process. These two samples were annealed with the same process as Fig. 3.1, and the background Si pressure was changed to flowing argon silane mixture. In order to match the Si adatoms in background, the background pressure for the mixture gas is 2.0×10^{-4} Torr. The gas mixture contains 0.7% of silane

which means about 1.5×10^{-6} Torr of Si background pressure.

In order to achieve this annealing process near phase-transition line, 20 minutes annealing at 800° C and another 20 minutes annealing at 1200° C as two pre-heat processes were done before achieving 1350° C. After growth, routine LEED measurement was done
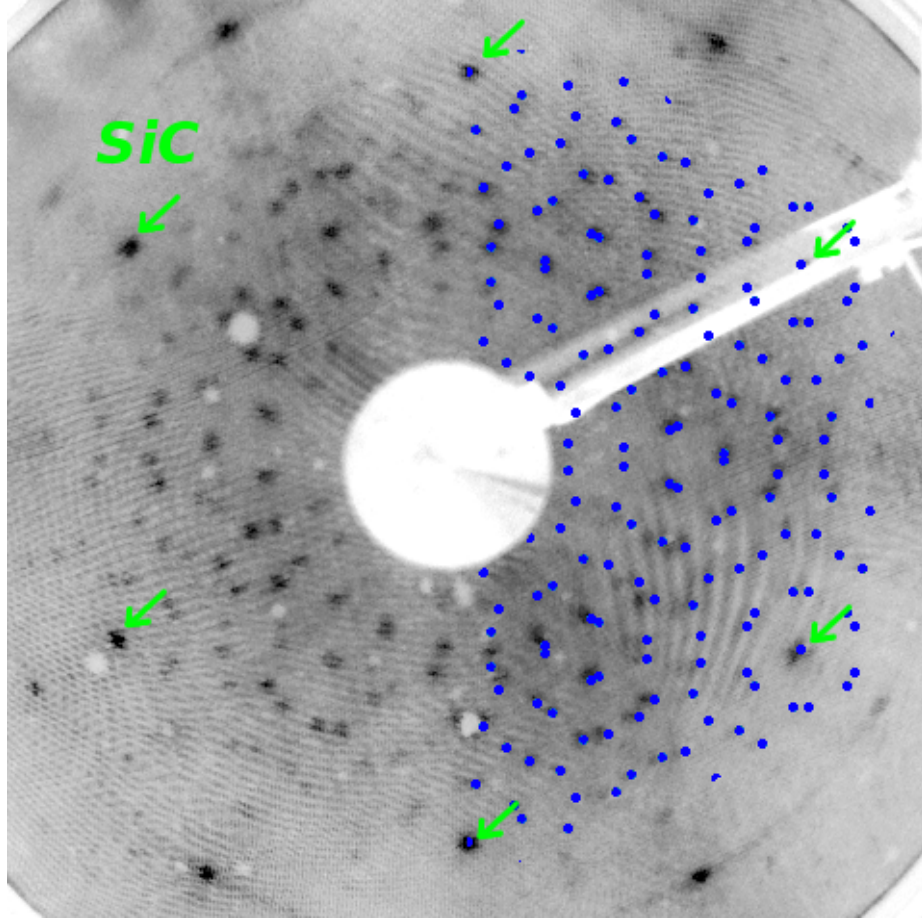
Figure 3.2: LEED image for C-face of a 4H-SiC sample annealed at 1350° C under 1.5×10^{-6} Torr Si. This image shows graphene ring and 1×1 SiC spots and a well ordered reconstruction $\sqrt{43} \times \sqrt{43}$ pattern as shown in blue dots. Sample ID: LF43

on both faces for both samples. As expected, Si-face on both samples are similar. Each Si-face contains a buffer layer pattern; however, C-face shows a ring feature, indicating rotationally-disordered graphene, with 1×1 spots from SiC substrate and other complex but well-ordered reconstruction spots, as shown in Fig. 3.2. This pattern was identified as $\sqrt{43} \times \sqrt{43}$ R±7.6°, which was previously observed by He et al. [79].

This $\sqrt{43} \times \sqrt{43}$ was found in Si-rich environment while annealing, and this suggests

that the structure is a Si thin layer instead of a C thin layer on the substrate. However, LEED image is a combination of all well-ordered structure on the surface, so to this point there is no information whether this layer is overlapping with graphene.

The LEED pattern displays the 1×1 spots from SiC substrate instead of Si 1×1 from bulk Si or 1×1 graphene, which means that this pattern is epitaxial to the substrate, and this suggests that this Si structure is on top of SiC substrate instead of on top of the rotationally-disordered graphene. In other words the Si-rich layer most likely forms an interface layer (or buffer layer) intercalated between SiC and graphene. This scenario has been confirmed recently using transmission electron microscopy [62].

The $\sqrt{43} \times \sqrt{43}$ LEED pattern indicates a well-ordered structure on the surface, and the rings still indicate a rapid growth of somewhat rotationally-disordered graphene. In order to understand how Si background pressure affects graphene growth and how Si can be deposited on hexagonal surface epitaxially, we turned our focus to Si face.

3.1.2   Si face

As mentioned in the previous section, the Metastable Phases denotes a P, T region that contains many unknown or non-reproducible patterns produced during the annealing process [28] (see also Fig. 3.6). With the ability to grow Si thin films under quasi-equilibrium conditions we chose to investigate the Metastable Phases to find potential Si-rich 2D equilibrium phases. As a guide to this work and that of others, Table 3.1 provides a partial list

Table 3.1: Si-rich surface reconstructions on SiC(0001).

Phase	3×3	$\sqrt{43} \times \sqrt{43}$	$2\sqrt{3} \times 2\sqrt{13}$	$2\sqrt{3} \times 2\sqrt{3}$	12×12	$\sqrt{3} \times \sqrt{3}$	2×2
Reference	[45]	[this work]	[57, 60]	[61]	[57]	[45]	[55]
Si density (ML)	13/9	56/43	34(33)/28	13/12	1	1/3	1/4
	(1.44)	(1.30)	(1.21)	(1.08)		(0.33)	(0.25)

of reconstructions previously characterized on Si-rich SiC, as well as a main result from this work. Note that most of these phases are obtained after heating a SiC(0001) surface with a thick layer of Si predeposited (i.e., nonequilibrium conditions).

We used three different annealing processes, some of which did allow us to successfully obtain a new stable $\sqrt{43} \times \sqrt{43}$ phase on the Si face. During these different annealing processes, each P, T stage was 30 minutes long with flowing argon and silane mixture to ensure to reach quasi-equilibrium condition. Some unknown LEED patterns also were found.

(a)   (b)   (c)
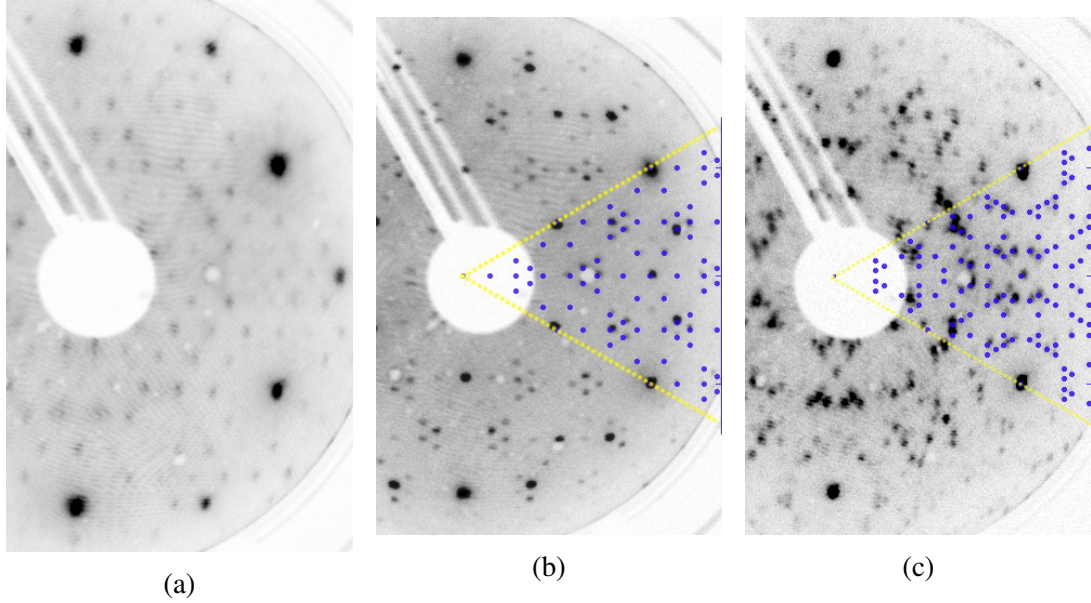
Figure 3.3: LEED images for some of the annealing conditions in Metastable Phases. (a) Unknown pattern. (b) $2\sqrt{3} \times 2\sqrt{13}$. (c) $\sqrt{19} \times \sqrt{21}$. Growth condition: $950°$C, 1.0×10^{-5} Torr flow argon and silane mixture, 30 min. Sample ID: 6H-HB019

Figure 3.3 shows some LEED phases found during this annealing process. The sample was annealed under the same Si background pressure with $50°$C increment in order to find the range of Metastable Phases. From Heinz et al. [28], the growth method were not able to achieve quasi-equilibrium status due to the fact that Si was pre-deposited on the surface before annealing under vacuum. With flowing argon and silane mixture, we are able to achieve the equilibrium phases in this region for longer annealing time. Fig. 3.3a shows an unknown pattern. Some reconstruction patterns could fit part of the reconstruction spots, but none of the currently known hexagonal reconstruction patterns could fully fit this pattern. This suggests that multiple well-ordered structures form on the surface. After finding out some unknown patterns in the Metastable Phases, different temperature and

pressure conditions were used to find other LEED patterns, and for most of the patterns found, same annealing process was repeated in order to see if the phase is reproducible.

Even though some unknown patterns were found from initial annealing procedures, for different annealing process or repeated process from here resulted in some identifiable patterns. Fig. 3.3b shows a $2\sqrt{3} \times 2\sqrt{13}$ reconstruction pattern, which was found from Naitoh et al. [60]. However, Fig. 3.3c shows another pattern identified as $\sqrt{19} \times \sqrt{21}$, which is not found in the literature. Other annealing condition were used in this pressure region either to repeat the same process and confirm that the patterns found are reproducible or to change annealing temperature to look for other patterns. Growth conditions for specific samples discussed here can be found in Appendix A.

Metastable Phases and $\sqrt{43} \times \sqrt{43}$ Reconstruction

After obtaining some phases as shown in Fig. 3.3, the flow rate of Si pressure was fixed and temperature was increased in small increments to look for other patterns. All phases found were annealed more than once in order to be sure it is reproducible.

(a)   (b)   (c)
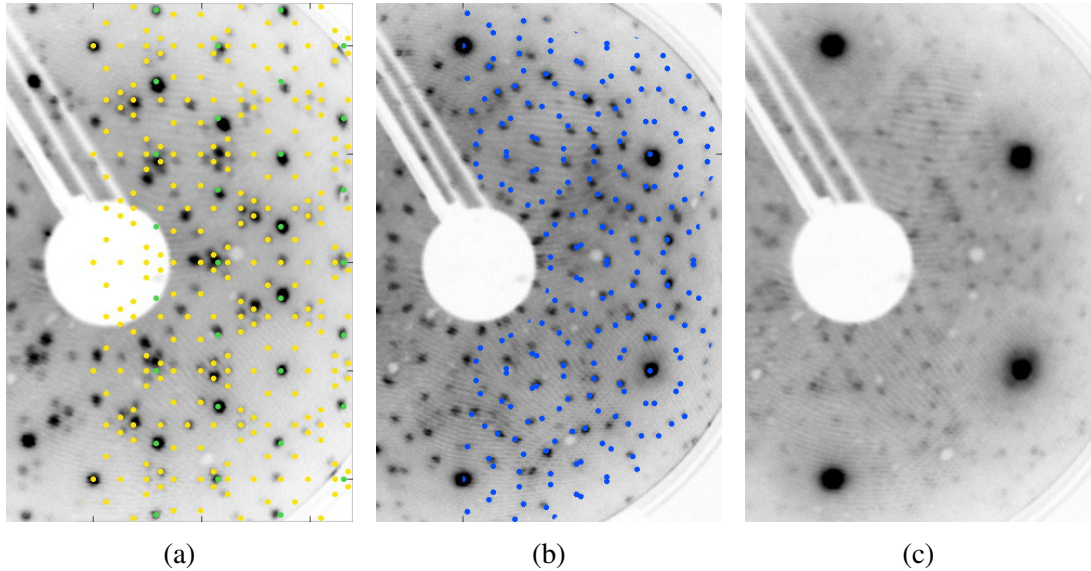
Figure 3.4: LEED images for some of the annealing conditions between 3×3 and 1×1. (a) 950° C, $2\sqrt{3} \times 2\sqrt{13}$ (yellow) and 3×3 (green). (b) 1000° C, $\sqrt{43} \times \sqrt{43}$. (c) 1050° C, unknown pattern. Pressure setting is all fixed in this process with 1.0×10^{-4} Torr Si background pressure. Sample ID: 6H-HB022

Figure 3.4 shows LEED patterns found under growth condition between $950°$ C and $1050°$ C. Fig. 3.4a shows a LEED phase with both 3×3 and $2\sqrt{3} \times 2\sqrt{13}$. This confirms the work from Naitoh et al. [60] especially with the presence of 3×3, and surprisingly $\sqrt{43} \times \sqrt{43}$ was obtained after increasing temperature by $50 °$ C as shown in Fig. 3.4b. Except for the lack of graphene diffraction, this is the same LEED pattern found on C-face (at $1350 °$ C). Each growth condition has been done twice to confirm the conditions. However, the LEED phases were apparently changing rapidly from one phase to another under these annealing conditions.
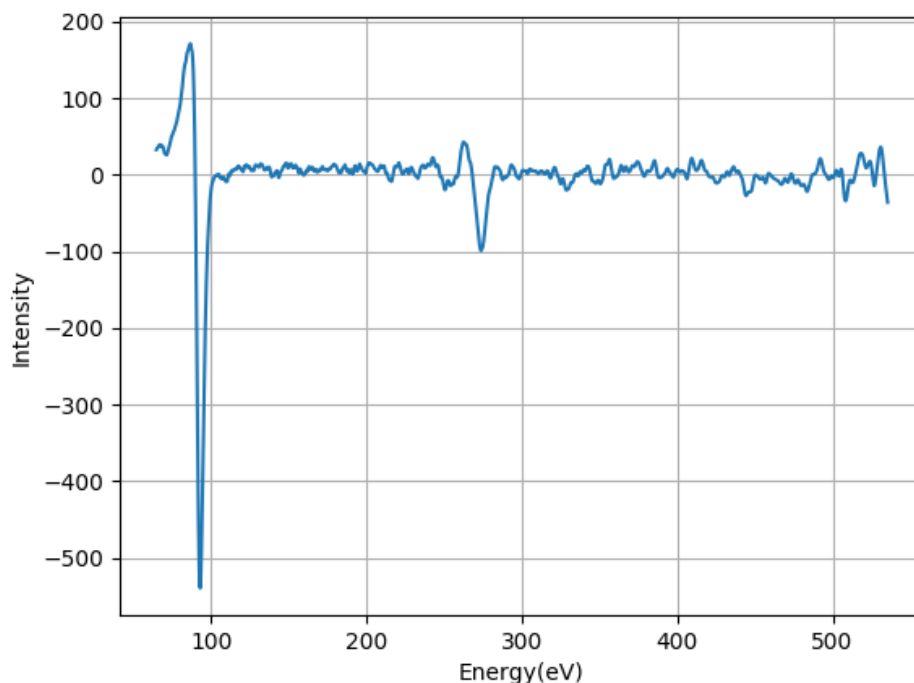
Figure 3.5: Auger spectrum for the $\sqrt{43} \times \sqrt{43}$. The Si peak at 92 eV and C peak at 272 eV were found, with no other confirmed peaks. Sample ID 6H-HB029

The Auger data for phases around this region shows Si and C element. Figure 3.5 shows the Auger spectrum for the $\sqrt{43} \times \sqrt{43}$ surface reconstruction. The larger peak where the valley is at around 92 eV indicates covalent bonding for Si atoms, and another valley at 272 eV indicates C atoms with covalent bonding. There is no other element including oxygen

visible in the Auger spectrum.

The Si structure that forms $\sqrt{43} \times \sqrt{43}$ phase found on Si-face could potentially be the key to either solve the structure found from C-face or, as discussed below, it could be an important 2D phase of silicon, e.g., silicene. It is essential to examine this structure carefully with further measurement.

Figure 3.6 shows an extended version of the Temperature - Pressure diagram from Tromp et al. [19]. The orange stars indicate the annealing condition from Naitoh et al. [60] and
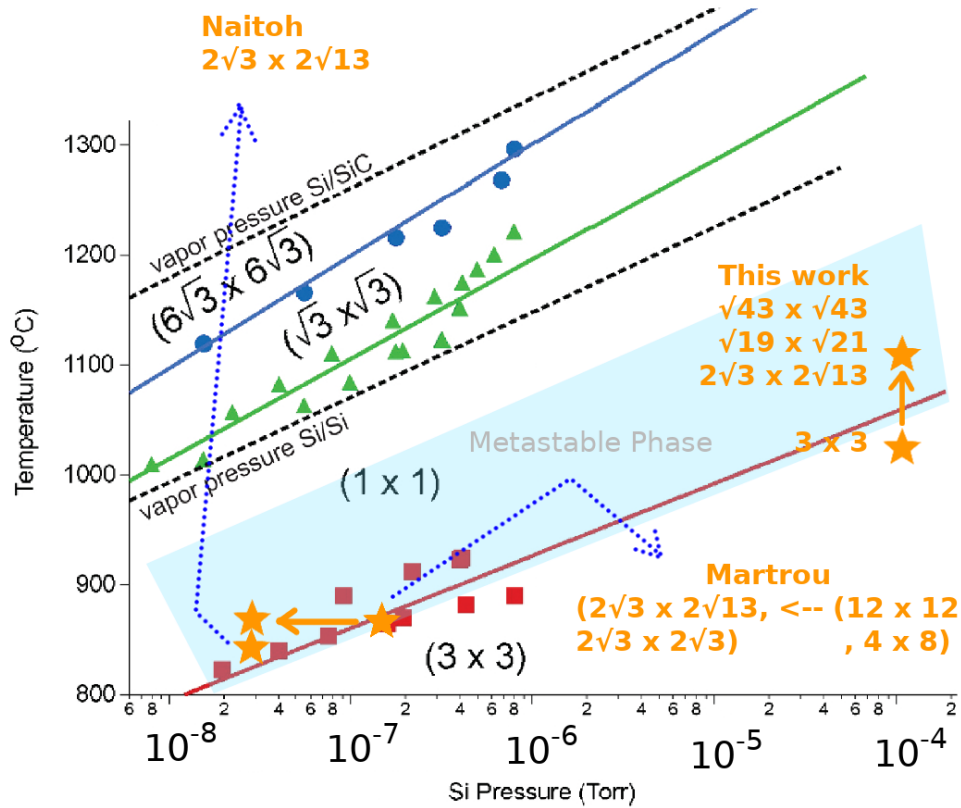
Figure 3.6: Extended Temperature v.s. Pressure diagram from Hannon et al. [19]. The light cyan region approximately indicate the Metastable Phases. The orange stars on the bottom left corner shows low Si background pressure growth with annealing temperature around 850° C. The stars on the right shows our result when annealing under approximately 1000° C with 10^{-4} Torr pressure.

from Martrou et al. [57] for the Si enrichment annealing process. The two stars on the right of the figure are the start and end points of our annealing process. All three growth process from different group show $2\sqrt{3} \times 2\sqrt{13}$ LEED pattern, and with a little higher annealing

temperature, we obtained some new phases such as $\sqrt{19} \times \sqrt{21}$ and $\sqrt{43} \times \sqrt{43}$.

Even though phases in Metastable Phases tend to evolve through different annealing paths, $\sqrt{43} \times \sqrt{43}$ is still the phase that most of the annealing path ended. In other words, this phase is slightly preferable with the annealing condition around here. This indicates that the $\sqrt{43} \times \sqrt{43}$ phase is potentially an equilibrium structure within this region. Also, this pattern is the only hexagonal structure of Si thin film found in Metastable Phases other than the most stable ones found such as 3×3 and $\sqrt{3} \times \sqrt{3}$. Because of the fact that hexagonally-ordered C atoms (graphene) can be obtained by epitaxial growth on Si-face of SiC on C-rich surface, it is possible that $\sqrt{43} \times \sqrt{43}$ is a hexagonal Si pattern obtained by epitaxial growth on Si-face of SiC, and a potential epitaxial match suggests silicene as a possibility. The lattice constant for $\sqrt{43} \times \sqrt{43}$ phase is $3.08 * \sqrt{43} = 20.2$Å, which is approximately five times that of the predicted lattice constant for silicene(3.866Å[64]) with approximately 4% mismatch (silicene under tension). Rotating the silicene lattice by $30°$ with respect to the $\sqrt{43} \times \sqrt{43}$ produces alignment over a $3\sqrt{3} \times 3\sqrt{3}$ silicene unit cell with a lattice mismatch of only -0.76% (silicene under compression).

To investigate this surface in more detail with other techniques, we tried various methods to prevent oxidation of the sample surface: Vacuum suitcase transfers to environmental cells or UHV, capping with amorphous silicon, and "capping" with graphene (i.e., intercalation of Si $\sqrt{43} \times \sqrt{43}$ under graphene).

3.1.3 Raman

As described in Chapter 2, a vacuum inline-valve (Figure 2.8) was used as a small chamber to transfer $\sqrt{43} \times \sqrt{43}$ samples under vacuum. After preparing the possible silicene phase, the sample with its graphite sample holder was dropped into the suitcase and the valve was closed to maintain UHV. The sample was then transferred into a glove box under pure Nitrogen and from there into a nitrogen-purged environmental cell (Linkam Scientific Instruments) to avoid oxidation (these Raman measurements were performed on instrumentation in the

group of Prof. Samuel Graham, Georgia Tech School of Mechanical Engineering).
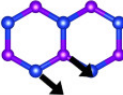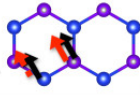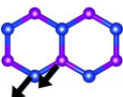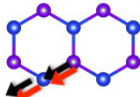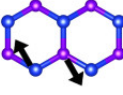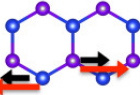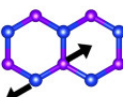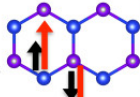
Figure 3.7a shows the calculation from Dr. Pan for possible silicene and silicane (hydrogenated silicene) vibration modes are from $185\,\mathrm{cm}^{-1}$ to $553\,\mathrm{cm}^{-1}$[93]. Figure 3.7b shows the Raman data for our potential silicene film. The dominant features are all due to the Nitrogen-doped SiC substrate; none of the predicted vibrational peaks are found in our data. However, a small but consistent peak at $520\,\mathrm{cm}^{-1}$ can be seen in the data. This is where crystalline Si has a characteristic Raman peak. This suggests that the $\sqrt{43} \times \sqrt{43}$ 2D Si reconstruction has predominantly sp^3 bonding, consistent with the model developed in Chapter 4.

Two other methods for protecting the $\sqrt{43} \times \sqrt{43}$ reconstruction from atmospheric oxidation were attempted: Deposition of a thick layer of amorphous Si using the GGS, and growth of the $\sqrt{43} \times \sqrt{43}$ underneath a protective layer of graphene. Unfortunately (but as anticipated), the only resolved Raman features after depositing amorphous Si were from amorphous Si, Si, and oxides of silicon. Results from our attempts to grow $\sqrt{43} \times \sqrt{43}$ underneath graphene, i.e., Si intercalation under graphene, are described in the next section.

Si intercalated graphene

One way to avoid oxidation is to cover the structure with other material. Growth on C-face SiC under Si-rich conditions results in a $\sqrt{43} \times \sqrt{43}$ reconstruction *beneath* a layer (or layers) of graphene [62]. Could the same configuration be created on the Si-face? If so, the graphene layer may protect the 2D Si phase from oxidation. Unfortunately, graphene growth on the Si-face occurs at a higher temperature, where the $\sqrt{43} \times \sqrt{43}$ would not survive. So one possible way to obtain this protective cap is to create the graphene first, then intercalate Si atoms beneath the graphene, to a density sufficient to form (one hopes) the $\sqrt{43} \times \sqrt{43}$ structure. This will require the proper equilibrium Si pressure and temperature.

Experimental methods for detaching buffer layer from substrate by intercalating other elements have been studied [94]. Si intercalated graphene on SiC was also studied [35,

Band #	Frequency(cm^{-1})	Vibration mode (Silicene)	Frequency(cm^{-1})	Vibration mode (Silicane)
1.	0		0	
2.	0		0	
3.	0		0	
4.	*185*		*383*	
5.	*553*		*485*	
6.	553		485	

(a)
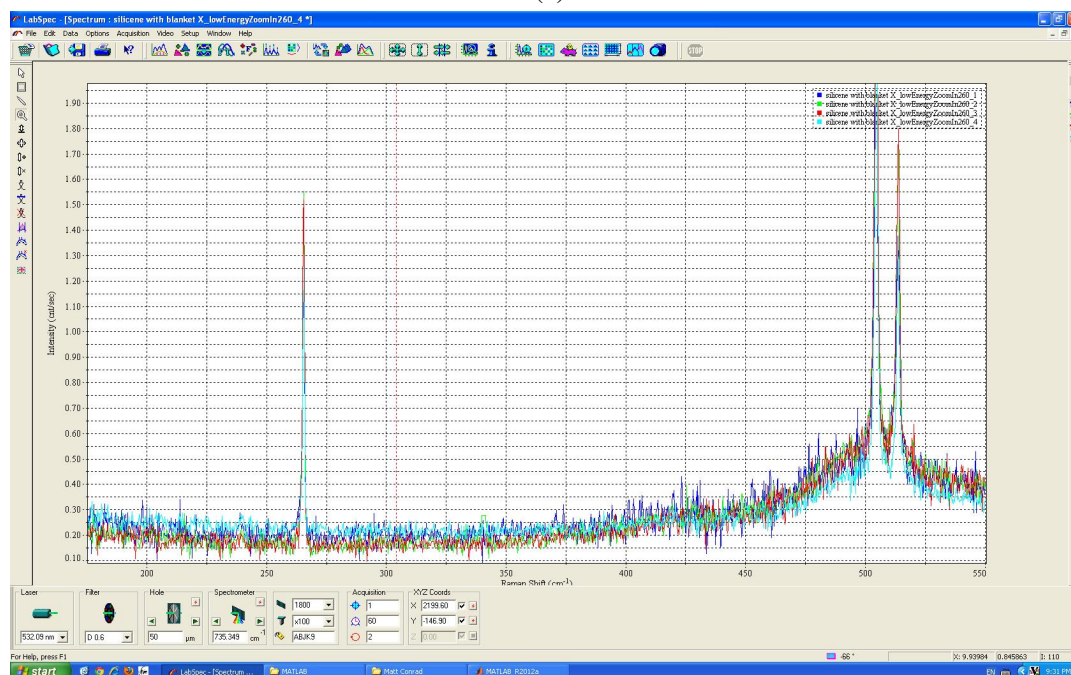
(b)

Figure 3.7: (a) Silicene and silicane vibration modes calculated by Dr. Chi-Ruei Pan. (b) Spectrum between 175 cm^{-1} and 550 cm^{-1}. The Raman spectrum is essentially identical to SiC, except for a possible peak at 520 cm^{-1}. Sample ID: 6H-HB019

56

95]. In order to intercalate a buffer layer, we first prepared a sample with one buffer layer grown on Si-face and deposited Si on the surface. After that we annealed gradually to reach Si intercalated graphene layer. Figure 3.8 shows the major annealing process in order
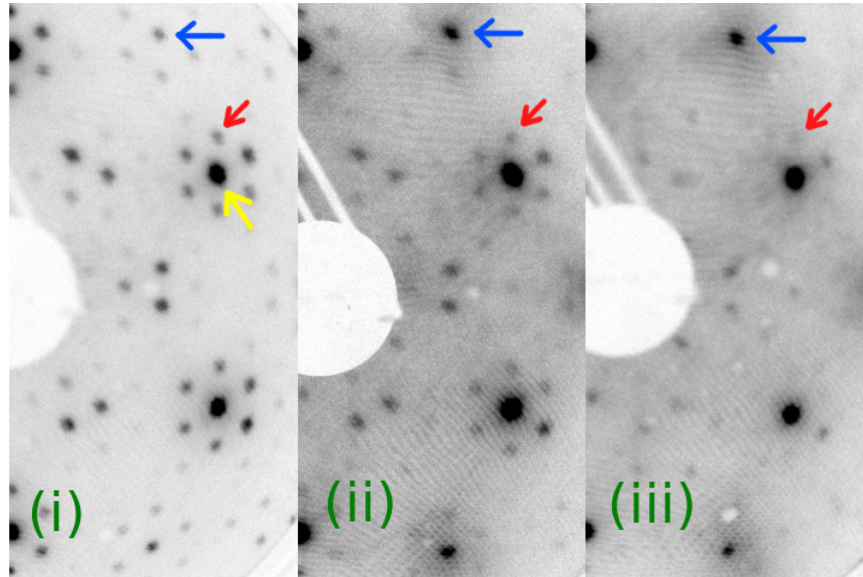
Figure 3.8: A series of LEED images at 105eV taken through out annealing process. The yellow arrow indicate SiC 1×1 spot, the blue arrows indicate the graphene spot, and the red arrows indicate the $6\sqrt{3} \times 6\sqrt{3}$ satellite spots around 1×1. (i) $1300°$ C, 1.0×10^{-4} Torr Silane, 10 min to obtain $6\sqrt{3} \times 6\sqrt{3}$ for buffer layer (ii) $700°$ C, 1.0×10^{-4} Torr Silane, 30 min to deposit Si (iii) $800°$ C, 1.0×10^{-4} Torr Silane, 10 min to saturate bonds from substrate in order to obtain intercalated graphene. Sample ID: 6H-HB024

to achieve this goal. The sample was annealed under Si background pressure in order to reach quasi-equilibrium condition, and annealing temperature was increased gradually until LEED image shows a well-ordered buffer layer on the surface as shown in Fig. 3.8(i). After a buffer layer was obtained, large amount of Si was deposited on the surface by annealing the sample under $700°$ C as shown in Fig. 3.8(ii). The reconstruction spots in (ii) is not as sharp as (i) due to large amount of Si deposited on the surface. The sample was then annealed couple times from $700°$ C with $10°$ C increment for 10 min each time in order to intercalate Si between graphene and substrate. A few cycles later, intercalation was found when annealing at $800°$ C as shown in Fig. 3.8(iii).

The LEED image in Fig. 3.8(iii) shows a combination of clear SiC spots and clearer

and brighter graphene spots, and the $6\sqrt{3} \times 6\sqrt{3}$ which indicates buffer layer is almost gone especially around graphene spots. This indicates that most area of the buffer layer on the surface was intercalated and become graphene layer so that this C layer was not bonding to the substrate.

After successfully obtaining Si between graphene and substrate, the sample is transferred to STM system for investigation before growing $\sqrt{43} \times \sqrt{43}$ reconstruction.

The intercalated graphene is able to prevent oxidation for the Si under it, so this sample is not transferred under vacuum by our designed vacuum suitcase. Instead, the sample was taken out from the furnace chamber and exposed to air first and then put into STM system.

After transferring the sample into UHV system, it is degassed at around 500 $^\circ$ C for one hour before measurement.

(a) V_{sample} = 4.0 V and I = 50 pA

(b) V_{sample} = -0.8 V and I = 50 pA
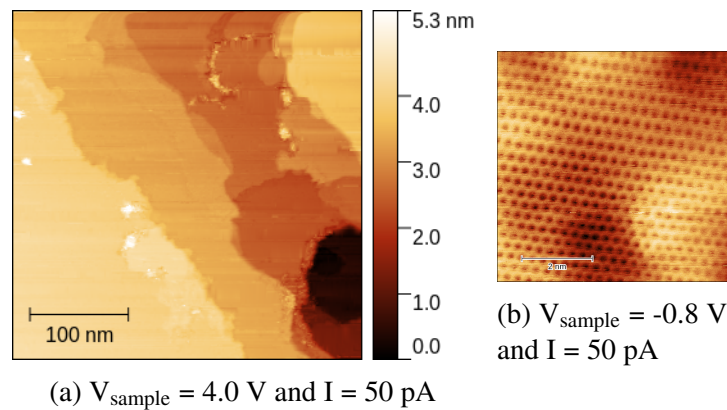
Figure 3.9: (a) 350 x 350 nm scan for the intercalated graphene sample after annealing at 800° C, 1.0×10^{-4} Torr Silane for 10 min. The surface still shows well-ordered steps with relatively flat area locally. (b) Zoom-in image near top left corner of (a) which shows graphene lattice. Sample ID: 6H-HB024

Figure 3.9 shows STM image of basic feature of the sample surface. The flat surface without Si or other mounds on the surface suggests intercalated graphene. Rough surface with mounds, on the other hand, suggests buffer layer. In Figure 3.9b, a zoom-in scan near the top left corner of Fig. 3.9a shows a well ordered graphene layer which confirmed the surface condition. Figure 3.10a shows a local defect on the surface. Two strips in the hole are one layer of intercalated graphene, and the flat area around the hole is another layer of

(a) V_{sample} = 3.0 V and I = 50 pA

(b) V_{sample} = 0.4 V and I = 50 pA
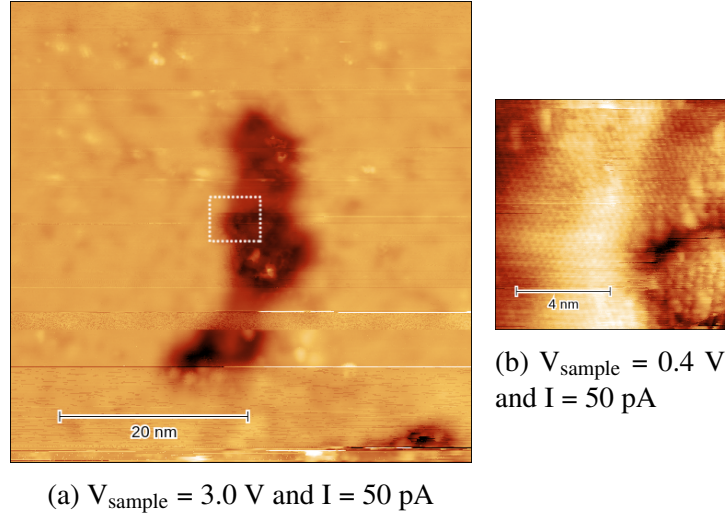
Figure 3.10: (a) Same sample as Fig.3.9. A local defect in a 50 x 50 nm scan. (b) The zoom-in image from the white box from (a) shows periodic pattern locally. Top left part of the image indicating graphene lattice. The bottom right part shows another pattern indicating possible 6×6 buffer layer. Sample ID: 6H-HB024

graphene that was grown originally instead of intercalated. The rough surface between the strips is possibly buffer layer with Si atoms on the top. Figure 3.10b is a zoom-in image on the left edge of the defect near the middle with graphene lattice showing on the left part and the top right corner of the image. Some detailed feature indicates graphene lattice on left half and top right area. It also shows buffer layer on the bottom right corner of the image.

The LEED phase for this annealing condition at $800°$ C, 1.0×10^{-4} Torr Si background pressure suggests a 3×3 reconstruction if no graphene present as discussed in Fig. 1.2b. However, there is no indication of such phase on the surface. This could mean that beneath the graphene Si adatoms are not sufficiently dense to form the tetramer structure, or the annealing process is not long enough to allow enough Si atoms to diffuse into the space between substrate and graphene layer. Of course, the graphene layer could change the energetics of the surface sufficiently to eliminate the possibility of a protected $\sqrt{43} \times \sqrt{43}$ phase.

Figure 3.11 shows a local area on the surface. The bottom left corner shows an intercalated layer, and the top right corner shows a smooth surface. Fig. 3.11b are images

(a) V_{sample} = 3.0 V and I = 50 pA

(b) Zoom-in image on local area.
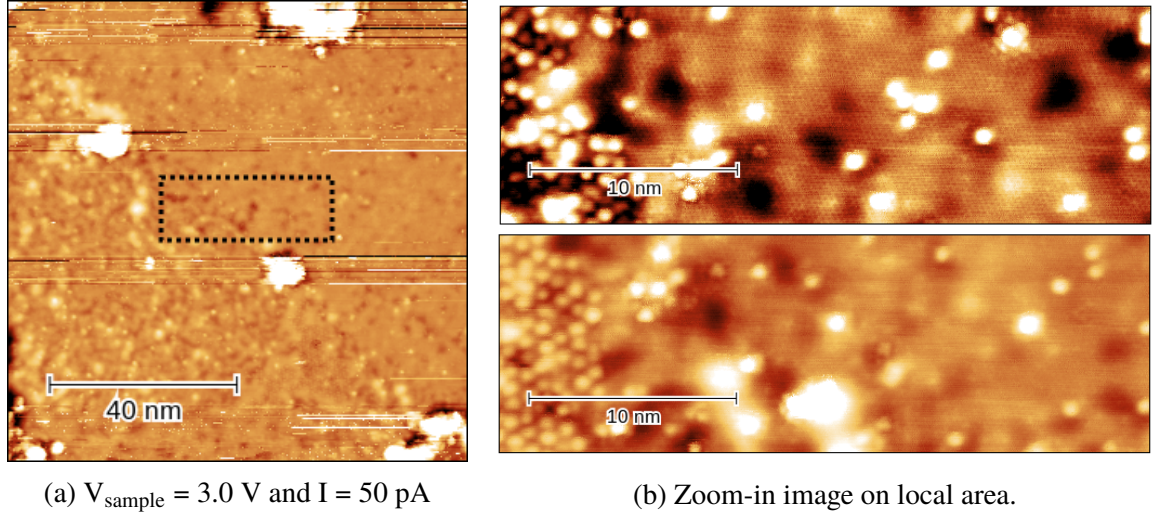
Figure 3.11: (a) The image shows a 100 x 100 nm scan. Bottom left part shows buffer layer features, and the top right corner shows intercalated graphene. (b) A zoom-in image from dotted rectangular area with sample bias values of 1.4 V (top) and 2.0 V (bottom). This images shows buffer layer on the left side of the boundary (regular bumps), and graphene lattice on the right side. This suggests that the left side of the boundary is the original buffer layer, and the right side of the boundary is intercalated graphene with saturated surface by extra Si atoms. Couple mounds can be seen under graphene indicating that they are extra Si atoms. Sample ID: 6H-HB024

scanned right above the mounds near the center as shown in dotted box from (a). Top figure of Fig. 3.11b shows clear graphene lattice on the right indicating intercalated graphene layer.

As discussed in the literature, it is likely that Si atoms diffuse at this annealing temperature and reach the substrate under the buffer layer through defect holes or step edges. However, a clear straight-line boundary is seen separating intercalated and non-intercalated graphene in this image of a step-free area. So far, no explanation was found to explain this boundary. It is possible that a boundary was formed because Si atoms were not sufficient, but it still does not explain the reason the boundary is a straight line. It is possible that the boundary is formed based on the location of defect since Si atoms need to be diffused through the defect holes, but as seen in Fig. 3.11, there are also other defects on the top and bottom left/right corner of the image. The boundary line is not likely to depend on the location of the defect.

To this end, it is clear that a free graphene layer was formed, and Si adatoms were between graphene layer and substrate. The intercalated sample was then sent back to the GGS for obtaining $\sqrt{43} \times \sqrt{43}$.

With Si intercalated graphene on the substrate, the sample was annealed again under the growth condition in order to form $\sqrt{43} \times \sqrt{43}$ reconstruction. Figure 3.12a shows the LEED image for the SiC sample with intercalated graphene before annealing. The LEED image

(a)　　　　　　　　　　　　　　　(b)
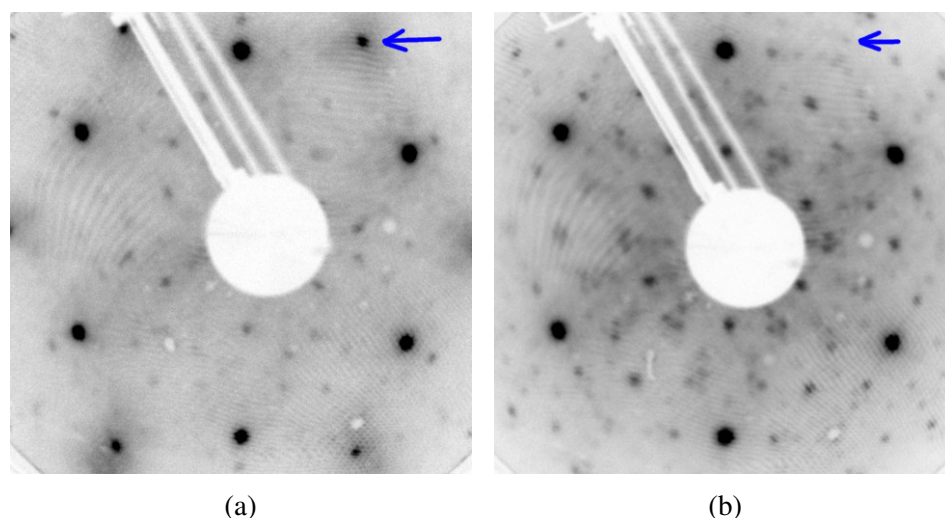
Figure 3.12: LEED images before and after annealing under growth condition for $\sqrt{43} \times \sqrt{43}$ pattern. (a) Graphene spot indicated by blue arrows right after degassing in UHV chamber with intercalated graphene. (b) Graphene spots disappear after annealing at $1000°$ C, 1.0×10^{-4} Torr Silane, 40 min. Sample ID: 6H-HB024

shows that the surface condition is still the same after the STM measurement. Figure 3.12b shows the LEED image after annealing under the same condition for obtaining $\sqrt{43} \times \sqrt{43}$ reconstruction. The first order graphene spots disappeared, and an unknown reconstruction has shown. Also, the area of the six SiC spots were broader comparing to the spots before annealing, and this suggests that the Si-face surface order consists of smaller domains as compared to the surface before annealing.

The unknown pattern is similar to some unknown pattern obtained previously, which indicates that it is still possible to obtain the hexagonal Si structure with additional annealing; however, the disappearing graphene spots indicate that the intercalated graphene has been

turned back to SiC. The LEED measurement suggests that the intercalated graphene layer has turned back to SiC. The surface became a Si-rich surface after annealing. This also indicates that it is less likely to grow $\sqrt{43} \times \sqrt{43}$ Si structure between substrate and graphene layer.

It is known that once a graphene layer (buffer layer or multiple layers) has formed, it is not possible to change the structure when annealing around this temperature range (800 °C to 1000 °C) when annealing under vacuum. Also, depositing sufficient amount of Si on top of buffer layer before intercalating also did not turn the buffer layer back to SiC. To this end, the fact that intercalated graphene can be turned back to SiC suggests that the Si-C bonding is favored within this range rather than the sp^2 C-C bond. The result for this experiment suggests that it is not likely to form hexagonal Si structure covered by graphene.

The result obtained from LEED data shows that the hexagonal Si 2D structure can only be on top of the substrate without graphene layer. In order to have further investigate, transferring under vacuum is needed. Two experiments were done by transferring under vacuum. First, we attempted to transfer samples under pure nitrogen environment to measure Raman spectrum (described earlier), and after that the samples were also transferred to do STM.

3.1.4   STM

In previous experiments, Raman spectrum did not show any peak indicating possible silicene structure. After that, another sample was prepared for transferring into our STM system for further investigation. We used the vacuum suitcase to transfer the possible silicene sample several times, and the surface of the sample could easily be contaminated due to transferring time. The best transferring condition was obtained with a copper feedthrough in contact with liquid nitrogen as a cooling system to avoid contamination. The estimation of pressure in the suitcase is about 1.0×10^{-8} Torr.

Figure 3.13 shows a comparison for two LEED images taken before and after transfer-

<div align="center">(a)   (b)</div>
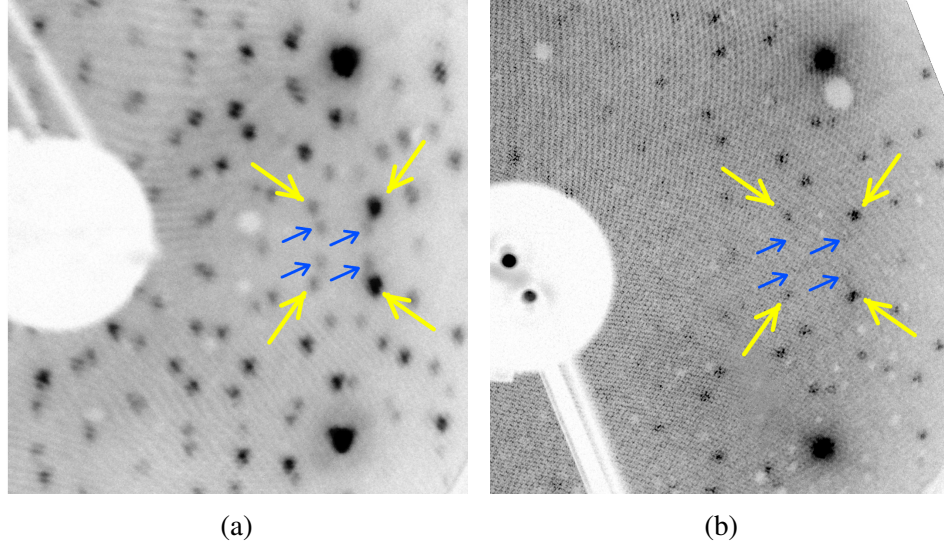
Figure 3.13: A comparison of two LEED images showing the $\sqrt{43} \times \sqrt{43}$ pattern before and after transferring with vacuum suitcase. The largest two spots are SiC. (a) Before transferring (b) after transferring. Yellow arrows indicate the reconstruction spots from $\sqrt{43} \times \sqrt{43}$ with less intensity but sharp. The blue arrows indicate the spots that are much less intensity but still sharp. Sample ID: 6H-HB031

ring. The brightest two spots are the 1×1 SiC spots. Fig. 3.13a is the LEED image from GGS, and Fig. 3.13b is the LEED image taken in our STM system after transfer. Comparing the details between the 1×1 SiC spots, both LEED images show sharp reconstruction patterns which indicates a well-ordered surface. Some details in LEED image are missing as shown in blue arrows, and some are missing at the center area. The missing detail between SiC spots suggests that while some area of the surface are still well-ordered, the sample surface is not as clean after transferring so that higher order reconstruction spots disappeared. The missing detail near the center could be due to the equipment. After confirming the LEED phase, the sample was then prepared for STM measurement.

Figure 3.14 shows the configuration of our STM tip and the sample holder. The handle of the holder is pointing directly upward, and the sample is designed to have the longer edge perpendicular to the handle. This makes the scanning direction parallel to the longer edge (i.e., along the SiC [$10\bar{1}0$] direction.)

The large area STM scan of Fig. 3.15a shows the $\sqrt{43} \times \sqrt{43}$ reconstruction. Figure 3.15

(a)	(b)	(c)
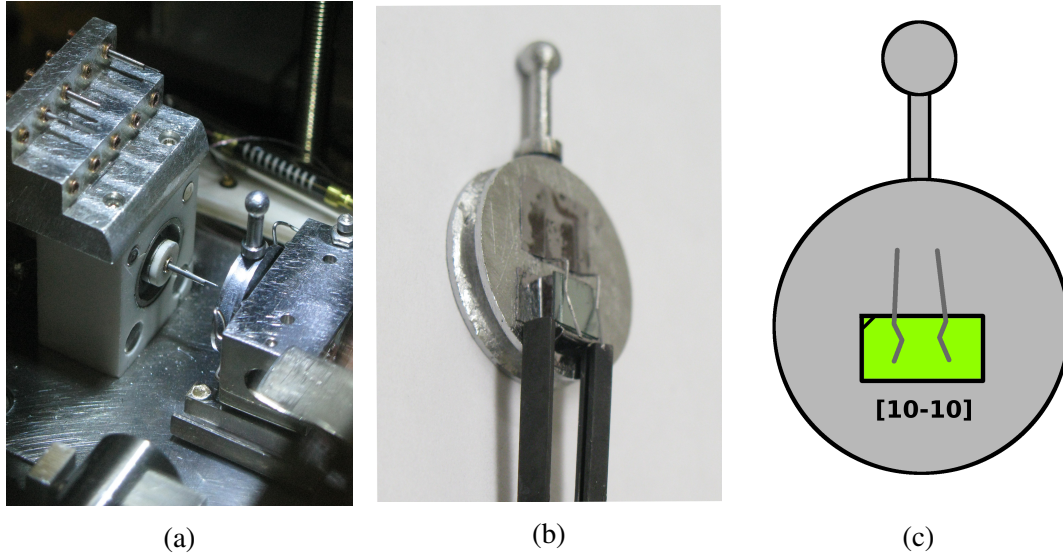
Figure 3.14: (a) An image for configuration of our STM. (b) A demonstration for transferring a SiC sample from graphite sample holder to STM holder (c) A schematic drawing of the STM holder and the sample direction.

(a)	(b)	(c)
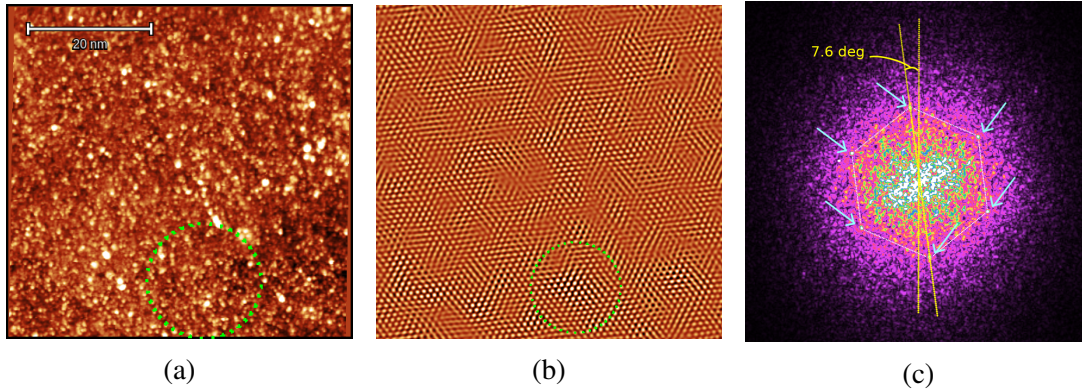
Figure 3.15: (a) 50x50 nm scan. V_{sample} = -3.0 V and I = 50 pA. (b) FFT-filtered image showing regions of $\sqrt{43} \times \sqrt{43}$. (c) FFT showing periodic pattern indicating a hexagonal structure with lattice constant about 20 Å. The FFT shows a 7.6° angle tilted from vertical line which is along SiC direction. Sample ID: 6H-HB031

shows a flat area for which the fast Fourier transform (FFT) in Fig. 3.15c shows a clear hexagonal structure with 7.6° rotated from SiC lattice direction. Some large meshes are shown in this image, and there is no SiC structure found. A circled area in the FFT-filtered image of Fig. 3.15b shows a local well-ordered area of the $\sqrt{43} \times \sqrt{43}$.

(a)

(b)
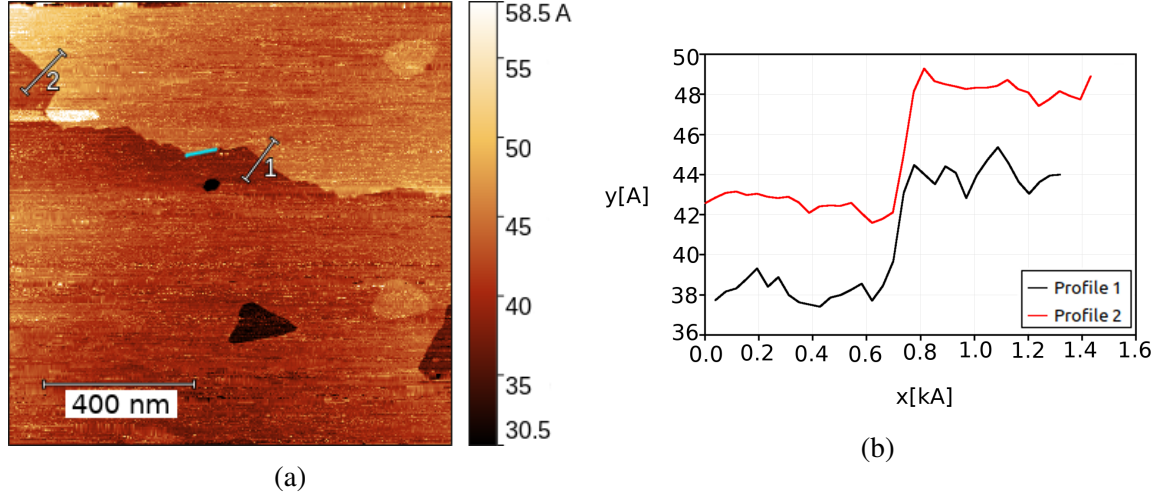
Figure 3.16: (a) A 1x1 μm scan. The edge of the step aligns with the direction 7.6° counterclockwise from SiC lattice direction as marked in the blue line. (b) Height profile indicating the step height for this sawtooth step. V_{sample} = -3.0 V and I = 40 pA. Sample ID: 6H-HB031

Figure 3.16 shows a 1 x 1 μm scan. In this image, a saw-tooth edge with step height of (6.8 ± 0.5) Å separates the image into two large uniform areas. Unfortunately, the uncertainty is large enough that this step could consist of SiC/SiC, Si/SiC, or Si/Si. The direction of the saw-tooth edge might be able to help determining the combination, but without resolving any periodic structures, those directions are also somewhat uncertain. What can be said is that for these growth conditions, Si apparently forms relatively flat and uniform layers on the SiC surface over large areas. Still, without resolving any periodic structure in this area, we cannot determine whether we are imaging a pure Si phase, bare SiC, or a contaminated surface phase. However, the preparation conditions give us high confidence that these are Si-rich layers.

After moving to another local area (separated by millimeters), some flat areas with $\sqrt{43} \times \sqrt{43}$ have been found. The change in imaging could be due to a difference in the

65
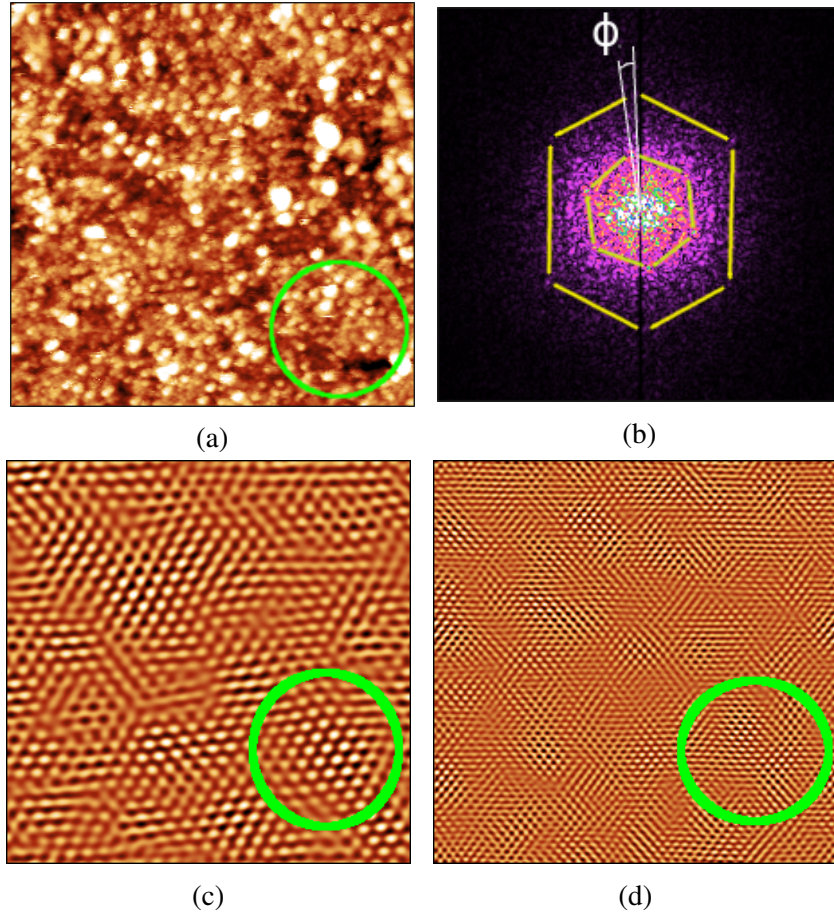
Figure 3.17: (a) A 50 x 50 nm scan. V_{sample} = -2.5 V and I = 50 pA. (b) FFT shows two hexagonal patterns with lattice constant 20 Å and 9.17 Å. ϕ = 7.6° after correction for image drift. (c)(d) FFT-filtered images from the hexagonal spots in (b). The green circles in (a),(c) and (d) show an area where both 3×3 and $\sqrt{43} \times \sqrt{43}$ features are strong. Sample ID: 6H-HB031

sampled areas or, perhaps more likely, a change in the condition of the STM tip. Fig. 3.17 shows one of the local area of flat Si layer. The FFT in Fig. 3.17b shows two hexagonal periodic spots. The inner hexagonal pattern corresponds to Si structure with lattice constant about 20.5 Å. This agrees with the LEED reconstruction and indicates that this periodic pattern is the $\sqrt{43} \times \sqrt{43}$ pattern, which the lattice constant is 3.08 Å $\times \sqrt{43} = 20.2$ Å. Another hexagonal spots in the FFT is 7.6° counterclockwise from the $\sqrt{43} \times \sqrt{43}$ structure with a lattice constant 9.17 Å. The orientation aligns with lattice of the substrate. This suggests that it is the 3×3 pattern, which the lattice constant is 3.08 Å $\times 3 = 9.24$ Å.

The 3×3 structure was well studied from Heinz et al. [28]. It is also the LEED phase before entering the Metastable Phases on the phase diagram. The coexistence suggests that the $\sqrt{43} \times \sqrt{43}$ structure is related to the 3×3 structure. Figure 3.18 shows a zoom-in

(a)

(b)
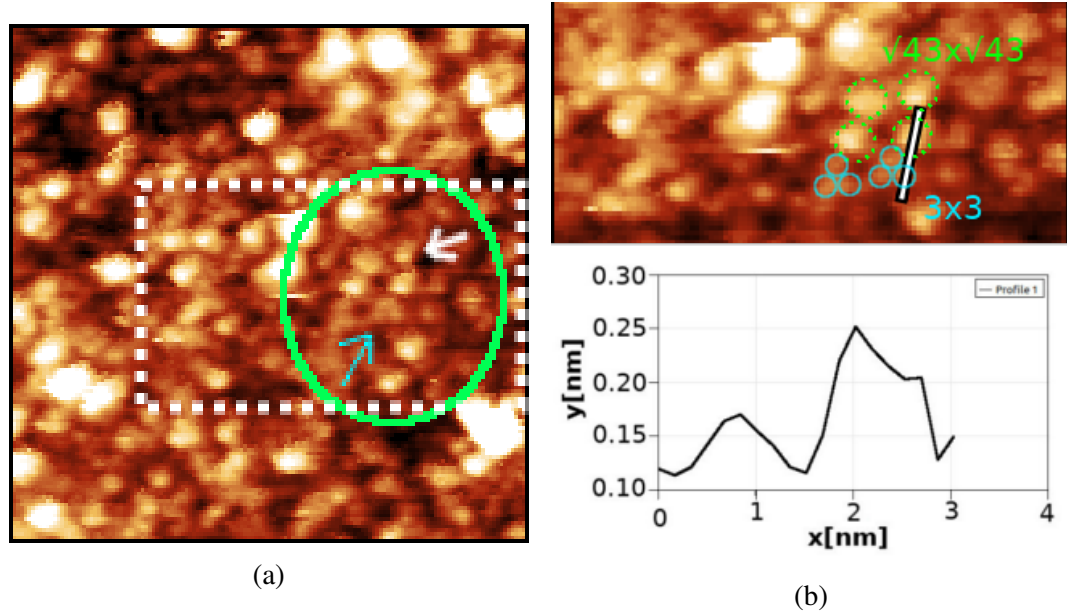
Figure 3.18: (a) Zoom-in image of Fig. 3.17a. The green circle indicates a relatively clear structure for $\sqrt{43} \times \sqrt{43}$ and 3×3, and the blue arrow indicates three points for 3×3. The white arrow indicates the points for $\sqrt{43} \times \sqrt{43}$. (b) A zoom-in image from the white dotted box from (a) with a line profile to compare the height of 3×3 and $\sqrt{43} \times \sqrt{43}$ sites. Sample ID: 6H-HB031

image at the bottom right corner of the 50 nm image from Fig. 3.17. The circled area shows a relatively clear structure. There are four larger mounds as indicated by the white

arrow, and another two sets of three small mounds form two triangular groups (blue arrow). By comparing the STM image, FFT-filtered image, and the location of the mounds, it is suggested that the four big mounds are corresponding to $\sqrt{43} \times \sqrt{43}$, and the two sets of small mounds corresponds to 3×3.

To wrap up, in this chapter the experimental data has confirmed known LEED phases, and some new (and some unknown) reconstructions phases are found in Metastable Phases. We believe that the newly-discovered $\sqrt{43} \times \sqrt{43}$ reconstruction corresponds to an equilibrium Si-rich 2D phase. Considering epitaxial matching, silicene was considered as a candidate for this phase, but Raman data does not support that interpretation. STM data is hampered by potential surface contamination, but images show the $\sqrt{43} \times \sqrt{43}$ periodicity as well as features similar to those found on the 3×3 surface. The magnitude of the surface corrugation also does not favor silicene. In Chapter 4 we will use the information gathered so far to develop a model structure of the $\sqrt{43} \times \sqrt{43}$ reconstruction.

CHAPTER 4

PROPOSED MODEL AND ITS DEVELOPMENT

Based on the information collected, a model for the Si-rich $\sqrt{43} \times \sqrt{43}$ R±7.6° structure is proposed. We first motivate and show the model, then follow with a discussion of the ideas behind its development.

(a)   (b)
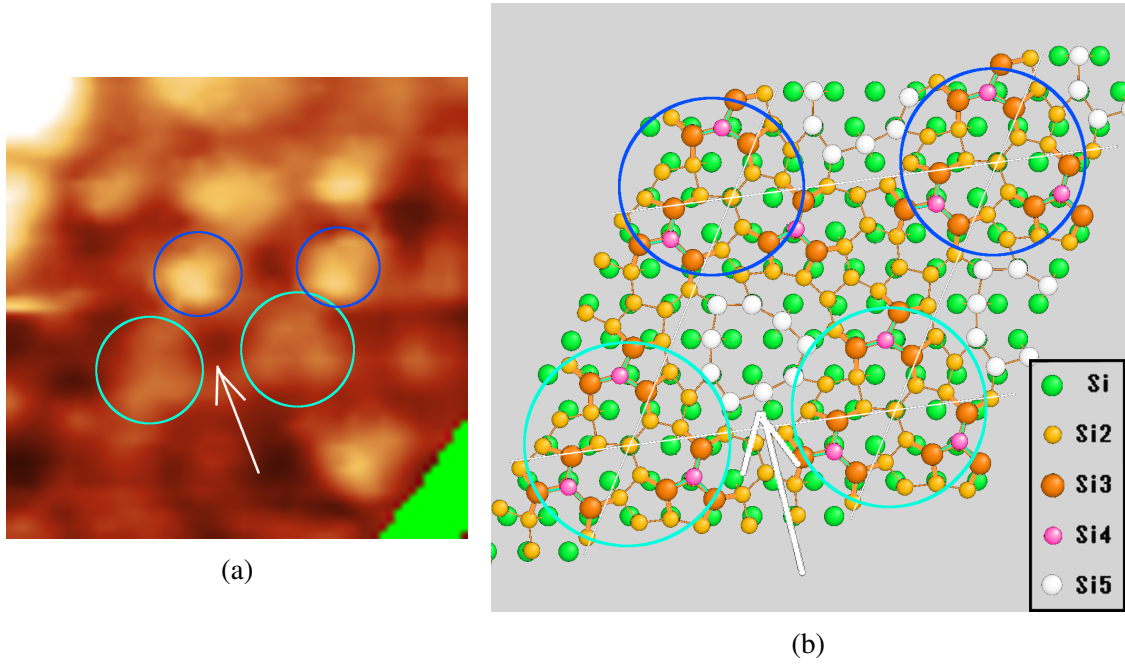
Figure 4.1: (a) Zoom-in image of the lower-right corner of Fig. 3.18. The cyan circles indicate the $\sqrt{43} \times \sqrt{43}$ sites from an FFT-filtered image. The blue circles show higher mounds and the white arrow indicates one of the local low spot between the circle. (b) The proposed structure with blue, cyan circles and white arrows comparing to (a). The cyan circles shows three dangling bonds, and the blue ones are presumed to have additional contaminant adatoms on top to produce the mounds shown in (a).

Figure 4.1a shows a zoom-in image of the circled area from Fig. 3.18. Figure 4.1b shows a plotted version of the proposed $\sqrt{43} \times \sqrt{43}$ structure. Five kinds of Si atoms are marked. "Si" is from substrate, "Si2" is from the adlayer, "Si3" denotes trimer atoms on top of adlayer, "Si4" is the top atom of the tetramer structure on top of each trimer, and "Si5" are adlayer atoms that are part of the bridge formations. The cyan circles in Fig. 4.1a

indicate the two sets of small mounds, which corresponds to the three "Si4" atoms as the only three dangling bonds inside the circle in Fig. 4.1b. The blue circles indicate another two sets of small mounds, and some additional adatoms (e.g., oxygen contamination) might be on top of this structure to form a big mound in Fig. 4.1a. In this figure, the white arrow on STM image indicates a low spot, which corresponds to a local area possibly with no dangling bonds. This is also shown in the proposed structure by a white arrow and "Si5" atoms for the bridge formation. The detail about the proposed structure derived from 3×3 in the following.
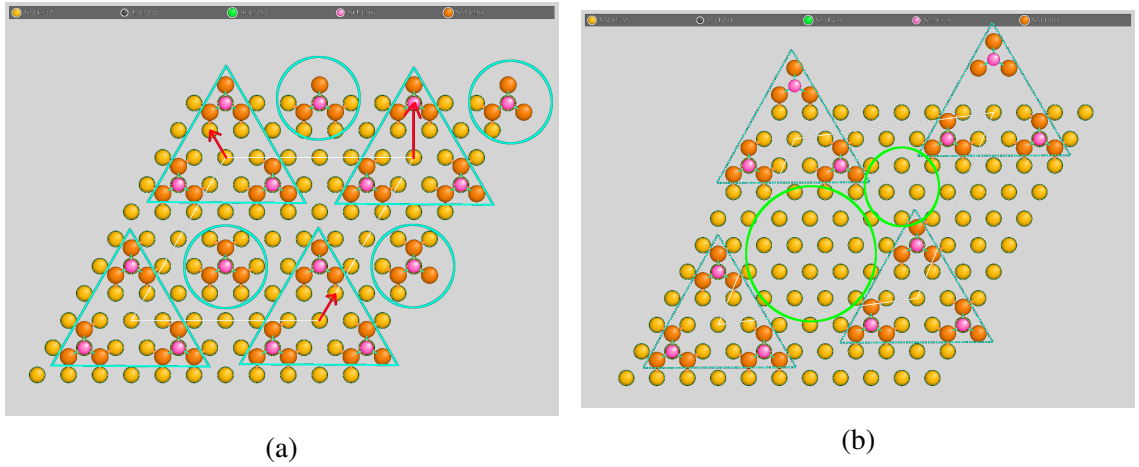
Figure 4.2: (a) Plotted version of unrelaxed 3×3 and the shifting groups. The red arrows indicates the shifting distance and direction for three mounds as a group. (b) The groups after shifting.

Figure 4.2a is a plotted model for unrelaxed 3×3 structure from Starke et al. [33]. The "Si" atoms marked in green is right below "Si2" from adlayer. Each of the four cyan triangles indicates a triangular grouping of 3 tetramers (3-tet), which which are similar to the groups of three small mounds in Fig. 4.1a. The white lines in diamond shape which connect the centers of 3-tets form a 6×6 unit cell, which is close to the lattice constant of $\sqrt{43} \times \sqrt{43}$ reconstruction. The circled tetramers correspond to the positions of the low areas in STM so that the tetramer on this spot is removed. Then, the 3-tets shift in different directions as shown by red arrows. This forms a new hexagonal structure, which is $\sqrt{43} \times \sqrt{43}$ as shown in white lines in Fig. 4.2b. This figure also shows the 3-tets after

shifting. The two 3-tets at the bottom of the picture are similar to the groups of small mounds in the STM image.

The other two 3-tets in Fig. 4.2b do not show on the STM image of Fig. 4.1a. Instead, these two 3-tets are replaced by two higher mounds. The proposed structure can not explain the two large mounds, but it is probable that there are extra contaminant adatoms (likely to be oxygen) on top of two 3-tets so that they image as higher mounds.

The two green circles in Fig. 4.2b indicate some buffer areas after shifting. Before shifting, the 3×3 structure would satisfy all dangling bonds except the top adatoms, and this is no longer the case after shifting. Also, by comparing to the STM image, there is still no dangling bond in those area as well. Therefore some arrangement needs to be done to satisfy the dangling bonds. A few versions of rearrangement in these two areas were done in order to satisfy the bonds, and considering the proper bond length and bonding angle, we obtain the proposed structure with only three dangling bonds in each set in the triangular group in Fig. 4.1b by using bridge formation (see, e.g., Figs. 1.7 and 4.4). Finally, by applying the relaxed bonding condition from Schardt et al. [31] and approximately shorten the bond lengths for the rest of the atoms, we obtained the proposed structure as Fig. 4.1b

In conclusion, some proposed structures for Si thin film grown on SiC surface has been discussed after the LEED phase $\sqrt{43} \times \sqrt{43}$ was found, and after having measurements via transferring under vacuum method, a structure is proposed based on 3×3 structure.

Corrugation of the Si layer.

Although a characteristic step height of (6.8 ± 0.5)Å was measured in Fig. 3.16 this does not provide information about the thickness of the 2D Si adlayer bonded to the substrate. On the other hand, Fig. 3.17a which shows both 3×3 and $\sqrt{43} \times \sqrt{43}$ Fourier components might be able to help. Figure 4.3 shows the same image as Fig. 3.17. The green triangle shows the boundary which aligns with the direction of the substrate. The blue circle indicates the location of relatively clear $\sqrt{43} \times \sqrt{43}$ reconstruction sites.

By comparing to the FFT-filtered image in Fig. 4.3, the four large mounds to lower right

(a)   (b)
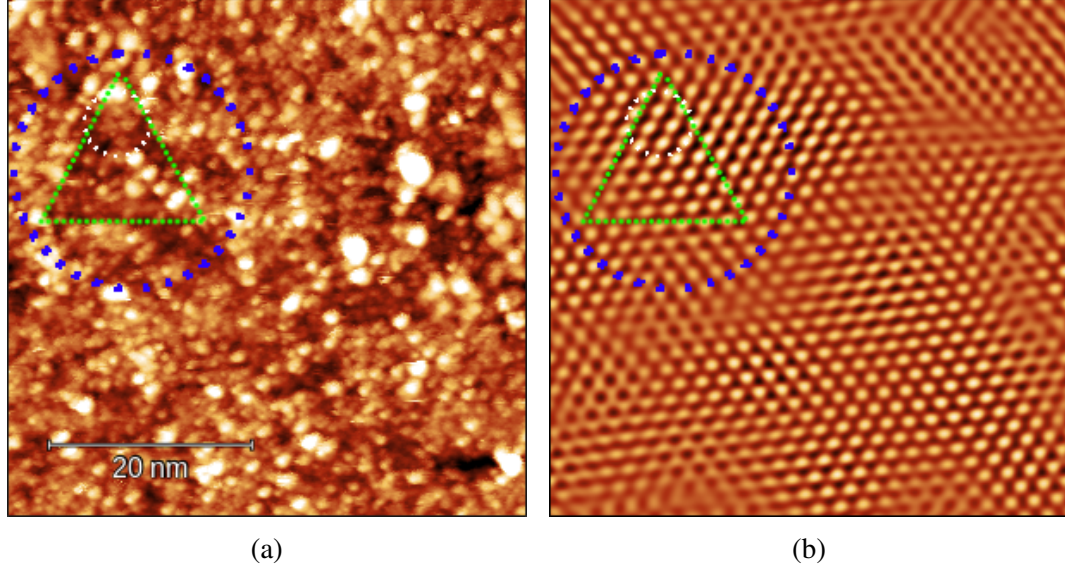
Figure 4.3: (a) The green triangle indicates symmetry directions of the SiC substrate (a small surface depression aids alignment). (b) FFT-filtered image showing the $\sqrt{43} \times \sqrt{43}$ reconstruction sites within the blue circle Markings are placed identically in (a) and (b).

within the triangle indicate a $\sqrt{43} \times \sqrt{43}$ area, which is rotated from the substrate symmetry directions denoted by the green triangle. Another area near the top corner of the triangle, inside the white circle, could be a group of four 3-tets. The height difference between the lowest point and the presumed 3-tets is about 1.4 Å. This is close to our proposed structure which is 1.6 Å.

Si adlayer coverage could depend on local area.

The characteristic step height after Si growth is 6.8 Å, and this can be used to bound the Si coverage on the surface. Based on the STM scan in Fig. 3.16, there are approximately one full layer and one-third of the image with another Si layer. With no clear LEED pattern other than $\sqrt{43} \times \sqrt{43}$, the Si covered here could be amorphous Si, which the mass density is 2.285 g cm^{-3}. One and one-third layers of amorphous Si give approximately 3.85 ML of Si on the surface where one monolayer is defined as one Si atom per unit cell of SiC on Si-face. Comparing to Si coverage for 3×3, which is 13/9 = 1.44 layers. The Si coverage is far more than we expected.

On the other hand, the STM image in Figure 3.18 has relatively less Si coverage on

the surface. There is no step found around this area, and on the top left corner of this image, there is a triangular area which indicates the bare SiC with not much Si coverage. As for the Si coverage, the proposed structure shows three tetramers in the unit cell with some adatoms removed due to the bridge formation. The number of total Si adatoms is 52, and this gives this proposed structure $52/43 = 1.209$ monolayers of Si coverage. This Si coverage is less than 3×3 coverage, which is 1.44, and it is very close to the coverage from other reconstruction structures. The Si coverage for $2\sqrt{3} \times 2\sqrt{13}$ structure, for example, from Naitoh et al. [60], is 1.21.

To this end, it is possible that with the annealing condition at this temperature and background pressure, the Si-rich surface can form two different structure: The area with relatively high Si density will form amorphous Si and $\sqrt{43} \times \sqrt{43}$ for less Si density area.

This could be contradicted with the LEED phase diagram from Tromp et al. [19] since changing annealing temperature or pressure could change the LEED phase. However, the Metastable Phases was not indicated in their P-T Diagram, and it takes longer time under the quasi-equilibrium condition to obtain such phase. So it is still possible that the LEED phases shown in this region is not relatively stable comparing to other phases such as 3×3 and $\sqrt{3} \times \sqrt{3}$.

Three tetramers move as a group.

As discussed previously, the annealing condition is at least 30 minutes which suggests that it is a relatively stable structure in Metastable Phases. However, STM data from other research groups also shows single protrusion per unit cell. By comparing to the well accepted 3×3 structure [31], it is reasonable to assume that the single dangling bond from STM data is from tetramer structure, and our STM data also suggests that three tetramers (3-tets) move as a group. This also shows for the large mounds that represent $\sqrt{43} \times \sqrt{43}$ sites with additional adatoms.

In other words, it is suggested that starting with a 3×3 surface, with higher temperature the tetramer structure tend to "shift" instead of aligning closely as 3×3 structure. Either

the tetramer decompose and reform at this temperature or the adatoms on top of the adlayer diffuse away from it's original site.

In the case of decomposing and reforming, the Si bonds tend to break easily under this condition, and since the tetramer structure consist of all sp^3 bonding, this also suggests that the whole tetramer structure will decompose. Therefore the reforming part of this process might not necessary become a tetramer. Instead, it could only form one adatom on top of the adlayer. This could explain not only the reason the phases found in Metastable Phases can change rapidly even with the same annealing condition, but also explain the height of the STM data from other research group is lower than a tetramer such as $2\sqrt{3} \times 2\sqrt{13}$ structure from Naitoh et al. The Si surface density fluctuates in local area, and some tetramers in that area will break and reform with only one adatom on top of the adlayer, and another area still stay 3×3 since the bonds for tetramer structure did not break in that area.

Bridge formation is the main cause for different phases in Metastable Phases.

While it is possible that the tetramers decompose and reform while annealing, it still does not necessary mean that it is the cause for the $\sqrt{43} \times \sqrt{43}$ formation. There could be other factors that is involved in this process to determine the final structure. In the following, we will discuss additional cause for this phase by using bridge formation from Martrou et al.

The experimental detail in that paper indicates that Si enrichment method has been used to study the surface structure by slowly increasing Si coverage on Si-face. They addressed one important component to form different Si structure through out this process, and that is the bridge formation.

As discussed previously, Figure 1.7 from Chapter 1.2 shows that Si adatoms are freely moving around one of the peak site in $\sqrt{3} \times \sqrt{3}$ structure, and one Si adatom will bond with the adatom bonded on the surface. This will introduce additional dangling bonds and eventually form a bridge to saturate the bonding for the middle Si atom with substrate and therefore to form the bridge. Figure 4.4a shows a plotted model for a unit cell of SiC on
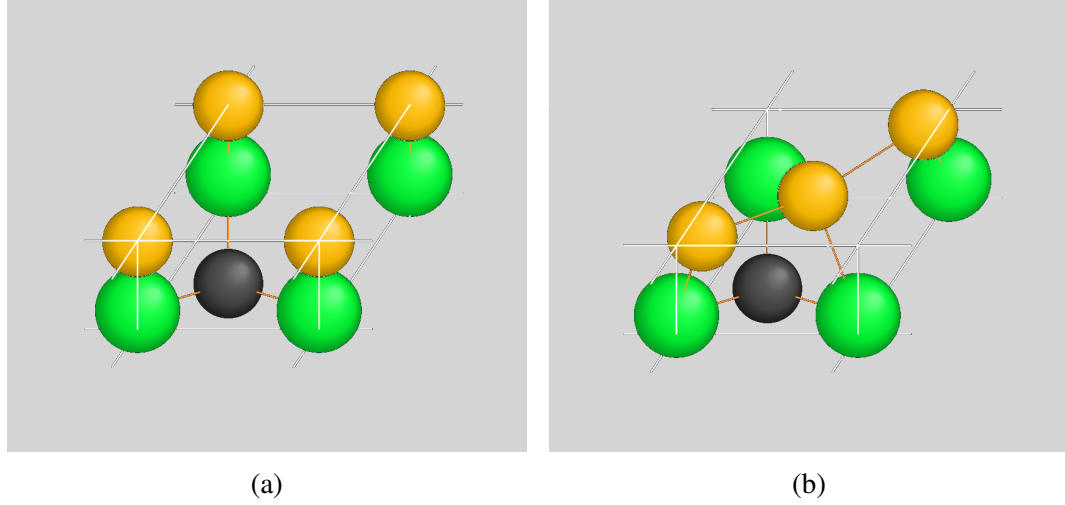
Figure 4.4: (a) Unit cell of SiC (Green Si and Black C) with one Si adlayer(Yellow). (b) Bridge formation on the adlayer. One Si adatom is removed, and the Si atom in the middle has two bonds to the Si atoms from substrate.

Si-face and one adlayer. Fig. 4.4b shows the bridge formation. One Si adatom is removed from the adlayer, and the Si atom in the middle has two bonds with two Si atoms from substrate. This plotted model has the bonds relaxed manually. Calculation is needed for a real relaxed position for all atoms.

From Martrou et al., their experiment started with $\sqrt{3} \times \sqrt{3}$ reconstruction surface and slowly increase Si density to enrich the surface until 3×3[57]. However, in our experiment, the $\sqrt{43} \times \sqrt{43}$ is close to the other end of the Metastable Phases, which means the Si coverage is relatively more. As discussed in previous paragraphs, the annealing condition for obtaining $\sqrt{43} \times \sqrt{43}$ could create both high and low Si density in local area and therefore have both thick Si layers and thin 2D structure. To this end, it is also possible that the relatively low Si density area starts from $\sqrt{3} \times \sqrt{3}$ to start accumulating Si atoms. It is also possible that the bridge formation happens even though excessive Si adatoms are on the substrate.

By saturating the dangling bonds when forming a bridge, the energy configuration is considerably lower relative to pure Si adlayer. Once a bridge is formed, both ends of the bridge will still need additional atoms to minimize number of bonds.

To this end, considering the low energy configuration of the bridges and the possibility that the tetramer structure could be shifting, this suggests that the triangular bridges are formed first in our proposed structure, and then Si adatoms start piling up and form the tetramers around it, and they would start shifting (or they would form at the right location directly) until all tetramers around the triangular bridges start to bond and minimize the dangling bond.

The bridge formation could be one of the main factors to obtain $\sqrt{43} \times \sqrt{43}$ structure, and the tetramers (or only three trimers) shift around the bridges. To this end, it is possible that other reconstruction patterns in the Metastable Phases are formed in the same method. In the following, we will discuss some structures found in this region and how the bridge formation could be applied.

According to Martrou et al., some other reconstruction patterns were also found during the Si enrichment process including 12×12 and 4×8 [57]. They address the bridge formation in that paper and applied it to their structure. Figure 4.5 shows the bridge structures in some of the proposed structure from Martrou et al. and our proposed $\sqrt{43} \times \sqrt{43}$ structure in Fig. 4.5d. The blue dotted boxes show the location of the bridge structure. Fig. 4.5a and 4.5b are the two basic structures in the large 12×12 reconstruction unit cell. The first one is a regular hexagonal pattern with three bridges symmetrically aligning to the center. The second one is a distorted hexagon where the three bridges were shifted. Fig. 4.5c is the $2\sqrt{3} \times \sqrt{7}$ firstly found from Naitoh et al. [60]. The shaded rectangular indicate the thin belts, and the blue dotted box indicate the bridges. Fig. 4.5d is our proposed structure for $\sqrt{43} \times \sqrt{43}$. The shaded area indicates several sets of small mounds, and the three bridges with totally nine adatoms were formed at the center.

While the bridge formation does explain some reconstruction patterns found, it is also possible that other patterns in the Metastable Phases could be from bridge formation as well. There are some reconstruction patterns found during the annealing process that could not be recognized. The only one recognized is the $\sqrt{19} \times \sqrt{21}$. The proposed structure for

76
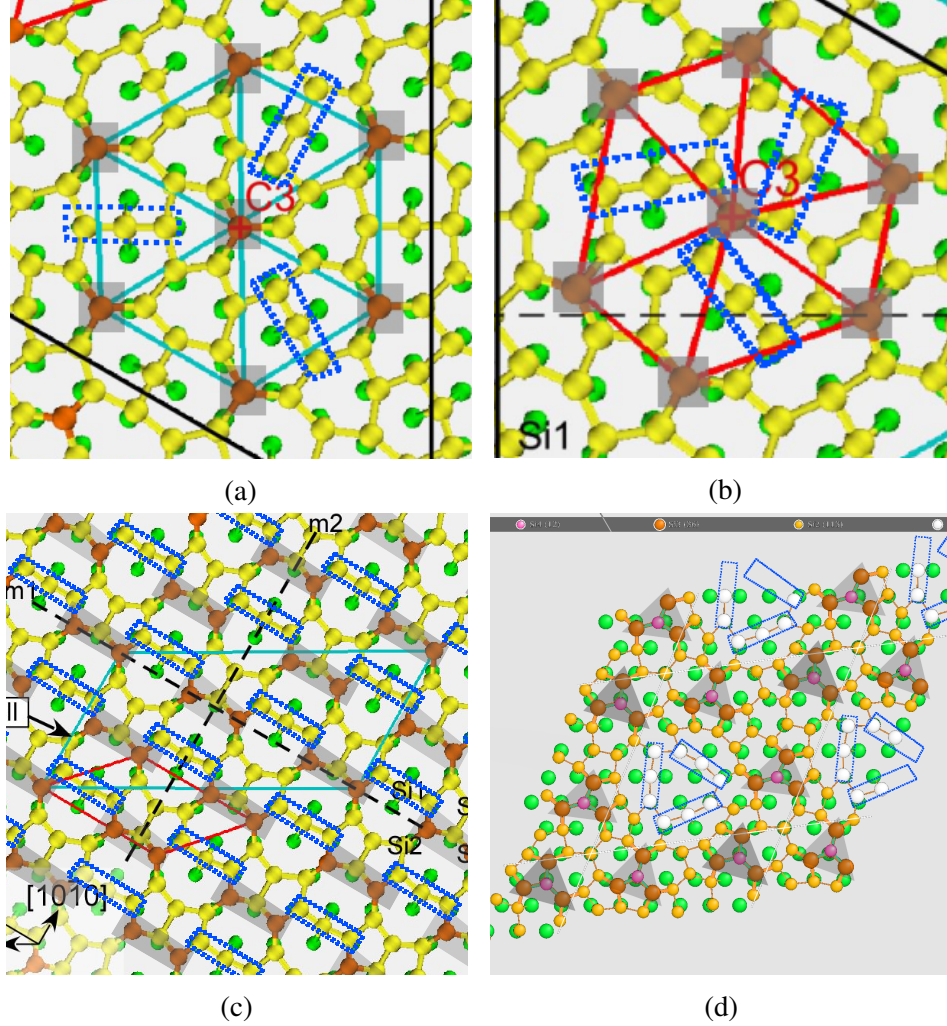
Figure 4.5: (a) A regular hexagon center in 12×12. (b) A distorted hexagon in 12×12. (c) Proposed structure for $2\sqrt{3} \times \sqrt{7}$. (d) Our proposed structure [57].

this phase with bridge formation has not been constructed yet. On the other hand, some of the unknown patterns did appear more than once in all annealing process we had, so it is still possible to reveal the structure with proper STM data to support our theory.

Forming bridges first, and then trimers or tetramers.

Our proposed structure is derived from tetramer structure in 3×3, and in the following, we will summarize the possible main factors that would allow this structure to form.

Even though the Metastable Phases contains a lot of reconstruction patterns, the structures on both ends are known, which are 3×3 on the Si-rich side and $\sqrt{3} \times \sqrt{3}$ on the condition with almost no Si adatoms. To this end, most of the experiment done in this area

would either start from 3×3 to start evaporating Si adatoms or from $\sqrt{3} \times \sqrt{3}$ to enrich Si density. The 3×3 structure from Starke et al. [28] is widely accepted, and the LEED phase found near Si-rich side of the Metastable Phases usually coexist with 3×3, so it is reasonable to start a proposed structure with only a few Si adatoms less then 3×3 structure. In other words, number of Si adatoms on top of the adlayer could be different, and the bonding arrangement for the adlayer could also be different.

Another important factor to form reconstruction pattern is the annealing condition. The STM image from our data indicate that even though a quasi-equilibrium Si background pressure was provided, the surface area still consists of two very different Si coverage. Either the annealing condition could be very different in local area to cause this result or the $\sqrt{43} \times \sqrt{43}$ structure actually prevent extra Si adatoms to be deposited on top of this 2D film structure. Therefore, excessive Si atoms phase segregate as (perhaps) amorphous Si in another local area.

Bond length distribution.

After setting up the bridge formation and the location of tetramers, some bonds relaxation have been applied. The relaxation of bonds for tetramers are already done in previous work [31], so for this process, all the tetramers start with the relaxed position. After that, all the bond length reductions are done manually from rearranging atoms horizontally and then vertically for the combined structure with other Si atoms.

Figure 4.6 shows our proposed structure, the side view, and the bond length distribution. The process of reducing bond length starts with the relaxed version of the tetramers from Schardt et al. [31], after taking out some atoms from the adlayer to form three bridges and shifting all tetramers to form, all atoms were examined and adjusted manually to minimize the bond lengths (approximately; substrate atom positions remained fixed, and limited vertical adjustments of adlayer atoms were made). Fig. 4.6c shows the bond length distribution. The x-axis is length in Å, and y-axis is the number of bonds. In this figure, there are three peaks and one region which represent the average bonding length for different

78
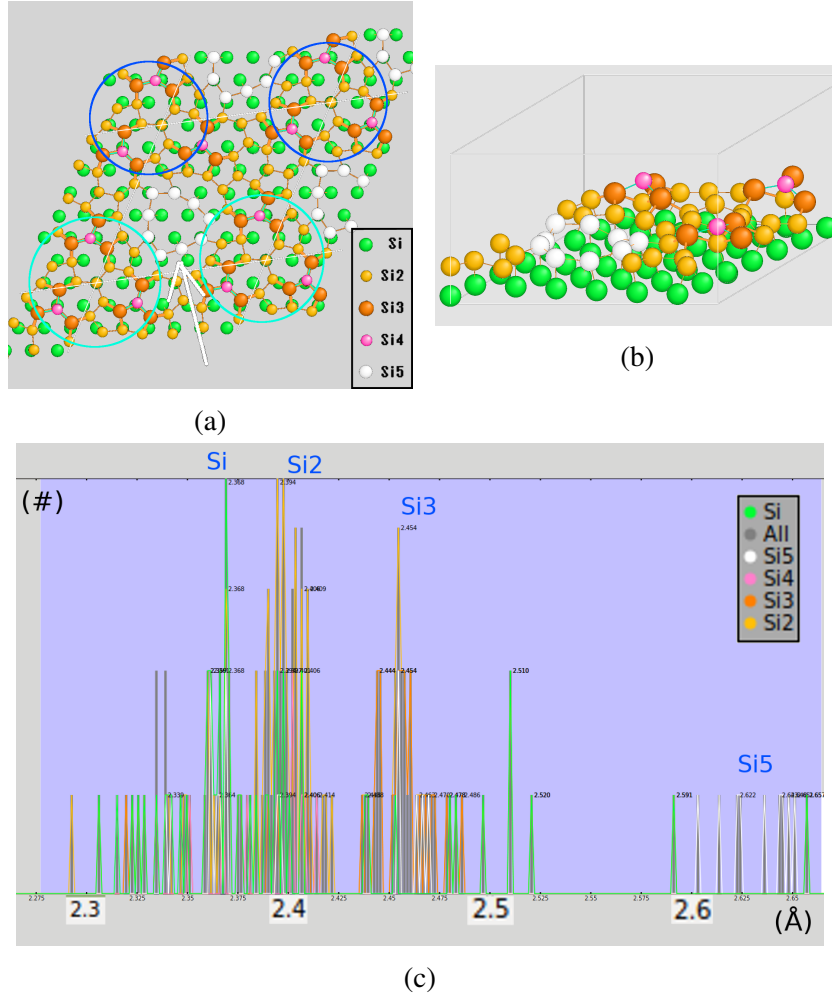
Figure 4.6: (a) Proposed structure for $\sqrt{43} \times \sqrt{43}$ structure. (b) Sideview of the structure. (c) Bond lengths distribution in the proposed structure.

atoms in this model.

The green peak is at 2.368 Å, and this is the bond lengths for the "Si" atoms from the substrate. The yellow peak is at 2.394 Å, and this represents the average bond length for "Si2" in the adlayer. The orange peak is at 2.45 Å which represents "Si3". The pink ones for "Si4" did not show clearly here since there are only three atoms with only six bonds. The bond length is about 2.4 Å. The white ones as "Si5" represents the nine white Si atoms from bridge formation. The (unrelaxed) bond length is about 2.62 Å.

The ideal Si-Si bonds for bulk Si is 2.35 Å, and the bond lengths for most of the Si atoms in this model are slightly longer but close to this value. However, the "Si5" from

bridge formation in this model is clearly apart from this group. This is not unexpected as discussed previously in Fig. 4.4. Judging by the bonding direction, the bridges do need to "shrink" from both end of the bridge in order to lower the energy. As a result, the additional two dangling bonds on both ends which seek for other adatoms to bond will start to stretch and therefore the bond length would eventually be longer than others. The longer bonding length could be one of the reasons to have unstable structures in the Metastable Phases, even though we do expect that the actual bond lengths for the "Si5" atoms would decrease appreciably after relaxation of both adlayer and substrate atom positions.

Extra adatoms on top of three tetramers for big mounds.

While the height measurement of the proposed $\sqrt{43} \times \sqrt{43}$ structure for the three sets of the small mounds agrees with our STM data, how three tetramers at the local $\sqrt{43} \times \sqrt{43}$ site became a single apparent mound is still unknown. Figure 3.18 does indicate four large mounds that clearly show the $\sqrt{43} \times \sqrt{43}$ period. The height difference from three tetramers to the top is approximately 0.87 Å in Fig. 3.18b. This suggests that additional structure were formed on top of three tetramers. We speculate that the new structure involves oxygen contamination.

$\sqrt{43} \times \sqrt{43}$ structure on C face.

The annealing condition and STM data collected from our experiments indicate some surface features for the $\sqrt{43} \times \sqrt{43}$ phase. Because of that a structure has been proposed. In previous discussion, the main process for forming this structure from 3×3 is discussed. While the proposed structure is based on experimental data on Si-face, this LEED phase was firstly found from C-face. In the following, we will discuss the $\sqrt{43} \times \sqrt{43}$ structure on C-face.

Based on our experimental method and proposed structure, we concluded that $\sqrt{43} \times \sqrt{43}$ structure need the following growth environment and condition:

- One dangling bond sticking out of the substrate per unit cell periodically with lattice constant like Si-face.

- Sufficient Si adatoms on the surface

The graphene growing experiment from He et al. [79] where the $\sqrt{43} \times \sqrt{43}$ was found does have very similar growth condition. The C-face on SiC does have one dangling bond per unit cell with proper lattice constant on the substrate. However, the growth condition indicate that the surface is a C-rich surface, and this suggests that Si adatoms on the surface at this condition is very limited. This surface condition was then updated from Li et al. [62]. This paper indicates the preferable model calculated by ab initio density functional theory (DFT) which suggests that it is preferable to have 1.3 ML when annealing with elevated temperature higher than 380 K. In other words, higher temperature annealing will form one adlayer of Si even if the surface is C-rich. This adlayer preference supports our proposed structure as well. This suggests that while the C-face start forming graphene at this annealing temperature and pressure, the local area other than graphene still is kept relatively high Si density to form at least one adlayer of Si coverage and $\sqrt{43} \times \sqrt{43}$ structure.

To this end, the growth condition on C-face for obtaining $\sqrt{43} \times \sqrt{43}$ is similar to the same LEED phase structure on Si-face. This suggests that both $\sqrt{43} \times \sqrt{43}$ from Si-face and C-face could have similar structure.

Even though the surface condition is very similar for obtaining $\sqrt{43} \times \sqrt{43}$ on both faces, there are still some inconsistencies. For example, the annealing temperature for Si-face is $1020°$ C, and it's $1220°$ C for C-face [79]. Possible reasons for this $200°$ C difference is coming from the Si-Si bond or Si-C bond between the structure and substrate. The bond length for the adlayer and substrate on C-face could also be a factor. However, further investigation is still needed such as STM on C-face to confirm.

In the paper from Li et al. [62], a proposed structure for $\sqrt{43} \times \sqrt{43}$ was also discussed as shown in Fig. 1.8. While the calculation and bonding distortion provide a low energy configuration on the surface with proper Si coverage, as applied to the Si-face, there are some inconsistencies with our data. Based on the structure proposed in Ref. [62], there are 13 dangling bonds per unit cell, and our STM data suggests that there are only three dangling

bonds per $\sqrt{43} \times \sqrt{43}$ unit cell. Dangling bond density is considered to be a main driver for surface reconstructions. For example, DFT calculations from Starke et al. indicate that their 3×3 structure was "designed to saturate as many dangling bonds as possible." [43, 96]. The $\sqrt{43} \times \sqrt{43}$ structure from Li et al. have 13 dangling bonds per unit cell, which gives 13/43 dangling bonds per SiC unit cell. On the other hand, our proposed structure have 3 dangling bonds per unit cell, which gives 3/43 bonds per SiC unit cell. However, we note that the overlying graphene layer for the C-face also could affect the energetics of the $\sqrt{43} \times \sqrt{43}$ reconstruction for that case.

In conclusion, we compare our proposed Si thin film structure to the structures found and proposed so far. We also provide growth condition and annealing environment to see if our proposed structure could apply to the LEED phase on C-face.

CHAPTER 5

CONCLUSION

Motivation and goals: The motivation for this work was the development of tools for the epitaxial growth of electronic-grade 2D materials. As a mix of the two elements highlighted as the kings of present and future electronics—and an excellent semiconductor itself—single-crystal silicon carbide was chosen as the ideal substrate material. The (0001) facet of SiC is known to support epitaxial growth of graphene, and work presented in this Thesis, in particular the discovery of the Si-rich $\sqrt{43} \times \sqrt{43}$ reconstruction, showed that it could potentially serve as a substrate for epitaxial silicene, the silicon equivalent of graphene. Our goal has been to understand and control the growth of these 2D materials and surface phases, by controlling conditions of pressure and temperature to achieve quasi-equilibrium. Most related research has focused on the growth of graphene, in the C-rich portion of the Si-C phase diagram. In this work, we developed an understanding of the Si-rich surface reconstructions, with an eye toward creating electronically useful 2D phases of silicon.

Findings: The major findings of this work are as follows:

- Discovery of the $\sqrt{43} \times \sqrt{43}$ Si-rich surface phase on SiC(0001).

  Within the chosen P, T regime of the quasi-equilibrium growth, many different Si-rich reconstructions were found—with at least two newly discovered ($\sqrt{19} \times \sqrt{21}$ and $\sqrt{43} \times \sqrt{43}$). However, their sensitivity to annealing time prompts us to classify all but one of these reconstructions as metastable phases. Due to its reproducibility and stability (under UHV), we postulate that the $\sqrt{43} \times \sqrt{43}$ reconstruction corresponds to an equilibrium surface phase, with density slightly below that of the stable 3×3 phase (1.44 ML) and in the range of previously-observed metastable phases such as

the $2\sqrt{3} \times 2\sqrt{13}$ (1.21 ML). One intriguing possibility is silicene, with an epitaxial mismatch of about +4% (tensile strain) for the 5×5 silicene unit cell (density of about 1.16 ML) or -0.76% (compressive strain) for silicene $3\sqrt{3} \times 3\sqrt{3}$ R30° on the SiC $\sqrt{43} \times \sqrt{43}$ R7.6° unit cell (1.26 ML).

- Silicon intercalation density under graphene is limited.

  Although Si intercalation was achieved at lower temperatures, under pressure and temperature conditions tuned to produce the $\sqrt{43} \times \sqrt{43}$ phase, graphene converts to SiC. Therefore, it was not possible to grow a graphene-protected $\sqrt{43} \times \sqrt{43}$ surface phase on SiC(0001).

- Surface topography of the $\sqrt{43} \times \sqrt{43}$ phase.

  Step orientations, surface corrugation amplitude, and partially-resolved details of the surface structure were obtained after vacuum transfer. The new phase grows as micron-scale flat regions, with height corrugation of $\sim$ 1.5 Å and characteristic features, some of which appear similar to adatom tetramer structures known for the 3×3 surface phase.

- Elimination of silicene as the $\sqrt{43} \times \sqrt{43}$ phase.

  Raman spectroscopy of air-exposed, Si-capped, and N_2 protected $\sqrt{43} \times \sqrt{43}$ samples showed no phonon features near those predicted for silicene. STM imaging of vacuum-transferred $\sqrt{43} \times \sqrt{43}$ samples also does not favor silicene.

- A model for the $\sqrt{43} \times \sqrt{43}$ phase.

  Applying principles based on the known physics of semiconductors and experimental results from surface phases of similar density, we propose a structural model for the $\sqrt{43} \times \sqrt{43}$ phase.

To elaborate on the last finding, a model for the $\sqrt{43} \times \sqrt{43}$ phase was constructed to obey the following postulates:

- Surface energy is minimized by eliminating dangling bonds to the greatest extent possible.

- The surface density should be slightly smaller than the 3×3 coverage and larger than 1 ML, consistent with AES results and model densities for experimentally-known phases prepared under Si-rich conditions.

- Major structural elements experimentally identified from 3×3, and metastable phases such as $2\sqrt{3} \times 2\sqrt{13}$ should comprise most of the reconstruction. Since the 3×3 structure is very stable and STM results indicate 3×3 Fourier components coexisting with $\sqrt{43} \times \sqrt{43}$ components, we view the $\sqrt{43} \times \sqrt{43}$ as a perturbation/distortion of the 3×3 to smaller coverage. Thus we retain major features of the 3×3 (tetramers) which resemble STM-resolved features of the $\sqrt{43} \times \sqrt{43}$ phase.

- Outside of the major structural elements, bond lengths should be as close as possible to the Si-Si bond length in bulk Si.

Following these postulates, we arrive at a model which has 3 dangling bonds in a unit cell of 43 bulk-termination sites. This can be compared to the Si(111) 7×7 reconstruction, which retains 19 dangling bonds in a unit cell with 49 bulk-termination sites.

Impact: We anticipate that these findings will have practical impact for silicon carbide electronics and for electronic materials derived from silicon carbide. It is conceivable that the $\sqrt{43} \times \sqrt{43}$ reconstruction could provide a path to epitaxial growth of Si on SiC or to improved Si-SiC wafer bonding, either of which would be beneficial for high-voltage, high-speed integrated Si+SiC electronics. This ordered layer might also be useful as a precursor to a uniform oxide on the SiC surface, enabling an abrupt interface and high mobility channel for SiC MOSFET devices. Furthermore, the $\sqrt{43} \times \sqrt{43}$ reconstruction and the metastable reconstructions newly discovered in this work, can provide P, T markers for the determination of furnace conditions in the growth of graphene or (perhaps) another

2D phase. Note that achieving a single rotational domain ($+7.6°$ or $-7.6°$ may be possible by enforcing registry with step edges through a substrate polished slightly off axis.

Recognizing that the similarly complex 7×7 reconstruction of Si(111) required 25 years of community effort to solve, we don't expect that our proposed model of the $\sqrt{43} \times \sqrt{43}$ phase can be entirely correct. However, our approach to "solving" the $\sqrt{43} \times \sqrt{43}$ reconstruction is very successful in reducing the number of dangling bonds on the surface. Perhaps similar methods will be useful for addressing other surface phases with large unit cells. On a related topic, it is tempting to conclude that the C-face $\sqrt{43} \times \sqrt{43}$ interface reconstruction, occurring at a nearly identical Si surface density [62], is similar to that observed for the Si-face of SiC. However, despite the similarities, there are bound to be differences because the Si-C bond length is much shorter than the Si-Si bond, which, for instance, could make the bridge configuration higher energy on the C-face. Note that the theoretical structure proposed for C-face SiC [62] is substantially different than the model introduced here.

5.1 Future Work

More research is required to confirm or refine our proposed model of the SiC(0001) Si-rich $\sqrt{43} \times \sqrt{43}$ surface phase. This could range from conventional surface techniques for both physical and electronic structure to electrical transport measurements of the stable surface phases. All measurements are complicated by the fact that the surface is easily oxidized, so appropriate methods must be implemented for in situ measurement, environmentally-controlled transfer, or surface encapsulation.

One possible way to confirm the proposed structure is the HLEED method. The STM data implies 3 dangling bonds per unit cell for the $\sqrt{43} \times \sqrt{43}$, with local atomic arrangements similar to those found on the 3×3 surface, which was previously solved using HLEED (made possible by the "beam-splitter" effect of the topmost Si adatoms). With the addition of quantitative video data acquisition to our LEED system and spot-profile analysis software, it should be possible to perform similar measurements for the $\sqrt{43} \times \sqrt{43}$ phase. This could

confirm one of the most prominent features of the reconstruction. More advanced techniques at external beamline facilities would also be useful for structural studies. These include photoelectron diffraction, surface extended X-ray absorption fine structure spectroscopy, and X-ray standing wave measurements.

In order to access other techniques, a more effective means of sample transfer should be developed. The vacuum suitcase used in our experiments worked moderately well, but is limited because it has no standalone pumping unit. Cryopumping via an in-vacuum copper braid cooled through a feedthrough with liquid nitrogen was the sole pumping source. A better design for the suitcase with integrated pumping (e.g., a non-evaporable getter pump) would reduce the pressure in the suitcase. A more flexible design for the adapter also would be beneficial for connecting to different UHV systems.

It is possible to construct a proposed structure for every phase found in Metastable Phases. According to our process for constructing the proposed structure, the bridge formation is the main reason to form different reconstruction patterns. It is possible to use this method to construct other known patterns. Improved STM measurements are also needed for confirmation. If "beam-splitter" adatoms are found, then HLEED can also be used to verify subsurface structures. There are still a few unknown patterns found in Metastable Phases. One of them was recognized as $\sqrt{19}\times\sqrt{21}$, and others are still unknown.

The $\sqrt{43} \times \sqrt{43}$ structure on C-face from Li et al. could contain structures similar to those proposed in this Thesis. However, the C-face reconstruction is an *interface* reconstruction, with an overlying layer of graphene. Furthermore, the bond lengths for Si-Si (2.35 Å in bulk Si) and Si-C (1.89 Å in bulk SiC) are much different, and this could affect especially the bridge configuration from the Si adlayer. In our model, the bridging Si atoms have bond lengths already larger than for bulk Si, and this configuration may not be energetically favorable for the C-terminated surface. STM data is needed to confirm the vertical corrugation of the C-face $\sqrt{43} \times \sqrt{43}$ reconstruction. If the STM imaging shows similar features to those of the Si-face, HLEED could help to confirm critical features of

the C-face structure.

Looking at the bigger picture of epitaxial growth of 2D materials on semiconducting substrates, it would be interesting to apply methods similar to those described in this Thesis to the growth of other potential 2D materials on SiC. For instance, germanium in its 2D sp^2-bonded version, germanene, has a lattice constant slightly under $4\,\text{Å}$, which would match the $\sqrt{43} \times \sqrt{43}$ SiC superlattice with about 1% tensile strain. So far, germanene has been created only on metallic substrates. It is an appealing material scientifically, because spin-orbit coupling and sublattice buckling could produce interesting topological effects on its electronic structure.

The path to electronic-grade 2D materials is long. I hope that the findings of this Thesis provide some small amount of guidance.

Appendices

APPENDIX A

SAMPLE GROWTH PARAMETERS

For the Si-rich region of the Si/SiC(0001) phase diagram studied in this thesis, metastable surface reconstructions were found, and one apparently stable reconstruction, i.e., the $\sqrt{43} \times \sqrt{43}$ reconstruction. Since reproducibility of results is inherently difficult within this regime, for the benefit of future research I include here the logbook entries of growth and characterization for each of the samples presented in this thesis.

The naming system for our first wafer is to have two letters followed by a number. The first letter is either "H" or "L" which indicate high (Nitrogen n-doped, $\sim 0.02 \, \Omega - cm$) or low conductive (semi-insulating) wafer. For example, "LF42" indicates the 42nd low conductive sample used. "F" refers to the name of a specific wafer.

After that, we added "4H" or "6H" to indicate the polytype, and "A" or "B" refers to the name of the wafer.

2013

1/11

AFM Si 00000 9b/9c/a1/a2/a3/a4
C 000-1 a5/a6/a7/a8/a9/aa

1/14

1400 LEED Si 600-01 blur √3x√3 + 3fold
C 597-99 √3x√3
1500 Auger Si 1.12 0.33
C 1.15 0.4

1/15

anneal@500/850C,1.9e-2torr(ArSilane),5/10min (look for 3x3)
1500 LEED Si 602 1x1 +3fold
C 603 √3x√3
anneal@1000C,2.0e-2torr(ArSilane),30min
LEED Si 607-08 ████████████████ update:2√3x2√13
C 604-06 2x2 + satellite
Auger Si 4.49 0
C 3.42 0

1/18

1200 LEED Si 611-12 weaker (to see if stable)
C 613-14 weaker
Auger Si 2.51
C 3.45
1/24 LEED Si 616 weaker (to see if stable)
C 617 1x1
anneal@1100C,2.0e-2torr(ArSilane),30min
LEED Si 620-21 √19x√21
624
C 622-23 2x2 + satellite
Auger Si 4.4
C 3.59

1/25

anneal@1100C,vacuum,30min
1200 LEED Si 625-26 √3x√3 + 2√3x6family
C 2x2 + satellite
1445 Auger Si 2.82
C 2.89
anneal@1100C,vacuum,30min
1700 LEED Si 629-30 √3x√3 + 6√3x6√3
C 631-32 3x3

1/27

Auger Si 1.50
C 1.70

1/28

anneal@1100/950C,2.0e-4(ArSilane),5/30min
LEED Si 634-35 √3x√3 + light 6√3x6√3
C 3x3

1/29

anneal@1100/950C,2.0e-3(ArSilane),5/30min (regrowth)
LEED Si 641-42 2√3x6 family
C 640 weak 3x3
Auger Si 3.26
C 1.95
anneal@950C,vacuum,20min
1500 LEED Si 643-44 √3x√3 + very weak 6√3x6√3
C 3x3

1/30
1000 Auger Si 1.88
    C 1.43
  anneal@1200C,2.0e-4(ArSilane),5min
   LEED Si 651-52 √3x√3 + super weak 6√3x6√3
   C 649-50 3x3
  Auger Si 2.42
   C 1.91
  anneal@1250C,2.0e-4(ArSilane),5min
 1700 LEED Si 653 √3x√3 + super weak 6√3x6√3
   C 654 1x1 + blur 2x2
  Auger Si 2.21
   C 2.52
1/31
  anneal@1250C,2.0e-4(ArSilane),30min
 1200 LEED Si 655 6√3x6√3 + graphene
   C 656 2x2 + graphene
  Auger Si 1.16
   C 0.75
  anneal@1250C,2.0e-3(ArSilane),30min
   LEED Si 659-60 6√3x6√3 + graphene
   C weaker 2x2 + graphene
  Auger Si 0.61   0.462ML
   C 0.47 0.352ML
2/1
 1220 LEED Si 661 6√3x6√3 + graphene
   C 662 much weaker 2x2 + graphene
 1315 Auger Si 0.68   0.462ML
   C 0.46 0.352ML
  anneal@1250C,2.0e-3(ArSilane),30min
  LEED Si 663 6√3x6√3 + ?
   C 664 weak 2x2 + graphene
  Auger Si 0.639   0.439ML
   C 0.268 0.629ML
  LEED Si 665 6√3x6√3 + graphene
2/2
  anneal@1300C,2.0e-3(ArSilane),30min
  LEED Si 668-70 6√3x6√3 + graphene
   C 666-67 weak 3x3 + graphene
  Auger Si 0.52 0.534ML
   C 0.083 1.353ML
2/4
  anneal@800C,vacuum,20min
  LEED Si 672-73 6√3x6√3 + graphene
   C 671 1x1 + graphene
  Auger Si 0.49 0.565ML
   C 0.093 1.27ML
2/5
  AFM Si 00001 50/51/52/53
   C 00001 44/45/4a/4b
  Raman 00001

2013
4/10

   1200 LEED Si 722 1x1 + blur √3x√3
       C 723 √3x√3
    1400 Auger Si 0,1,2 1.37/1.11/1.07 0.8/0.5/0.5
       C 0,1 1.14/1.140.33/0.33

4/11
  1100 **anneal@900C, 2e-3torr, 30min**
  1300 LEED Si 724 1x1 + blur √3x√3
      C 725 √3x√3   (both faces confirm with 6H-HB021)
  1400 Auger Si 0,1 1.00/1.110.5/0.5
      C 0,1 1.00/0.970.33/0.4

4/15
       anneal@900C, 2e-2torr, 30min
   LEED Si 728 1x1 + very blur √3x√3
      C 726-27 √3x√3 + super blur unknown
  1434 Auger Si 0 1.61 0.5
      C 0 2.39 0.33
  1500 **anneal@950C, 2e-2torr, 30min** (pressure drop to 1.2e-2 at the end)
   LEED Si 732-33 3x2√3? (731@edge)
      C 729-30 √3x√3
  1800 Auger Si 1 6.09 0
      C 0 3.26 0(this one might not be true)

4/16
  1100 **anneal@950C, 2.04e-2torr, 30min** (to see if the complex pattern is stable)
  1600 LEED Si 734-35 2x2 + 2√3x2√13
      C 736 √3x√3
  1714 Auger Si 0,1 6.17/7.1(6.692/7.6)   3.48ML/3.79
      C 0,1 3.64/3.35

4/17
 1115**anneal@1000C, 2e-2torr, 30min**
   LEED Si 738-41 √43x√43R52.4 + 2x2 +?
      C 737 1x1 + super weak 2x2
   Auger Si 0 4.66
      C 0 3.55
  1511 **anneal@1000C, 2e-2torr, 30min**   (so see if the pattern is stable)
   LEED Si 742-43 √43x√43R52.4 + 2x2 +?
      C 744 1x1 only
   Auger Si 1,2 6.15/6.17(6.729/6.714)   3.5ML/3.49
      C 1,2 3.65/3.98

4/18
  1037 **anneal@1050C, 2e-2torr, 30min**   (Ion gauge is down, use PG2=8.1e-3)
   LEED Si 745-46 2√3x6 + mixed?
      C 747 2x2 + satellite
   Auger Si 0,1 3.51/3.47
      C 0,1 2.97/3.38
  1630 **anneal@1050C, 2e-2torr(PG=6e-3), 30min**   (to get better pattern)
    LEEDSi 748 very blur √43x√43R52.4
      C N/A 1x1
   Auger Si 2 3.15
      C 2 3.08

4/19
  0030 **anneal@1100C, 2e-2torr(PG=6e-3), 30min**
   LEED Si 1x1 + blur pattern
      C like 2x2@high energy
  1400 **AFM** Si 00017 041902 1e/1f/20/21/22/23

C   00018   041902   2a/2b/2c/2d/2e/2f

Due to the fact that EDM9 and CMP1 are not good for our exp(both of them are not H etched), one has decided to go back to 6H-HB022 & 024(H etched furnace shut down, so no new samples)

10/7
- 1100   **anneal@1000C, 8.2e-3torr(ArSilane), 50min (to get rid of Oxygen)**
- 1300   **LEED**   Si   805 1x1 w/ blur pattern(rt7xrt7??)
- 1400   **Auger**   Si   0,1   4.55/4.70 0.5/0.5
- 1600   **anneal@800C, vacuum, 60min (to get rid of Si)**

10/8
- 1100   **LEED**   Si   t20(60eV)1x1 w/ blur pattern (relate to √43?)
- 1122   **Auger**   Si   0,1   4.18/4.52 0.3/0.3
- 1400   **anneal@800C, vacuum, 60min (to get rid of Si)**
- 1500   **LEED**   Si   t048 sharper 1x1 w/ dimmer blur pattern
- 1642   **Auger**   Si   0,1   4.04/4.135   0/0?
- 1800   **anneal@1000C, 8.2e-3torr(ArSilane), 60min**

10/9
- 1100   **LEED**   Si   807 unknown sharp pattern
- 1200   **Auger**   Si   0,1   5.07/5.00
- 1300   **anneal@1020C, 8.2e-3torr(ArSilane), 60min**
- 1500   **LEED**   Si   809 many sharper unknown pattern
- 1600   **Auger**   Si   2,3   4.78/5.28
- 1715   **anneal@1025C, 8.2e-3torr(ArSilane), 60min**
- 1820   **LEED**   Si   811 many sharp unknown pattern
- 1920   **Auger**   Si   0,1(10/10)   5.77/4.81

10/10
- 0900   sample taken out
- 1000   **AFM**   Si   00035(4/2/2014)   101000 21/22/23/24/25/26   20x20/10x10/20x20(um)
                    island: 3 in 20x20(um)
                        height:69.6(nm)
                        width:0.74(um)
- 1530   **anneal@1020C, 8.2e-3torr(ArSilane), 60min (to get rid of Oxygen)**
- 1800   **LEED**   Si   813 √43x√43 w/ unknown patterns
- 1900   **Auger**   Si   2,3   4.59/4.69
- Sample ready to transfer to downstairs system

10/13
- valve to main chamber is opened while baking out, so need to bake out the whole system.
-      (Sample is inside furnace chamber)

10/17
- 1130   **LEED**   Si   t080(60eV)   unknown patterns
- 1300   **anneal@1020C, 8.2e-3torr(ArSilane), 60min**
- 1400   **LEED**   Si   t082(60eV)   same unknown patterns
- 1700   **anneal@800C, 8.2e-3torr(Ar), 60min   (put Ar b/c might coat the window)**
- 1950   **LEED**   Si   t084(54eV)   similar unknown patterns(rt7xrt7? or 2rt3x4??)
- 2000   **anneal@1020C, 8.2e-3torr(ArSilane), 60min**
- 2200   **LEED**   Si   815 many unknown patterns

10/18
- 0930   **Auger**   Si   0   4.29
- 1000   **anneal@900C, vacuum, 120min**
- 1245   **LEED**   Si   t90-99(45-72eV)   many unknow patterns
- 1350   **Auger**   Si   1,2,3   4.88/4.84/4.77
- sample transfer to downstairs and dropped inside the RTSTM system(need to start over)

10/23
- take out sample from RTSTM and put it into upstairs system again
- bake out first

10/24
- 0530   stop baking out

0630   open manipulator chamber to main chamber
0700   anneal@1020C, 8.2e-3torr(ArSilane), 60min
0900   **LEED**   Si   816 $\sqrt{43}x\sqrt{43}$(major) w/ unknown patterns
0950   **Auger**   Si   0,1 4.79/5.02
                      5.15/5.46(new Auger model)
      transfer to do STM

12/2

transfer in w/ 6H-HB024 and test if under vacuum w/o pumping is affecting the surface
1000   **anneal@1020C, 8.2e-3 torr ArSilane, 1HR**
1330   **LEED**   824 $\sqrt{43}x\sqrt{43}$(but not as sharp as before)
start (sec)
    0
    350 close valve to main chamber for 30 min
    2150   open
    pressure file: PressMoni2013-12-03_13:37.txt
    LEED   Si   825 weaker
start (sec)
    0
    300 close valve to main chamber for 30 min
    2100   open
    pressure file: PressMoni2013-12-03_15:55.txt
    LEED   Si   826 weaker

12/4
1057   close valve again
1357   open
     pressure file: PressMoni2013-12-04_10:55.txt
1530   **LEED**   Si   827

12/5
1055   **Auger**   Si   0,1   4.1 / 3.9

12/9
      Auger   Si   0,1
      LEED   Si   828
baking out the suitcase and start again

12/12
0900   **anneal@1020C, 8.2e-3 torr ArSilane, 1HR**
    LEED   Si   829 1x1 w/ sth blur
1340   **anneal@950C, vacuum, 15 min (to see if Si on surface will be off)**
    Auger   Si   0,1
1553   **anneal@1000C, 8.2e-3 torr Ar, 10 min (to get rid of Si)**

12/13
1000   **anneal@1020C. 8.2e-3 tor ArSilane , 1HR**
1149   LEED   Si   830 $\sqrt{43}x\sqrt{43}$ sharp!!!
transfer to do STM → have some STM images, but not indicating $\sqrt{43}x\sqrt{43}$pattern

2013
6/17
    1730   AFM   Si   00030   10/11/12/13/14/15
            C   00031   16/17/18/19/1a/1b
6/18
    1000   **transfer into system**
    1300   LEED   Si   n/a   blur √3x√3
            C   n/a   sharp √3x√3
    1310   Auger   Si   0,1   0.91/0.96 0.5/0.5
            C   0,1   1.2/1.23   sth/sth
    1440   **anneal@950C,PG2=8.1e-3(Ar Silane),30min (to get rid of oxygen and√3x7+2√3x√13)**
    1600   LEED   Si   n/a   √3x√3
    1610   Auger   Si   2   Still have Oxygen
    1730   **anneal@950C,PG2=8.1e-3(Ar Silane),30min (to get rid of oxygen and√3x7+2√3x√13)**
    2100   Auger   Si   3   Still have Oxygen
7/3
    1040   LEED   Si   t002 very blur √3x√3
            C   t003 sharp √3x√3
    1050   Auger   Si   0   1.157   sth   Oxygen peak
            C   0   1.066   sth   Clear Si peak from SiO2
    1140   **anneal@1000C,PG2=8.2e-3(Ar Silane),30min (to get rid of oxygen and√3x7+2√3x√13)**
    1340   LEED   Si   778 √3x7+2√3x√13(not as strong as previous sample)
            C   t006 blur but better √3x√3
    1400   Auger   Si   1   6.059(5.422)   0
            C   1   1.475   sth
7/4
    1100 **anneal@1000C,PG2=8.2e-3(Ar Silane),30min (to see if the pattern is stable)**
    1300 LEED   Si   780 √43x√43
          C   781 2x2(w/ satellite) + √3x√3
    1400 Auger   Si   0   4.847   similar ratio by eyes
          C   0   2.819   0 or sth
7/5
    1110 **anneal@1000C,PG2=8.2e-3(Ar Silane),30min (to see if the pattern is stable)**
    1400 LEED   Si   782 blurer √43x√43
          C   783 2x2(w/ satellite) + √3x√3
    1450 Auger   Si   0   5.188   similar ratio by eyes
          C   0   3.404   0   ratio increase
7/8
    1030   **anneal@1000C,PG2=8.2e-3(Ar Silane),30min and**
         anneal@from 1000C to 700C,PG2=8.2e-3(Ar Silane),30min
         anneal@700C,PG2=8.2e-2(Ar Silane),30min
    1330   LEED   Si   784 3x3
            C   785 √3x√3
    1400   Auger   Si   0,1,2   7.34/7.02/7.2   Si peak increase &C peak decrease
            C   0   2.713   Si peak decrease
7/12
    not record yet
7/18
    not record yet

Due to the fact that EDM9 and CMP1 are not good for our exp(both of them are not H etched), one has decided
to go back to 6H-HB022 & 024(H etched furnace shut down, so no new samples)
All the data in highlight is for 6H-HB022, but 024 is inside with this series of exp

10/7
    1100   **anneal@1000C, 8.2e-3torr(ArSilane), 50min (to get rid of Oxygen)**
    1300   LEED   Si   805 1x1 w/ blur pattern(rt7xrt7??)
    1400   Auger   Si   0,1 4.55/4.70 0.5/0.5

1600 **anneal@800C, vacuum, 60min (to get rid of Si)**
10/8
1100 LEED Si t20(60eV)1x1 w/ blur pattern (relate to √43?)
1122 Auger Si 0,1 4.18/4.52 0.3/0.3
1400 **anneal@800C, vacuum, 60min (to get rid of Si)**
1500 LEED Si t048 sharper 1x1 w/ dimmer blur pattern
1642 Auger Si 0,1 4.04/4.135 0/0?
1800 **anneal@1000C, 8.2e-3torr(ArSilane), 60min**
10/9
1100 LEED Si 807 unknown sharp pattern
1200 Auger Si 0,1 5.07/5.00
1300 **anneal@1020C, 8.2e-3torr(ArSilane), 60min**
1500 LEED Si 809 many sharper unknown pattern
1600 Auger Si 2,3 4.78/5.28
1715 **anneal@1025C, 8.2e-3torr(ArSilane), 60min**
1820 LEED Si 811 many sharp unknown pattern
1920 Auger Si 0,1(10/10) 5.77/4.81
10/10
0900 sample taken out
1000 AFT Si
1530 **anneal@1020C, 8.2e-3torr(ArSilane), 60min (to get rid of Oxygen)**
1800 LEED Si 813 √43x√43 w/ unknown patterns
1900 Auger Si 2,3 4.59/4.69
Sample ready to transfer to downstairs system
10/13
valve to main chamber is opened while baking out, so need to bake out the whole system.
(Sample is inside furnace chamber)
10/17
1130 LEED Si t080(60eV) unknown patterns
1300 **anneal@1020C, 8.2e-3torr(ArSilane), 60min**
1400 LEED Si t082(60eV) same unknown patterns
1700 **anneal@800C, 8.2e-3torr(Ar), 60min (put Ar b/c might coat the window)**
1950 LEED Si t084(54eV) similar unknown patterns(rt7xrt7? or 2rt3x4??)
2000 **anneal@1020C, 8.2e-3torr(ArSilane), 60min**
2200 LEED Si 815 many unknown patterns
10/18
0930 Auger Si 0 4.29
1000 **anneal@900C, vacuum, 120min**
1245 LEED Si t90-99(45-72eV) many unknow patterns
1350 Auger Si 1,2,3 4.88/4.84/4.77
sample transfer to downstairs and dropped inside the RTSTM system(need to start over)
10/23
take out sample from RTSTM and put it into upstairs system again
bake out first
10/24
0530 stop baking out
0630 open manipulator chamber to main chamber
0700 **anneal@1020C, 8.2e-3torr(ArSilane), 60min**
0900 LEED Si 816 √43x√43(major) w/ unknown patterns
0950 Auger Si 0,1 4.79/5.02
5.15/5.46(new Auger model)
transfer to do STM
11/18
transfer in to test if Auger beam is affecting the surface
anneal@1020C, 8.2e-3 torr ArSilane 1HR
LEED Si 817 not √43x√43
Auger Si 0,1 seems no Oxygen (might need outgas furnace)(update:no need)
outgas@1100C, 8.2e-3 torr Ar, 30 min
11/19

take out sample and put it back in
1110anneal@1020C, 8.2e-3 torr ArSilane, 1HR
1700   LEED   Si   818 $\sqrt{43}$x$\sqrt{43}$ + weak(but sharp) sth
1740   Auger   Si   0,1
1755   LEED   Si   819 weaker $\sqrt{43}$x$\sqrt{43}$ (WEAKER AFTER Auger!!!)
11/20
1030   LEED   Si   820 $\sqrt{43}$x$\sqrt{43}$(→ stay i vacuum is fine)
1049   Auger   Si   0,1
1120   LEED   Si   821
1133   left Auger beam on for 1 HR
1330   LEED   Si   823
1350   Auger   Si   2,3
conclusion: Auger beam will affact the surface, but staying in the vacuum or doing LEED won't

12/2
transfer in w/ 6H-HB024 and test if under vacuum w/o pumping is affecting the surface
1000   anneal@1020C, 8.2e-3 torr ArSilane, 1HR
1330   LEED   824 $\sqrt{43}$x$\sqrt{43}$(but not as sharp as before)
start (sec)
    0
    350 close valve to main chamber for 30 min
    2150   open
    pressure file: PressMoni2013-12-03_13:37.txt
    LEED   Si   825 weaker
start (sec)
    0
    300 close valve to main chamber for 30 min
    2100   open
    pressure file: PressMoni2013-12-03_15:55.txt
    LEED   Si   826 weaker
12/4
1057   close valve again
1357   open
    pressure file: PressMoni2013-12-04_10:55.txt
1530   LEED   Si   827
12/5
1055   Auger   Si   0,1   4.1 / 3.9
12/9
    Auger   Si   0,1
    LEED   Si   828
baking out the suitcase and start again
12/12
0900   anneal@1020C, 8.2e-3 torr ArSilane, 1HR
    LEED   Si   829 1x1 w/ sth blur
1340   anneal@950C, vacuum, 15 min (to see if Si on surface will be off)
    Auger   Si   0,1
1553   anneal@1000C, 8.2e-3 torr Ar, 10 min (to get rid of Si)
12/13
1000   anneal@1020C. 8.2e-3 tor ArSilane , 1HR
1149   LEED   Si   830 $\sqrt{43}$x$\sqrt{43}$ sharp!!!
transfer to do STM → have some STM image, but not indicating $\sqrt{43}$x$\sqrt{43}$pattern

10/31
sample is used for growing buffer layer and exp for Si intercalation

outgas sample holder @1600C, 5 min

send in the sample

outgas@1050C, vacuum, 10 min
LEED   Si   n/a   rt3 x rt3 (pure)

11/2
anneal@1200C, 1e-1 Torr ArSilane, 5 min
anneal@1300C, 1e-1 Torr ArSilane, 10 min
LEED   Si   IMG4974(105eV)   6rt3 x 6rt3
Auger   Si   0,1   Si/C=   (0.66/0.65ML)
anneal@800C, 8e-3 Torr ArSilane, 10 min (to intercalate)
LEED   Si   IMG4975(105eV)   not changed
anneal@800C, 8e-3 Torr ArSilane, 40 min (to intercalate)
LEED   Si   IMG4977(105eV)   not changed

next: increase pressure ten times and see what happened

11/11
anneal@800C, 8e-2 Torr ArSilane, 10 min (to intercalate)
LEED   Si   IMG1307(103eV)   6rt3 x 6rt3 not changed
Auger   Si   0   Si/C=0.864   (0.39ML)
anneal@750C, 8e-2 Torr ArSilane, 10 min (to deposit more Si)
LEED   Si   IMG4993(105eV)   not changed
Auger   Si   1   Si/C=1.14   (0.21ML)
anneal@700C, 8e-2 Torr ArSilane, 10 min (to deposit more Si)
LEED   Si   IMG4999   not changed
Auger   Si   2   Si/C=0.99   (0.3ML)
anneal@700C, 8e-2 Torr ArSilane, another 10 min (to deposit more Si)
LEED   Si   IMG5000   not changed
Auger   Si   0   Si/C=1.262   (0.15ML)
anneal@800C, 8e-2 Torr ArSilane, another 20 min (to deposit more Si)
LEED   Si   876   intercalated
Auger   Si   1,2   Si/C=1.251   (0.16ML)

2014

3/12

1730　H-etched　　　　　　　　1400C　30min　Si face

5/23

　　　　　AFM　Si　　00056　　　　　uniform half unit cell height step

5/27

1200　sample stay at the front of the sample holder, so try to use transfer arm to adjust it
　　　sample holder crash in the furnace chamber and sample drop inside
　　　open furnace chamber and pick it

After repairing furnace and obtain new sample holder

6/26

2000　anneal@1020C, 8e-3 torr ArSilane, 1HR
　　　　　final pressure: 9.5e-3 torr

6/27

1500　LEED　Si　　850(60-120eV)　$2\sqrt{3}x\sqrt{13}$

　　　might need to anneal at higher temperature
1600　anneal@1050C, 8e-3 torr ArSilane, 1HR
1800　LEED　Si　　t12-16(50, 60, 90, 105,51eV)　　new unknown patter
　　　　　feature: m shape around middle of two SiC spots(2x2 position)

　　　I don't know what I was thinking, raising 50C is too high.

6/28

1600　anneal@1030C, 8e-3 torr ArSilane, 1HR
　　　a sudden pressure drop @ 2000 sec, from 8.5e-3 to 6e-3, and start oscillating after that
　　　start pumping @ 500C after it's done
1800　LEED　Si　　N/A　　crazy pattern

1820　try to clean surface
　　　anneal@950C, vacuum, 15 min
　　　(previous data shows that it's useless, I don't know what the hell I was thinking)

　　　Start to feel like 1HR is not really necessary, and still don't know the temperature to grow
　　　found out that Silane break to Si and H at 420C
1900　anneal@1010C, 8e-3 torr ArSilane, 20 min
　　　start to pump @ 370C

6/29

1500　LEED　Si　　N/A　　$\sqrt{3}x\sqrt{3}+2\sqrt{3}x\sqrt{13}$
　　　again, temperature is not high enough

1515　anneal@1020C, 8e-3 torr ArSilane, 30 min
　　　start pumping @400C
　　　pressure oscillate @ 1400 sec, may be caused by RF freq 196k Hz
1600　LEED　Si　　N/A　　not the right pattern

1700　use another one method to clean surface
　　　anneal@1000C, 8e-3 torr Ar, 10 min
　　　anneal@1030C, 8e-3 torr ArSilane, 1 HR
　　　furnace shaking @ 2000 sec RF:196k Hz
2200　LEED　Si　　851&t18(105eV)　$\sqrt{43}x\sqrt{43}+2x2 +sth$ (finally!!!)
　　　　　pattern shows clear 2x2 which doesn't overlap with $\sqrt{43}x\sqrt{43}$ and something
else

6/30

    1000   heat sample to 400 degree to see if the pattern will be gone
                anneal@400C, vacuum, 10 min

    1030   LEED   Si   852(51-60eV)   blur$\sqrt{43}$x$\sqrt{43}$+2x2 +sth (weaker but the same pattern)

                try previous recipe to make it clear
                anneal@1000C, 8e-3 torr Ar, 10 min

    1300   LEED   Si   853(51-60eV)   super **sharp $\sqrt{43}$x$\sqrt{43}$**
                      note: pure $\sqrt{43}$x$\sqrt{43}$ pattern, no other pattern or spots
    1400   Auger   Si   0,1   Si/C = 5.019/5.1(new model, and comapare to before, it's similar)

                now try to destroy the pattern by change the phase back to 3x3
                anneal@800C, 8e-3 torr ArSilane, 5 min
                start pumping right after it's done
    1430   LEED   Si   N/A   blur $\sqrt{43}$x$\sqrt{43}$
             Auger   Si   2   4.922

                either 5 min is not enough or temperature is not low enough
    1700   anneal@700C, 8e-3 torr ArSilane, 10 min
    1750   LEED   Si   N/A   3x3 (no other pattern)
             Auger   Si   0   5.~
             Auger peak doesn't show right peak shape so it's estimate by me, and it shows that there is more
Si on the surface

    2100   maybe with right amount of Si on surface with the same temperature can get $\sqrt{43}$x$\sqrt{43}$ structure
                anneal@1030C, 8e-3 torr Ar, 10 min
             LEED   Si   N/A   1x1
             fine! it's not working.

7/1

                try to get $\sqrt{43}$x$\sqrt{43}$ again, with less time annealing
    1000   anneal@1030C, 8e-3 torr ArSilane, 30min
                furnace vibrate again
                start pumping right after it's done
    1140   LEED   Si   854   crazy pattern
                     note: this pattern might have the same pattern from previous crazy pattern, but it has more
other spots which seems to be another crazy pattern

                try "clean surface" again to see what happen
    1700   anneal@1000C, 8e-3 torr Ar, 10min
             LEED   Si   855   weak but the same crazy pattern with sharp $\sqrt{3}$x$\sqrt{3}$

                8e-3 torr Ar is not useful , so clean it under vacuum will be the same thing
                try again
    2130   anneal@1030C, 8e-3 torr ArSilane, 30min
                furnace vibrate @ 1200 sec and stop @ 1400
                start pumping @ 400C
    1040   LEED   Si   856   same pattern as the first crazy pattern(1050C, 8e-3 torr, 1HR)
7/2

    1100   anneal@1000C, 8e-3 torr Ar, 10min
    1130   LEED   Si   857   weak but the same crazy pattern (no $\sqrt{3}$x$\sqrt{3}$)

    start to think it might be true that sample is needed to anneal for 1 HR

	1400	anneal@1030C, 8e-3 torr ArSilane, 1 HR

note: doesn't have LEED data, I probably forgot to write it down, which means it's not worth mentioning

7/3

1030   try to get 3x3 again and start over, 5 min was not enough last time
         anneal@700C, 8e-3 torr ArSilane, 10 min
         anneal@1030C, 8e-3 torr ArSilane, 30 min
         start pumping @ 400C
1200   LEED   Si   858   same crazy pattern

1300   try to get 3x3 again and confirm if it's actually 3x3 by LEED
         anneal@700C, 8e-3 torr ArSilane, 10 min
1400   LEED   Si   859   blur √43x√43 (oh, what the hell)

1430   clean surface again to see if it gets sharper LEED pattern
         anneal@1000C, 8e-3 torr Ar, 10min
         LEED   Si   860   super sharp √43x√43 (oh, what the hell!!!)

7/7

1100   transfer to do Raman

7/8

LEED   1x1

7/22

send in sample again
1020   outgas @600C, vacuum, 10 min
1030   record pressure for calculating flow rate
                 "PressMoni2014-07-22_10:37.txt"
                 leak valve: 7 ⅝ turn
                 turbo pump valve: fully open and then fuuly closed, and then open a little until 8e-3torr
1048   anneal@1030C, 8e-3torr ArSilane, 30 min
1300   LEED   Si   862   crazy pattern

1400   anneal@700C, 8e-3torr ArSilane, 10 min
         LEED   Si   863   pure 3x3
1530   AUger   Si   0,1   5.461/4.893

1600   anneal@1030C, 8e-3torr ArSilane, 40 min
1630   LEED   Si   864   repeated crazy pattern from before

1730   anneal@700C, 8e-3torr ArSilane, 10 min
2000   LEED   Si   865   √43x√43 with 2x2
2030   anneal@1000C, vacuum, 10 min
2055   LEED   Si   866   sharp √43x√43 !!(reproducible)

7/23

1100   anneal@400C, vacuum, 10 min
1230   LEED   Si   867   weaker √43x√43
1250   anneal@1000C, vacuum, 10 min (see if the pattern stay)
1850   LEED   Si   N/A   pure 1x1

8/5

1600   anneal@1000C, 8e-3torr ArSilane, 40 min
2100   LEED   Si   N/A   1x1 with sth related to √43

8/6

1000   anneal@1000C, vacuum, 10 min

```
1030    LEED    Si      N/A     1x1 with sth related to √43
```
1130   anneal@1020C, 8e-3torr ArSilane, 40 min
```
1230    LEED    N/A     crazy pattern same as reproducible process

1300    anneal@1000C, 8e-3torr ArSilane, 10 min
1400    LEED    N/A     super sharp √43x√43
```

crazy pattern will lead to √43x√43
"getting sharper √43x√43 can be done under Silane pressure"

```
1530        anneal@700C, 8e-3torr ArSilane,15 min (to get 3x3)
1600    LEED    Si      t001(60eV)      2x2 + √3x√3 +  2√3x2√13

1610        anneal@700C, 8e-3torr ArSilane,10 min (to get 3x3)
1630    LEED    N/A     sharp 3x3(nothing else)

1644        anneal@1030C, 8e-3torr ArSilane,40 min
            anneal@1000C, 8e-3torr ArSilane,10 min
1800    LEED    Si      N/A     same reproducible crazy pattern

1810        anneal@400C, vacuum ( 1e-8 torr) ,10 min
1830    LEED    Si      N/A     same reproducible crazy pattern but weaker

2030        anneal@600C, vacuum(1e-8torr),10 min
            LEED    Si      N/A     √3x√3 + very very weak √43x√43
```

8/7
```
1000        anneal@700C, 8e-3torr ArSilane,20 min(to get 3x3)
1030    LEED    Si      N/A     not super sharp 3x3

1037        anneal@ 1030C, 8e-3torr ArSilane,40 min
            anneal@700C, 8e-3torr ArSilane,10min(rt43)
1150    LEED    Si      N/A     very weak but sharp reproducible crazy pattern

1155        anneal@1000C, vacuum(1e-8torr),10 min
            LEED    Si      N/A     same crazy pattern with something else

1400        anneal@700C, 8e-3torr ArSilane,10 min
            anneal@1000C, 8e-3torr ArSilane,10 min
            LEED    Si      N/A     unknown blur pattern

1444        anneal@1020C, 8e-3torr ArSilane,40 min
            LEED    Si      N/A     reproducible crazy pattern

1600        anneal@700C, 8e-3torr ArSilane,10 min
            LEED    Si      N/A     same crazy pattern

1600        anneal@1000C, vacuum(2e-7torr),10 min
            LEED    Si      t009(57eV)      unknown(what the fuck)
```
8/25
```
1345        anneal@1030C, 8e-3torr ArSilane,40 min
            LEED    Si      N/A     reproducible crazy pattern
```
install vacuum suitcase and bake out
8/27

```
1300    LEED    Si      N/A       same
1340    anneal@700C, 8e-3torr ArSilane,10 min
        LEED    Si      N/A       3x3(a little blur)
1430    anneal@700C, 8e-3torr ArSilane,10 min (to get pure 3x3)
        anneal@1030C, 8e-3torr ArSilane,40 min (to get rt43)  (start pumping right after)
        LEED    Si      N/A       rt3 x rt3 + same crazy pattern
        anneal@1000C, vacuum, 10 min
        LEED    Si      N/A       same
        anneal@700C, 8e-3torr ArSilane,15 min (to get 3x3 and start over)
        LEED    Si      N/A       1x1      weak crazy pattern
        anneal@1000C, vacuum,15 min (to get rt3 x rt3, clean surface)
2100    anneal@1050C, vacuum, 20 min (to get rt3 and clean surface)
        LEED    Si      N/A       rt3 x rt3

8/28

        anneal@1030C, 8e-3torr ArSilane,40 min (rt43)
        LEED    Si      N/A       1x1
        anneal@1030C, 8e-3torr ArSilane,40 min (rt43)
        (pressure suddenly drop at 500 sec, decide to stop and do LEED to see what's going on)
        LEED    Si      N/A       1x1
        anneal@1050C, vacuum, 40 min (start over)
        LEED    Si      N/A       rt3 x rt3
        anneal@1030C, 8e-3torr ArSilane,40 min (rt43)
        anneal@1000C, vacuum,40 min (rt3)
        LEED    Si      N/A       rt3 x rt3
        anneal@1030C, 8e-3torr ArSilane,40 min
        LEED    Si      N/A       1x1
        anneal@700C, 8e-3torr ArSilane,15 min (3x3)
        LEED    Si      n/a       1x1 with sth
        anneal@1030C, 8e-3torr ArSilane,40 min(rt43)
        LEED    Si      n/a       1x1 with weak unknown
        anneal@700C, 8e-3torr ArSilane, 40(?) min
        LEED    Si      IMG4708(57eV)   2rt3 x 6 with sth(?)

8/29

        anneal@1050C, vacuum,50 min (rt3)
        LEED    Si      n/a       rt3 x rt3
        anneal@750C, 8e-3torr ArSilane,15 min (3x3)
        LEED    Si      IMG4709(57eV)   4x4
        anneal@750C, 8e-3torr ArSilane,15 min (3x3)
        LEED    Si      IMG4711(54eV)   ?

        there might be a temperature shift

        anneal@650C, 8e-3torr ArSilane,15 min (3x3)
        LEED    SI      N/A       3x3 (so, yes, there is a temp shift due to the Si caoting on furnace)
        anneal@950C, 8e-3torr ArSilane,40 min(rt43)
        LEED    Si      IMG4713(?)        ?
        anneal@970C, 8e-3torr ArSilane,40 min (rt43)
        LEED    Si      rt43 x rt43 + 2 x 2 (finally)
        anneal@950C, vacuum ,5 min
        LEED    Si      n/a       mixed pattern
        anneal@970C, vacuum,10 min (sharp)
        LEED    Si      n/a       1x1
        anneal@970C, 8e-3torr ArSilane,40 min(rt43)
        LEED    Si      IMG4714(54eV)   rt43 x rt43 + 2x2
```

9/2

LEED   Si   IMG4716(54eV)   rt43 x rt43 + 2x2
transfer to do STM

2014
3/12

    1730   H-etched   1400C   30min   Si face

9/23

        outgas@1050C, vacuum, 15 min
        anneal@650C, 8e-3 torr ArSilane, 15 min
        anneal@970C, 8e-3 torr ArSilane, 40 min (rt43)
        LEED   Si   n/a   blur sth(not rt43)

9/24

        anneal@970C, 8e-3 torr ArSilane, 10 min (rt43)
        LEED   rt43

        transfer under to do STM

        successfully transfered with clear rt43 pattern

2012

10/22

before anneal

LEED

      18 Si   576-8   √3x√3 a little sharp

      18 C   574-5   √3x√3 a little blur

10/23

Auger

      18

anneal@850C , PG2=3E-4 Torr(Silane Only) , 20min

LEED

      18 Si   579-80 sharp 1x1 + super blur √3x√3

      18 C   582-4   √3x√3 (intensity interesting)

Auger

      18   _2,3,0_C

              _0,1,2_Si

10/24

anneal@1300C , PG2=4E-4 Torr(Silane Only) , 20min

LEED

      18 Si   585-8   6√3x6√3 + some GR

      18 C   1x1 but not clear

      42 Si   not diffraction patter

      42 C   not diffraction patter

Auger

      18   _0,1_Si

              _0,1_C

      42   _0_C

LEED

      18 Si   589-90 6√3x6√3 + some GR (I think this is my practice)

10/26

<mark>**anneal@1350C , PG2=1E-4 Torr(Silane Only) , 20min**</mark>

LEED

      couldn't operate camera

Auger

      18   _0,1_Si

              _0,1_C

      42   _0,1,2_Si

              _0,1_C

10/30

LEED

      18 Si   591   6√3x6√3 + some GR

      18 C   592   1x1 + GR ring + hex 2 dots on ring(what is this?)

42 Si   593   6√3x6√3 + some GR
42 C   594   GR ring with some spots on ring

√43

40 Si   561
40 C   566
41 Si   564
41 C   567

2012

11/12

  (first growth)

  anneal@800C , PG2=2E-4 Torr(Silane, flow) , 20min

  anneal@1200C , PG2=2E-4 Torr(Ar Silane) , 20min

  anneal@1350C , PG2=2E-4 Torr(Ar Silane) , 20min

  LEED

    43 Si LEED_Louis $6\sqrt{3}x6\sqrt{3}$ + some GR

    43 C LEED_Louis 1x1+GR ring + √43x√43

    44 Si LEED_Louis $6\sqrt{3}x6\sqrt{3}$ + some GR

    44 C LEED_Louis 1x1+GR ring + √43x√43 (weaker)

11/14

  Auger

    43 _0,1,2_Si 0.467 ML

      _0,1,2_C 0.177 ML

    44 _0,1,2_Si 0. 467 ML

      _0,1,2_C 0. 173 ML

11/19

  (test quasi-equillibrium)

  (second growth)

  anneal@1350C , PG2=2E-4 Torr(Silane, flow) , 20min

  LEED

    43 Si LEED_Louis $6\sqrt{3}x6\sqrt{3}$ + some GR

    43 C LEED_Louis 1x1+GR ring (no √43)

    44 Si LEED_Louis $6\sqrt{3}x6\sqrt{3}$ + some GR

    44 C LEED_Louis 1x1+GR ring (no √43)

  Auger (GR is more this time. -> not equillibrium)

    43 _0,1_Si 0.717 ML

      _0,1_C 0.653 ML

    44 _0,1_Si 0. 653 ML

      _0,1_C 0. 815 ML

11/20

  (third growth, higher pressure, change to Ar Silane back filled)

  anneal@1350C , PG2=1E-3 Torr(Ar Silane, flow with leak valve) , 20min

  LEED

    43 Si LEED_Louis $6\sqrt{3}x6\sqrt{3}$ + some GR

    43 C LEED_Louis 1x1+GR ring + super blur √43

    44 Si LEED_Louis $6\sqrt{3}x6\sqrt{3}$ + some GR

    44 C LEED_Louis   1x1+GR ring (no √43)

  Auger

    43 _0,1_Si 0.618ML

      _0,1_C 0.77ML

44		0.688ML
		0.95ML

11/21

(fourth growth, higher pressure)

anneal@1350C , PG2=1.27E-2 Torr(Ar Silane, flow with leak valve) , 20min

LEED

43 Si	LEED_Louis	6√3x6√3 + some GR
43 C	LEED_Louis	1x1+GR ring (<mark style="background-color: red">no √43</mark>)
44 Si	LEED_Louis	6√3x6√3 + some GR
44 C	LEED_Louis	1x1+GR ring (<mark style="background-color: red">no √43</mark>)

Auger

43	_2,3,4_Si	0.7ML
	_0,1,2_C	0.78ML
44	_2,3,4_Si	0.688ML
	_0,1,2,3_C	1.072ML

√43

40 Si	561
40 C	566
41 Si	564
41 C	567

REFERENCES

[1] P. Miro, M. Audiffred, and T. Heine, "An atlas of two-dimensional materials," *Chem. Soc. Rev.*, vol. 43, pp. 6537–6554, 18 2014.

[2] N. D. Mermin, "Crystalline Order in 2 Dimensions," *Physical Review*, vol. 176, no. 1, pp. 250–&, 1968.

[3] K. S. Novoselov, A. K. Geim, S. V. Morozov, D. Jiang, Y. Zhang, S. V. Dubonos, I. V. Grigorieva, and A. A. Firsov, "Electric Field Effect in Atomically Thin Carbon Films," *Science*, vol. 306, no. 5696, pp. 666–669, 2004.

[4] C. Berger, Z. Song, T. Li, X. Li, A. Y. Ogbazghi, R. Feng, Z. Dai, A. N. Marchenkov, E. H. Conrad, P. N. First, and W. A. de Heer, "Ultrathin Epitaxial Graphite: 2D Electron Gas Properties and a Route toward Graphene-based Nanoelectronics," *The Journal of Physical Chemistry B*, vol. 108, no. 52, pp. 19 912–19 916, 2004.

[5] Y. Zhang, Y.-W. Tan, H. L. Stormer, and P. Kim, "Experimental observation of the quantum Hall effect and berry's phase in graphene," *Nature*, vol. 438, no. 7065, pp. 201–204, Nov. 2005.

[6] K. S. Novoselov, A. K. Geim, S. V. Morozov, D. Jiang, M. I. Katsnelson, I. V. Grigorieva, S. V. Dubonos, and A. A. Firsov, "Two-dimensional gas of massless Dirac fermions in graphene," *Nature*, vol. 438, no. 7065, pp. 197–200, Nov. 2005.

[7] M. Zeng, Y. Xiao, J. Liu, K. Yang, and L. Fu, "Exploring two-dimensional materials toward the next-generation circuits: From monomer design to assembly control," *Chemical reviews.*, vol. 118, no. 13, pp. 6236–6296, 2018.

[8] S. Z. Butler, S. M. Hollen, L. Y. Cao, Y. Cui, J. A. Gupta, H. R. Gutierrez, T. F. Heinz, S. S. Hong, J. X. Huang, A. F. Ismach, E. Johnston-Halperin, M. Kuno, V. V. Plashnitsa, R. D. Robinson, R. S. Ruoff, S. Salahuddin, J. Shan, L. Shi, M. G. Spencer, M. Terrones, W. Windl, and J. E. Goldberger, "Progress, Challenges, and Opportunities in Two-Dimensional Materials Beyond Graphene," *ACS Nano*, vol. 7, no. 4, pp. 2898–2926, Apr. 2013.

[9] M. Ashton, J. Paul, S. B. Sinnott, and R. G. Hennig, "Topology-Scaling Identification of Layered Solids and Stable Exfoliated 2D Materials," *Phys. Rev. Lett.*, vol. 118, p. 106 101, 10 2017.

[10] N. Mounet, M. Gibertini, P. Schwaller, D. Campi, A. Merkys, A. Marrazzo, T. Sohier, I. E. Castelli, A. Cepellotti, G. Pizzi, and N. Marzari, "Two-dimensional

materials from high-throughput computational exfoliation of experimentally known compounds," *Nature Nanotechnology*, vol. 13, no. 3, pp. 246–+, Mar. 2018.

[11]   S. Haastrup, M. Strange, M. Pandey, T. Deilmann, P. S. Schmidt, N. F. Hinsche, M. N. Gjerding, D. Torelli, P. M. Larsen, A. C. Riis-Jensen, J. Gath, K. W. Jacobsen, J. J. Mortensen, T. Olsen, and K. S. Thygesen, "The Computational 2D Materials Database: high-throughput modeling and discovery of atomically thin crystals," *2D Materials*, vol. 5, no. 4, p. 042 002, 2018.

[12]   J. A. Venables, *Introduction to Surface and Thin Film Processes*. Cambridge University Press, 2000.

[13]   A. J. van Bommel, J. Crombeen, and A. van Tooren, "LEED and Auger electron observations of the SiC(0001) surface," *Surface Science*, vol. 48, no. 2, pp. 463–472, 1975.

[14]   J. B. Hannon and R. M. Tromp, "Pit formation during graphene synthesis on SiC(0001): In situ electron microscopy," *Physical Review B*, vol. 77, no. 24, p. 241 404, Jun. 2008.

[15]   W. A. de Heer, C. Berger, M. Ruan, M. Sprinkle, X. Li, Y. Hu, B. Zhang, J. Hankinson, and E. Conrad, "Large area and structured epitaxial graphene produced by confinement controlled sublimation of silicon carbide," *Proceedings of the National Academy of Sciences of the United States of America*, vol. 108, no. 41, pp. 16 900–16 905, Oct. 2011.

[16]   N. Camara, B. Jouault, A. Caboni, B. Jabakhanji, W. Desrat, E. Pausas, C. Consejo, N. Mestres, P. Godignon, and J. Camassel, "Growth of monolayer graphene on 8 degrees off-axis 4H-SiC (000-1) substrates with application to quantum transport devices," *Applied Physics Letters*, vol. 97, no. 9, p. 093 107, Aug. 2010.

[17]   C. Celebi, C. Yanik, A. G. Demirkol, and I. I. Kaya, "The effect of a SiC cap on the growth of epitaxial graphene on SiC in ultra high vacuum," *Carbon*, vol. 50, no. 8, pp. 3026–3031, Jul. 2012.

[18]   M. Sprinkle, M. Ruan, Y. Hu, J. Hankinson, M. Rubio-Roy, B. Zhang, X. Wu, C. Berger, and W. A. de Heer, "Scalable templated growth of graphene nanoribbons on SiC," *Nat Nano*, vol. 5, no. 10, pp. 727–731, Oct. 2010.

[19]   R. M. Tromp and J. B. Hannon, "Thermodynamics and Kinetics of Graphene Growth on SiC(0001)," *Physical Review Letters*, vol. 102, no. 10, p. 106 104, Mar. 2009.

[20]   K. V. Emtsev, A. Bostwick, K. Horn, J. Jobst, G. L. Kellogg, L. Ley, J. L. McChesney, T. Ohta, S. A. Reshanov, J. Rohrl, E. Rotenberg, A. K. Schmid, D. Waldmann, H. B.

Weber, and T. Seyller, "Towards wafer-size graphene layers by atmospheric pressure graphitization of silicon carbide," *Nat. Mater.*, vol. 8, no. 3, pp. 203–207, Mar. 2009.

[21] F. Ming and A. Zangwill, "Model and simulations of the epitaxial growth of graphene on non-planar 6H–SiC surfaces," *Journal of Physics D: Applied Physics*, vol. 45, no. 15, p. 154 007, 2012.

[22] R. Kaplan, "Surface-structure and Composition of Beta-SiC and 6H-SiC," *Surface Science*, vol. 215, no. 1-2, pp. 111–134, 1989.

[23] W. J. Choyke, D. R. Hamilton, and L. Patrick, "Optical Properties of Cubic SiC: Luminescence of Nitrogen-Exciton Complexes, and Interband Absorption," *Phys. Rev.*, vol. 133, A1163–A1166, 4A 1964.

[24] M. Bhatnagar and B. Baliga, "Comparison of 6H-SiC, 3C-SiC, and Si for power devices," *Electron Devices, IEEE Transactions on*, vol. 40, no. 3, pp. 645–655, 1993.

[25] A. K. Agarwal, S. Seshadri, M. MacMillan, S. S. Mani, J. Casady, P. Sanger, and P. Shah, "4H-SiC p-n diodes and gate turnoff thyristors for high-power, high-temperature applications," *Solid-state Electronics*, vol. 44, no. 2, pp. 303–308, Feb. 2000.

[26] J. A. Lely, *Sublimation process for manufacturing silicon carbide crystals*, US Patent 2,854,364, 1958.

[27] Y. Tairov and V. Tsvetkov, "Crystal Growth and Polytypism in Silicon Carbide," English, in *Growth of Crystals*, E. Givargizov, Ed., Springer US, 1986, pp. 117–124.

[28] K. Heinz, J. Bernhardt, J. Schardt, and U. Starke, "Functional surface reconstructions of hexagonal SiC," *Journal of Physics-condensed Matter*, vol. 16, no. 17, S1705–S1720, May 2004.

[29] R. Cheung, *Silicon Carbide Microelectromechanical Systems for Harsh Environments*. Singapore: Imperial College Press, 2006.

[30] Wikipedia contributors, *Two-dimensional materials — Wikipedia The Free Encyclopedia*, [Online; accessed 28-November-2019], 2019.

[31] J. Schardt, J. Bernhardt, U. Starke, and K. Heinz, "Crystallography of the (3X3) surface reconstruction of 3C-SiC(111), 4H-SiC(0001), and 6H-SiC(0001) surfaces retrieved by low-energy electron diffraction," *Physical Review B*, vol. 62, no. 15, pp. 10 335–10 344, Oct. 2000.

[32] C. Riedl, C. Coletti, and U. Starke, "Structural and electronic properties of epitaxial graphene on SiC(0 0 0 1): a review of growth, characterization, transfer doping

and hydrogen intercalation," *Journal of Physics D-applied Physics*, vol. 43, no. 37, p. 374 009, Sep. 2010.

[33] U. Starke and C. Riedl, "Epitaxial graphene on SiC(0001) and SiC(0001bar) : from surface reconstructions to carbon electronics," *Journal of Physics: Condensed Matter*, vol. 21, no. 13, p. 134 016, 2009.

[34] J. Sforzini, L. Nemec, T. Denig, B. Stadtmüller, T.-L. Lee, C. Kumpf, S. Soubatch, U. Starke, P. Rinke, V. Blum, F. C. Bocquet, and F. S. Tautz, "Approaching Truly Freestanding Graphene: The Structure of Hydrogen-Intercalated Graphene on $6H-$SiC(0001)," *Phys. Rev. Lett.*, vol. 114, p. 106 804, 10 2015.

[35] C. Xia, S. Watcharinyanon, A. A. Zakharov, R. Yakimova, L. Hultman, L. I. Johansson, and C. Virojanadara, "Si intercalation/deintercalation of graphene on 6H-SiC(0001)," *Phys. Rev. B*, vol. 85, p. 045 418, 4 2012.

[36] S. Oida, F. R. McFeely, J. B. Hannon, R. M. Tromp, M. Copel, Z. Chen, Y. Sun, D. B. Farmer, and J. Yurkas, "Decoupling graphene from SiC(0001) via oxidation," *Physical Review B*, vol. 82, no. 4, p. 041 411, Jul. 2010.

[37] C. Virojanadara, M. Hetzel, L. I. Johansson, W. J. Choyke, and U. Starke, "Electronic and atomic structure of the 4H-SiC(1(1)over-bar02)-c(2x2) surface," *Surface Science*, vol. 602, no. 2, pp. 525–533, Jan. 2008.

[38] L. Li and I. S. T. Tsong, "Atomic structures of 6H-SiC(0001) and (0001) surfaces," *Surface Science*, vol. 351, no. 1-3, pp. 141–148, May 1996.

[39] S. Tanaka, R. S. Kern, and R. F. Davis, "Effects of Gas-flow Ratio on Silicon-carbide Thin-film Growth Mode and Polytype Formation during Gas-source Molecular-beam Epitaxy," *Applied Physics Letters*, vol. 65, no. 22, pp. 2851–2853, Nov. 1994.

[40] M. A. Kulakov, G. Henn, and B. Bullemer, "SiC(0001)3x3-Si surface reconstruction - A new insight with a STM," *Surface Science*, vol. 346, no. 1-3, pp. 49–54, Feb. 1996.

[41] K. Takayanagi, Y. Tanishiro, S. Takahashi, and M. Takahashi, "Structure analysis of Si(111)-7 × 7 reconstructed surface by transmission electron diffraction," *Surface Science*, vol. 164, no. 2–3, pp. 367–392, 1985.

[42] R. Kaplan and T. M. Parrill, "Reduction of SiC Surface Oxides by a Ga Molecular-beam - Leed and Electron-spectroscopy Studies," *Surface Science*, vol. 165, no. 2-3, pp. L45–L52, Jan. 1986.

[43] U. Starke, J. Schardt, J. Bernhardt, M. Franke, K. Reuter, H. Wedler, K. Heinz, J. Furthmuller, P. Kackell, and F. Bechstedt, "Novel reconstruction mechanism for

dangling-bond minimization: Combined method surface structure determination of SiC(111)-(3x3)," *Physical Review Letters*, vol. 80, no. 4, pp. 758–761, Jan. 1998.

[44] Y. Li, L. Ye, and X. Wang, "A new structural model for the SiC(0001)(3 x 3) surface derived from first principles studies," *Surface Science*, vol. 600, no. 2, pp. 298–304, Jan. 2006.

[45] K. Heinz, A. Seubert, and D. K. Saldin, "Holographic low-energy electron diffraction," *Journal of Physics: Condensed Matter*, vol. 13, no. 47, pp. 10 647–10 663, 2001.

[46] G. Baffou, A. J. Mayne, G. Comtet, G. Dujardin, L. Stauffer, and P. Sonnet, "SiC(0001) 3 x 3 Heterochirality Revealed by Single-Molecule STM Imaging," *Journal of the American Chemical Society*, vol. 131, no. 9, pp. 3210–3215, Mar. 2009.

[47] F. Owman and P. Martensson, "STM Study of the SiC(0001)root-3x-root-3 Surface," *Surface Science*, vol. 330, no. 1, pp. L639–L645, Jun. 1995.

[48] S. Nakanishi, H. Tokutaka, K. Nishimori, S. Kishida, and N. Ishihara, "The Difference between 6H-SiC (0001) and (0001) Faces Observed by AES, LEED and ESCA," *Applied Surface Science*, vol. 41-2, pp. 44–48, Nov. 1989.

[49] L. I. Johansson, F. Owman, and P. Martensson, "High-resolution core-level study of 6H-SiC(0001)," *Physical Review B*, vol. 53, no. 20, pp. 13 793–13 802, May 1996.

[50] J. M. Themlin, I. Forbeaux, V. Langlais, H. Belkhir, and J. M. Debever, "Unoccupied surface state on the (root 3x root 3) R30 degrees reconstruction of 6H-SiC(0001)," *Europhysics Letters*, vol. 39, no. 1, pp. 61–66, Jul. 1997.

[51] U. Starke, J. Schardt, J. Bernhardt, M. Franke, and K. Heinz, "Stacking transformation from hexagonal to cubic SiC induced by surface reconstruction: A seed for heterostructure growth," *Physical Review Letters*, vol. 82, no. 10, pp. 2107–2110, Mar. 1999.

[52] A. Coati, M. Sauvage-Simkin, Y. Garreau, R. Pinchaux, T. Argunova, and K. Aid, "(sqrt [3]× sqrt [3]) R30 reconstruction of the 6H-SiC (0001) surface: A simple T4 Si adatom structure solved by grazing-incidence x-ray diffraction," *Physical Review B*, vol. 59, no. 19, p. 12 224, 1999.

[53] J. B. Pendry, "Reliability factors for LEED calculations," *Journal of Physics C: Solid State Physics*, vol. 13, no. 5, p. 937, 1980.

[54] A. Seubert, D. K. Saldin, J. Bernhardt, U. Starke, and K. Heinz, "Avoidance of ghost atoms in holographic low-energy electron diffraction (LEED)," *Journal of Physics-condensed Matter*, vol. 12, no. 26, pp. 5527–5540, Jul. 2000.

[55] J. Bernhardt, A. Seubert, M. Nerding, U. Starke, and K. Heinz, "Atomic structure of 6H-SiC(000(1)over-bar)-(2x2)(c)," *Silicon Carbide and Related Materials - 1999 Pts, 1 & 2*, vol. 338-3, pp. 345–348, 2000.

[56] M. Naitoh, J. Takami, S. Nishigaki, and N. Toyama, "A (2sqrt(3) x 2sqrt(13)) surface phase in the 6H–SiC(0001) surface studied by scanning tunneling microscopy," *Applied Physics Letters*, vol. 75, no. 5, pp. 650–652, 1999.

[57] D. Martrou, T. Leoni, F. Chaumeton, F. Castanié, S. Gauthier, and X. Bouju, "Giant (1212) and (48) reconstructions of the 6*H*-SiC(0001) surface obtained by progressive enrichment in Si atoms," *Phys. Rev. B*, vol. 97, p. 081 302, 8 2018.

[58] X. Xie, H. Wang, A. Wee, and K. P. Loh, "The evolution of $3 \times 3, 6 \times 6, \sqrt{3} \times \sqrt{3}R30°$ and $6\sqrt{3} \times 6\sqrt{3}R30°$ superstructures on 6H-SiC (0001) surfaces studied by reflection high energy electron diffraction," *Surface Science*, vol. 478, no. 1-2, pp. 57–71, May 2001.

[59] E. Tok, W. Ong, and A. Wee, "6H-SiC(0001) phase transition: evolution of the (6x6) magic clusters," *Surface Science*, vol. 558, no. 1-3, pp. 145–158, Jun. 2004.

[60] M. Naitoh, J. Takami, S. Nishigaki, and N. Toyama, "A ($2\sqrt{3}$ x $2\sqrt{13}$) surface phase in the 6H–SiC(0001) surface studied by scanning tunneling microscopy," *Appl. Phys. Lett.*, vol. 75, no. 5, pp. 650–652, Aug. 1999.

[61] F. Amy, P. Soukiassian, and C. Brylinski, "Atomic cracks and (2sqrt (3)× 2× sqrt (3))-R30 reconstruction at 6H-SiC (0001) surface," *Applied physics letters*, vol. 85, p. 926, 2004.

[62] J. Li, Q. Wang, G. He, M. Widom, L. Nemec, V. Blum, M. Kim, P. Rinke, and R. M. Feenstra, "Formation of graphene atop a Si adlayer on the C-face of SiC," *Phys. Rev. Materials*, vol. 3, p. 084 006, 8 2019.

[63] N. Srivastava, G. W. He, Luxmi, and R. M. Feenstra, "Interface structure of graphene on SiC(000(1)over-bar)," *Physical Review B*, vol. 85, no. 4, p. 041 404, Jan. 2012.

[64] Z. Ni, Q. Liu, K. Tang, J. Zheng, J. Zhou, R. Qin, Z. Gao, D. Yu, and J. Lu, "Tunable Bandgap in Silicene and Germanene," *Nano Letters*, vol. 12, no. 1, pp. 113–118, 2012.

[65] B. Lalmi, H. Oughaddou, H. Enriquez, A. Kara, S. Vizzini, B. Ealet, and B. Aufray, "Epitaxial growth of a silicene sheet," *Applied Physics Letters*, vol. 97, no. 22, p. 223 109, 2010.

[66] B. Aufray, A. Kara, S. Vizzini, H. Oughaddou, C. Léandri, B. Ealet, and G. Le Lay, "Graphene-like silicon nanoribbons on Ag(110): A possible formation of silicene," *Applied Physics Letters*, vol. 96, no. 18, p. 183 102, 2010.

[67] R. Bernard, T. Leoni, A. Wilson, T. Lelaidier, H. Sahaf, E. Moyen, L. Assaud, L. Santinacci, F. Leroy, F. Cheynis, A. Ranguis, H. Jamgotchian, C. Becker, Y. Borensztein, M. Hanbücken, G. Prévot, and L. Masson, "Growth of Si ultrathin films on silver surfaces: Evidence of an Ag(110) reconstruction induced by Si," *Phys. Rev. B*, vol. 88, p. 121 411, 12 2013.

[68] S. Colonna, G. Serrano, P. Gori, A. Cricenti, and F. Ronci, "Systematic STM and LEED investigation of the Si/Ag(110) surface," *Journal of Physics: Condensed Matter*, vol. 25, no. 31, p. 315 301, 2013.

[69] P. Vogt, P. De Padova, C. Quaresima, J. Avila, E. Frantzeskakis, M. C. Asensio, A. Resta, B. Ealet, and G. Le Lay, "Silicene: Compelling Experimental Evidence for Graphenelike Two-Dimensional Silicon," *Phys. Rev. Lett.*, vol. 108, p. 155 501, 15 2012.

[70] M. R. Tchalala, H. Enriquez, H. Yildirim, A. Kara, A. J. Mayne, G. Dujardin, M. A. Ali, and H. Oughaddou, "Atomic and electronic structures of the (rt13xrt13)R13.9° of silicene sheet on Ag(111)," *Applied Surface Science*, vol. 303, no. 0, pp. 61–66, 2014.

[71] A. Fleurence, R. Friedlein, T. Ozaki, H. Kawai, Y. Wang, and Y. Yamada-Takamura, "Experimental Evidence for Epitaxial Silicene on Diboride Thin Films," *Phys. Rev. Lett.*, vol. 108, p. 245 501, 24 2012.

[72] L. Meng, Y. Wang, L. Zhang, S. Du, R. Wu, L. Li, Y. Zhang, G. Li, H. Zhou, W. A. Hofer, and H.-J. Gao, "Buckled Silicene Formation on Ir(111)," *Nano Letters*, vol. 13, no. 2, pp. 685–690, 2013.

[73] D. Jose and A. Datta, "Structures and Chemical Properties of Silicene: Unlike Graphene," *Accounts of Chemical Research*, vol. 47, no. 2, pp. 593–602, 2014.

[74] S. Soubatch, S. E. Saddow, S. P. Rao, W. Y. Lee, M. Konuma, and U. Starke, "Structure and morphology of 4H-SiC wafer surfaces after H2-Etching," *Silicon Carbide and Related Materials 2004*, vol. 483, pp. 761–764, 2005.

[75] *LK Technologies*, `http://www.lktech.com/`, Accessed: 2019-12-12.

[76] Wikipedia contributors, *Low-energy electron diffraction — Wikipedia, The Free Encyclopedia*, [Online; accessed 12-December-2019], 2019.

[77]   ——, *Louis de Broglie — Wikipedia, The Free Encyclopedia*, [Online; accessed 16-December-2019], 2019.

[78]   A. T. Hubbard, *The Handbook of Surface Imaging and Visualization*. CRC Press, 1995.

[79]   G. He, N. Srivastava, and R. M. Feenstra, "Formation of graphene on SiC(0001¯) surfaces in disilane and neon environments," *Journal of Vacuum Science & Technology B*, vol. 30, no. 4, 04E102, 2012.

[80]   Wikipedia contributors, *Auger electron spectroscopy — Wikipedia, The Free Encyclopedia*, [Online; accessed 17-December-2019], 2019.

[81]   ——, *Auger effect — Wikipedia, The Free Encyclopedia*, [Online; accessed 17-December-2019], 2019.

[82]   M. Lepper, *Insights into the Adsorption Behavior of a Prototype Functional Molecule: A Scanning Tunneling Microscopy Study*, ser. BestMasters. Springer Fachmedien Wiesbaden, 2015.

[83]   Wikipedia contributors, *Scanning tunneling microscope — Wikipedia, The Free Encyclopedia*, [Online; accessed 18-December-2019], 2019.

[84]   G. Binnig, H. Rohrer, C. Gerber, and E. Weibel, "7x7 Reconstruction on Si(111) Resolved in Real Space," *Physical Review Letters*, vol. 50, no. 2, pp. 120–123, 1983.

[85]   Wikipedia contributors, *Quantum tunnelling — Wikipedia, The Free Encyclopedia*, [Online; accessed 26-December-2019], 2019.

[86]   *Scanning Tunneling Microscopy (STM)*, https://www2.fkf.mpg.de/ga/research/stmtutor/stmpage.html.

[87]   J. Chen, "Introduction to Scanning Tunneling Microscopy: Second Edition," *American Journal of Physics*, vol. 62, Jun. 1994.

[88]   D. Bonnell, *Scanning Probe Microscopy and Spectroscopy: Theory, Techniques, and Applications*. Wiley, 2000.

[89]   J. Tersoff and D. R. Hamann, "Theory and Application for the Scanning Tunneling Microscope," *Physical Review Letters*, vol. 50, no. 25, pp. 1998–2001, 1983.

[90]   ——, "Theory of the Scanning Tunneling Microscope," *Physical Review B*, vol. 31, no. 2, pp. 805–813, 1985.

[91] A. Baratoff, "Theory of Scanning Tunneling Microscopy Methods and Approximations," *Physica B & C*, vol. 127, no. 1-3, pp. 143–150, 1984.

[92] S. Ohnishi and M. Tsukada, "Molecular-orbital Theory for the Scanning Tunneling Microscopy," *Solid State Communications*, vol. 71, no. 5, pp. 391–394, Aug. 1989.

[93] C.-R. Pan, "Properties of two-dimensional materials grown on metal substrates," PhD thesis, Georgia Institute of Technology, 2019.

[94] N. Briggs, Z. M. Gebeyehu, A. Vera, T. Zhao, K. Wang, A. D. Duran, B. Bersch, T. Bowen, K. L. Knappenberger, and J. A. Robinson, "Epitaxial graphene/silicon carbide intercalation: a minireview on graphene modulation and unique 2D materials," *Nanoscale*, vol. 11, no. 33, pp. 15 440–15 447, Sep. 2019.

[95] M. G. Silly, M. D'Angelo, A. Besson, Y. J. Dappe, S. Kubsky, G. Li, F. Nicolas, D. Pierucci, and M. Thomasset, "Electronic and structural properties of graphene-based metal-semiconducting heterostructures engineered by silicon intercalation," *Carbon*, vol. 76, pp. 27–39, Sep. 2014.

[96] J. Furthmuller, P. Kackell, F. Bechstedt, A. Fissel, K. Pfennighaus, B. Schroter, and W. Richter, "Model of the epitaxial growth of SiC-polytypes under surface-stabilized conditions," *Journal of Electronic Materials*, vol. 27, no. 7, pp. 848–852, Jul. 1998.

VITA

Hsin-Ju was born in Taipei, Taiwan. He enjoys breaking things, putting them together, and getting yelled by his parents for breaking things. He aced Math in high school but felt there is something missing, and after taking the first physics course in second year in high school, he realized this is what he loves. After the national exam in Taiwan, he enrolled in department of Physics at National Tsing Hua University, and after graduating from college and finishing military service, he enrolled in department of Physics at California State University, Los Angeles for his master degree. He then joined Dr. First's lab in School of Physics at Georgia Tech. He spent some time identifying a two dimensional structure. After his PhD, Hsin-Ju is going to be a K-12 science teacher in Taiwan to share what he learned about science and teaching.